

**Perfluorodecalin (PFD)-filled polypeptide capsules as  
artificial oxygen carriers**

**Dissertation**

by

**Huayang Feng**

For the degree of

Doctor of Natural Science

- Dr. rer. nat.-

Faculty of Chemistry

University of Duisburg-Essen

Germany

Essen, 2023

# DuEPublico

Duisburg-Essen Publications online

UNIVERSITÄT  
DUISBURG  
ESSEN

*Offen im Denken*

ub | universitäts  
bibliothek

Diese Dissertation wird via DuEPublico, dem Dokumenten- und Publikationsserver der Universität Duisburg-Essen, zur Verfügung gestellt und liegt auch als Print-Version vor.

**DOI:** 10.17185/duepublico/78904

**URN:** urn:nbn:de:hbz:465-20230921-135430-8

Alle Rechte vorbehalten.

The present dissertation was conducted from October 2019 to May 2023 at Physical Chemistry II group of Prof. Dr. rer. nat. Christian Mayer in the Faculty of Chemistry of the University of Duisburg-Essen.

Disputation date: 16.08.2023

Referees:

Prof. Dr. rer. nat. Christian Mayer

Universität Duisburg-Essen

Prof. Dr. rer. nat. Mathias Ulbricht

Universität Duisburg-Essen

Chairman:

Prof. Dr. rer. nat. Georg Jansen

Universität Duisburg-Essen



## Declaration of Originality

I confirm that the submitted thesis is original work and was written by me without further assistance.

Appropriate credit has been given where reference has been made to the work of others.

The thesis was not examined before, nor has it been published. The submitted electronic version of the thesis matches the printed version.

Essen, 21.08.2023

(Place, Date)

Huayang Feng

(Huayang Feng)



## Acknowledgements

The thesis couldn't be finished without so many people's help.

First, I want to thank my parents, my wife and my daughter. My mother tried her best to provide me a good living environment. She always encourages me to study hard to get a better performance in every exam, as a result I have chance to study in Zhengzhou university. My father is a warm-hearted person. He always shows up with warm-heart smiles as well as gifts like a toy car with eight tires, which made my childhood fun and happy. He also teaches me a lot of mathematics when I was in elementary school, which also helps me a lot to get good performance in math exams. My wife also gives me endless love. She will tell jokes to cheer me up when I am down. She will also be by my side to take care of me when I am sick. My lovely daughter is three-year-old now, but I have been with her for less than three months. However, whenever I recall the time I spent with her, whenever I see her photos with her lovely smile, I am moved to tears. Her lovely smile is one motivation for me to work hard. As a son, husband, and father, I owe too much to my family, and I will forever be grateful to them in the future.

Then, I want to thank my Ph.D. supervisor, professor Christian Mayer for giving me the chance to do research in his research group and providing me endless support throughout my Ph.D. period. His support starts since 2018 when I was looking for Ph.D. position and applying China Scholarship Council scholarship. He fully supported my application for the CSC grant and provided me with all the necessary documents to apply for the scholarship. His great support made it possible for me to get the scholarship, which made my studying overseas dream and doing Ph.D. dream come true. After I arrived at Essen, he helps me registration as a student in Duisburg-Essen university in international student office as well as registration as a Ph.D. candidate in chemistry department. The first year of my graduate career is not easy because I couldn't find an alternative way to synthesize polypeptide. I even considered to give up synthesizing polypeptide. But the unlimited trust I saw from his eyes and kind encouragement I heard from our talk made me feel I can do it, and it turn out that I really did it. Later, he shared me methods in literature reading, showed me different ways to interpretate results in NMR and AFM, revised my every manuscript in detail, shared his interesting and informative 'general

chemistry' course to me, and encouraged me to apply for CGCA young researcher awards two times. All the supports he provided me and incredible patience he showed me made it possible for me to complete this PhD thesis.

Then I want to thank all colleagues in our research group for all the helps they provided. First, I want to thank Mr. Uwe Bachorski for repairing the UV lamp so that I don't need to worry about the column chromatography. Then, I want to thank Ms. Kirsten Schwark for helping me order all the chemicals when I was not familiar with the order process, which really helped me a lot to start synthesis work quickly. Then I want to thank Dr. Maria Davila Garvin for always encouraging me join our group talking and eating. Then I want to thank Dr. Juergen Linders for always welcoming to talk with me and for helping me to do so many PFG NMR test. I would also like to thank professor Katja Bettina Ferez, Dr. Miriam Cantore and Ms. Eva Hillen from the University Hospital Essen for their help with all cell tests and for the helpful discussion of the results.

I also want to thank all students, including Mr. Jonas Fabrizi, Ms. Annika Kirsten, Ms. Bianka Ifflaender, Ms. Burcu Yucel, Mr. Sascha Myszkowska, for their help with my research. Especially I want to thank Mr. Jonas Fabrizi for communicating so many syntheses with me and also teaching me many basics on organic chemistry. Also I want to thank Ms. Annika Kirsten for her help with syntheses of polypeptide and capsules. Many data in this Ph.D. thesis are from her research course report.

I also want to thank Dr. qirong ke and Mr. Sebastian Buchholz for UV test and GPC test. Then I want to thank Ms. Andrea Hermsen for Raman test and Dr. Florian Uteschil for MS test. I also want to thank professor Mathias Ulbricht for accepting to be the referee of my Ph.D. thesis and professor Georg Jansen for accepting to be the chairman of my defense. I also want to thank my master thesis supervisor, Dr. Jingguo Li for his helpful discussion on my research and future career plans.

Finally, I would like to thank the China Scholarship Council for financial support so that I can have the opportunity to do my Ph.D. thesis in professor Mayer's research group in Duisburg-Essen university.

## I. Abstract

Artificial oxygen carriers (AOCs) based on perfluorocarbons (PFCs) have been studied and developed for about half a century. Since PFCs are not dissolvable in blood, they are often emulsified or encapsulated before intravenous administration. In this dissertation, it is attempted to prepare capsules from a synthetic protein as a membrane material. For that purpose, triblock polypeptides consisting of a hydrophilic aspartate block, a hydrophobic phenylalanine block, and a central cysteine block for cross-linking are synthesized to form spherical solid protein-like capsule walls around PFC droplets.

We first investigate the effect of hydrophilic chain length to hydrophobic chain length ratio on the size and morphology of PFC droplets. Three di-block polypeptides Asp<sub>40</sub>-Phe<sub>n</sub> with different hydrophilic chain length to hydrophobic chain length ratios, including Asp<sub>40</sub>-Phe<sub>5</sub>, Asp<sub>40</sub>-Phe<sub>9</sub>, and Asp<sub>40</sub>-Phe<sub>14</sub>, are first synthesized and investigated for their ability to emulsify PFC. When the ratio is smaller than 3:1, polypeptides are hardly soluble in water, and there are a large number of self-assembled micelles in the emulsion, which are well dispersed around the PFC droplets. When the ratio is larger than 8: 1, polypeptides are well dissolved in water and are suitable to stabilize PFC in water emulsions.

In the second step, single block oligo- or poly-cysteine peptides are synthesized and their free thiol group contents were studied, to make sure that cysteine block can crosslink properly. Two differently protected cysteine units, including S-benzyl-L-cysteine (BnCys) and S-carbobenzoxy-L-cysteine (CbzCys), are used as starting materials. Both amino acids can be efficiently converted into activated monomers, including N-(phenoxycarbonyl)-S-benzyl-L-cysteine (NPBnCys) and N-(4-nitrophenoxycarbonyl)-S-carbobenzoxy-L-cysteine (NNPCbzCys). Polymerization of the first monomer gives oligo- or poly-BnCys with good yields (around 80%) and narrow molecular weight distribution (PDI=1.2). However, polymerization of NNPCbzCys gives oligo- or poly-CbzCys with smaller yields (around 30%) and broad molecular weight distribution (PDI=1.8). Around 90% of the protecting groups of both differently protected oligo- or poly-cysteine units can be efficiently removed by acidolysis, and around 20% of free thiol groups can be detected for all the resulting oligo- or poly-cysteine peptides. If 1,2-ethanedithiol was used as carbon cation scavenger and reducing agent for the deprotection

reaction, around 39% of free thiol groups can be detected. Given that the polymerization of monomer NPBnCys is more efficient than that of monomer NNPCbzCys, it is better to synthesize triblock polypeptide with monomer NPBnCys.

Finally, various triblock polypeptides with different block ratios and different initiators are synthesized, and their ability to encapsulate PFC are studied. All triblock oligo- or poly-peptides can stabilize PFC in water efficiently. The capsule dispersion can be easily redispersed by shaking even after 1 month. Most of the capsules exhibit a diameter that ranges from 100 nm to 1000 nm. When cysteine chain dominates the peptide composition, the capsule wall exhibits enough mechanical strength to maintain spherical shape after a drying process, which indicates an existence of crosslinking between cysteine residues. As observed by NMR spectroscopy, the capsule wall allows for fast gas exchange and the gas exchange is completely reversible. The capsules also exhibit a large self-diffusion constant as around  $2.05 \times 10^{-12} \text{ m}^2/\text{s}$  in aqueous solution, which is good for oxygen delivery in the blood circulation. The capsules also exhibit little cytotoxicity when tested on cell cultures.

## II. Table of Contents

I.	Abstract.....	I
II.	Table of Contents.....	III
III.	List of Abbreviations .....	V
IV.	List of Tables .....	VI
V.	List of Figures.....	VII
1	Introduction and objectives .....	1
2	Theoretical background .....	4
2.1	Perfluorocarbon based artificial oxygen carriers.....	4
2.1.1	Perfluorocarbon in water emulsions .....	5
2.1.2	Perfluorocarbon filled capsules .....	7
2.2	Polypeptide synthesis .....	8
2.2.1	Ring-opening polymerization (ROP) of $\alpha$ -amino acid N-carboxy anhydrides (NCAs) .....	13
2.2.2	Polymerization of N-phenoxy carbonyl amino acid (NPCs).....	16
2.3	Perfluorodecalin-filled polypeptide capsules .....	17
2.3.1	Polypeptide surfactants .....	18
2.3.2	Polycysteine .....	19
2.4	Studying molecules' structure and diffusion properties by nuclear magnetic resonance (NMR).....	22
2.4.1	Principle of NMR spectroscopy.....	22
2.4.2	Spin interactions in molecules .....	29
2.4.3	Study diffusion properties of molecules .....	33
2.5	Studying nano-capsules.....	36
2.5.1	Determination of capsule size distribution by video microscopic particle tracking .....	36
2.5.2	Determination of capsule morphology and strength by atomic force microscopy.....	41
3	Materials and methods .....	45
3.1	Chemicals used .....	45
3.2	Syntheses of PFD in water emulsions stabilized by diblock polypeptide surfactants .....	46
3.2.1	Syntheses of activated amino acid monomers.....	46
3.2.2	Synthesis of polypeptide through polymerization of activated amino acid monomers .....	47
3.2.3	Preparation of PFD/water emulsion stabilized by diblock peptide emulsifier . .....	49
3.3	Syntheses of oligo- and polycysteines .....	49
3.3.1	Synthesis of activated amino acid monomers.....	49
3.3.2	Synthesis of peptide through polymerization of activated amino acid monomers .....	50
3.3.3	Deprotection of protected peptides.....	52
3.4	Syntheses of PFD filled triblock polypeptide capsules.....	53

## II. Table of contents

---

3.4.1	Synthesis of the homopolymers, the diblock-peptide, and the triblock-peptide .....	53
3.4.2	Synthesis of nanocapsules.....	57
3.5	Devices used .....	57
3.5.1	Nuclear magnetic resonance spectroscopy .....	57
3.5.2	UV-vis spectroscopy.....	57
3.5.3	MALD-TOF Mass spectroscopy.....	58
3.5.4	Gel permeation chromatography .....	58
3.5.5	Atomic force microscopy .....	58
3.5.6	Dark-field microscopy.....	58
4	Results and discussion.....	59
4.1	Investigation of PFD in water emulsions stabilized by di-block polypeptides .....	59
4.1.1	Discussion of activated monomers and polymers.....	59
4.1.2	Discussion of PFD in water emulsions.....	61
4.2	Comparison of polycysteine synthesized from differently protected cysteines.....	64
4.2.1	Discussion of activated monomers .....	64
4.2.2	Discussion of polymerization of each monomer.....	65
4.2.3	Discussion of deprotection of polycysteine .....	72
4.3	Investigation of PFD filled triblock polypeptide capsules .....	81
4.3.1	Discussion of triblock polypeptide syntheses.....	81
4.3.2	Discussion of PFD filled triblock polypeptide capsule .....	84
5	Summary and outlook.....	96
6	References.....	98
7	Appendices.....	101
7.1	Supporting information.....	101
7.1.1	Measured <sup>1</sup> H NMR spectra.....	101
7.2	List of publications .....	120
7.3	Conference participation .....	120
7.4	Students co-supervision.....	121

### III. List of Abbreviations

<b>Abbreviation</b>	<b>Meaning</b>
BnAsp	$\beta$ -Benzyl L-aspartate
BnCys	S-Benzyl L-cysteine
CbzCys	S-Carbobenzoxy L-cysteine
Phe	L-Phenylalanine
PFC	Phenyl chloroformate
NPCF	4-Nitrophenyl chloroformate
NPBnAsp	N-Phenoxycarbonyl- $\beta$ -benzyl L-aspartate
NPBnCys	N-Phenoxycarbonyl-S-benzyl L-cysteine
NPCbzCys	N-Phenoxycarbonyl-S-carbobenzoxy L-cysteine
NNPCbzCys	N-(4-nitrophenoxycarbonyl)-S-carbobenzoxy L-cysteine
NPPhe	N-Phenoxycarbonyl L-Phenylalanine
TFA	Trifluoroacetic acid
HBr	Hydrobromic acid
TFMSA	Trifluoromethanesulfonic acid
Asp	L-Aspartic acid
Cys	L-Cysteine
Phe	L-Phenylalanine
DEE	Diethyl ether
DMAC	<i>N,N</i> -Dimethylacetamide
EA	Ethyl acetate
CDCl <sub>3</sub>	Deuterated chloroform
DMSO-d <sub>6</sub>	Deuterated dimethyl sulfoxide
DTT	Dithiothreitol
NPC	N-Phenoxycarbonyl amino acid
NCA	N-Carboxyanhydride amino acid
UDs	$\alpha$ -Amino acid urethane derivative
AOCs	Artificial oxygen carriers
PFC	Perfluorocarbon
PFD	Perfluorodecalin
ROP	Ring-opening polymerization
SPPS	Solid phase peptide synthesis
SPM	Scanning probe microscopy
AFM	Atomic force microscopy
ANT	Advanced Nanoparticle Tracking
DFM	Dark-field microscopy
CCD	Charged-Couple-Device
NMR	Nuclear magnetic resonance

## IV. List of Tables

Table 2.1	Comparison between products.....	6
Table 2.2	Comparison between capsules filled with PFD.....	7
Table 3.1	Chemicals used.....	45
Table 3.2	Summarized syntheses of Bu-BnAsp <sub>40</sub> -Phe <sub>n</sub> .....	47
Table 3.3	Summarized de-protection reactions of Bu-BnAsp <sub>40</sub> -Phe <sub>n</sub> .....	48
Table 3.4	Summarized synthesis of Bu-BnCys <sub>c</sub> or Bu-CbzCys <sub>c</sub> .....	51
Table 3.5	Summarized de-protection reaction of Bu-BnCys <sub>c</sub> or Bu-CbzCys <sub>c</sub> .....	52
Table 3.6	Summarized syntheses of Bu-BnAsp <sub>m</sub> -CbzCys <sub>c</sub> -Phe <sub>n</sub> .....	54
Table 3.7	Summarized syntheses of Bu-BnAsp <sub>m</sub> -BnCys <sub>c</sub> -Phe <sub>n</sub> .....	55
Table 3.8	Summarized syntheses of DBnAsp-BnAsp <sub>m</sub> -BnCys <sub>c</sub> -Phe <sub>n</sub> .....	55
Table 3.9	Summarized de-protection reaction of triblock polypeptide.....	56

## V. List of Figures

Figure 2.1	(a)The structures of two broadly used PFCs, perfluorodecalin (PFD) and perfluorooctylbromide. (b)Illustration of chemically bound of O <sub>2</sub> to the central iron atom of hemoglobin. ....5
Figure 2.2	Structural organization of proteins [12].....9
Figure 2.3	The common 20 amino acids. The three- and one-letter codes for the amino acids are also given. The amino acids are classified into hydrophobic (hydrogen, aliphatic, aromatic, and sulfur containing) and hydrophilic (negatively charged, positively charged, and polar). The side chains are marked with oval boxes [12]..... 11
Figure 2.4	Solid-phase peptide synthesis: (a) coupling, (b) deprotection, (c) cleavage from resin. P = protecting group e.g. 9-fluorenylmethoxycarbonyl (Fmoc) or tert-butylcarbonyl (Boc). R <sub>1</sub> , R <sub>2</sub> , R <sub>n</sub> = peptide side chains. Reproduced according to reference [14]..... 12
Figure 2.5	Recombinant DNA technique to synthesize polypeptides [14]..... 13
Figure 2.6	(a) Leuchs method to synthesize NCAs, (b) Fuchs-Farthing method to synthesize NCAs. .... 14
Figure 2.7	Mechanism of primary amines initiated ROP of NCAs. .... 16
Figure 2.8	Synthetic methods to prepare NPC monomers ..... 17
Figure 2.9	Synthesis of polypeptides by polymerization of NPCs..... 17
Figure 2.10	Cysteine undergoes facile oxidative dimerization to form cysteine disulfide crosslinks. Reducing conditions can readily convert cysteines back into the free thiol-based cysteines [16]. .... 20
Figure 2.11	Two possible directions of spin and its z-component..... 24
Figure 2.12	(a) Precession of spins. (b) transition between spin states..... 25
Figure 2.13	Thermal equilibrium. .... 26
Figure 2.14	(a) Direction of M <sub>eq</sub> after a pulse. (b) Direction of every one nuclear spin after a pulse. (c) Precession of the transverse magnetization. .... 27
Figure 2.15	Decay and oscillation of the transverse magnetic moment [32]..... 28
Figure 2.16	The induction of an NMR signal [32]. .... 28
Figure 2.17	NMR signals and its Fourier transformed frequency spectrum [32]. .... 29
Figure 2.18	Orientation of B <sub>0</sub> in the principal axis system as defined by the polar angles $\theta$ and $\varphi$ . .... 31
Figure 2.19	Illustration of how multiplets are built up as a result of scalar coupling..... 32
Figure 2.20	Pulse sequence in PFG NMR experiment [35]. .... 33
Figure 2.21	Stejskal Tanner plot [35]..... 34
Figure 2.22	Plot of the rate constants for longitudinal and transverse relaxation, caused by random fields, as a function of the correlation time, $\tau_c$ . .... 35
Figure 2.23	Graphic representation of the dependence of NMR time signal after 90° pulse and the corresponding frequency spectrum on molecules with (a) extremely fast rotational diffusion and (b) extremely slow rotational diffusion [30]. .... 36
Figure 2.24	Light path of dark-field microscopy..... 39
Figure 2.25	Picture of an AFM system on an active damping table..... 42

Figure 2.26	Cantilever deflection due to force interaction between cantilever and sample [42].	42
Figure 2.27	Detection of cantilever deflection by beam deflection method [42].	43
Figure 4.1	Synthetic route for di-block peptide.	59
Figure 4.2	Photos of the reaction DMAc solution after two days' reaction of di-block peptides. (a) Bu-BnAsp <sub>40</sub> -Phe <sub>5</sub> . (b) Bu-BnAsp <sub>40</sub> -Phe <sub>9</sub> . (c) Bu-BnAsp <sub>40</sub> -Phe <sub>14</sub> .	60
Figure 4.3	Photos of the di-block peptide 0.1 M NaOH aqueous solution or dispersion. (a) Bu-Asp <sub>40</sub> -Phe <sub>5</sub> . (b) Bu-Asp <sub>40</sub> -Phe <sub>9</sub> . (c) Bu-Asp <sub>40</sub> -Phe <sub>14</sub> . (NaOH is used to help the Asp block be soluble in water).	60
Figure 4.4	Photos of the PFD emulsions stabilized by different di-block peptide. (a) Bu-Asp <sub>40</sub> -Phe <sub>5</sub> . (b) Bu-Asp <sub>40</sub> -Phe <sub>9</sub> . (c) Bu-Asp <sub>40</sub> -Phe <sub>14</sub> . PFD volume fraction is 5%.	61
Figure 4.5	Dilute PFD in water emulsions stabilized by Bu-Asp <sub>40</sub> -Phe <sub>14</sub> under dark-field (a) and bright-field (b) conditions. Yellow circles are some examples.	62
Figure 4.6	AFM image of a diluted sample of a PFD-filled Asp <sub>40</sub> -Phe <sub>5</sub> emulsion.	63
Figure 4.7	AFM image of a diluted PFD filled Asp <sub>40</sub> -Phe <sub>14</sub> emulsion.	63
Figure 4.8	AFM image of diluted Asp <sub>40</sub> -Phe <sub>14</sub> micelles.	64
Figure 4.9	Synthesis route of activated protected cysteines, including (a) NPBnCys, (b) NPCbzCys, and (c) NNPCbzCys.	65
Figure 4.10	Syntheses of protected oligo- or poly-cysteine, including (a) oligo- or poly-BnCys and (b) oligo- or poly-CbzCys.	65
Figure 4.11	<sup>1</sup> H NMR spectrum of Bu-CbzCys <sub>c</sub> obtained at 30 °C (solvent: DMSO-d <sub>6</sub> ).	66
Figure 4.12	<sup>1</sup> H NMR spectrum of Bu-CbzCys <sub>c</sub> obtained at 60 °C (solvent: DMSO-d <sub>6</sub> ).	67
Figure 4.13	<sup>1</sup> H NMR spectrum of Bu-BnCys <sub>c</sub> obtained at 60 °C (solvent: DMSO-d <sub>6</sub> ).	68
Figure 4.14	<sup>1</sup> H NMR spectrum of Bu-BnCys <sub>c</sub> obtained at 60 °C (solvent: DMSO-d <sub>6</sub> ).	68
Figure 4.15	MALDI-TOF mass spectrum of Bu-BnCys <sub>c</sub> .	70
Figure 4.16	MALDI-TOF mass spectrum of Bu-CbzCys <sub>c</sub> .	71
Figure 4.17	MALDI-TOF mass spectrum of Bu-CbzCys <sub>c</sub> reacted at 30 °C.	72
Figure 4.18	<sup>1</sup> H NMR spectrum of Bu-Cys <sub>17</sub> (solvent: DMSO-d <sub>6</sub> ).	73
Figure 4.19	<sup>1</sup> H NMR spectrum of Bu-Cys <sub>20</sub> (solvent: DMSO-d <sub>6</sub> ).	74
Figure 4.20	Possible amide-iminole-tautomerism.	75
Figure 4.21	(a) <sup>19</sup> F NMR of Bu-Cys <sub>20</sub> (solvent: DMSO-d <sub>6</sub> ). (b) <sup>19</sup> F NMR of 20 mg Bu-Cys <sub>20</sub> with 3 mg of TFA as a reference (solvent: DMSO-d <sub>6</sub> ).	76
Figure 4.22	PFG-NMR echo decay plots for peptide and the two acids. The slopes of the decay corresponds to the self-diffusion constants of the observed nuclei.	77
Figure 4.23	<sup>1</sup> H NMR spectrum of Bu-BnAsp <sub>11</sub> -BnCys <sub>15</sub> (solvent: DMSO-d <sub>6</sub> ).	78
Figure 4.24	<sup>1</sup> H NMR spectrum of Bu-Asp <sub>11</sub> -Cys <sub>15</sub> (solvent: DMSO-d <sub>6</sub> ).	79
Figure 4.25	<sup>1</sup> H NMR spectrum of Bu-Asp <sub>11</sub> -Cys <sub>15</sub> (solvent: DMSO-d <sub>6</sub> ) deprotected with anisole and 1,2-ethandithiol as carbocation scavengers.	80
Figure 4.26	<sup>1</sup> H NMR spectrum of Bu-Asp <sub>11</sub> -Cys <sub>15</sub> (solvent: DMSO-d <sub>6</sub> ) deprotected with 2-ethandithiol as carbocation scavengers.	81
Figure 4.27	Synthetic route of triblock polypeptide using NNPCbzCys as monomer and n-butylamine as initiator.	82
Figure 4.28	Synthetic route of triblock polypeptide using NPBnCys as monomer and n-	

	butylamine as initiator. ....	83
Figure 4.29	Synthetic route of triblock polypeptide using NPBnCys as monomer and 1,4-dibenzyl L-aspartate as initiator.....	84
Figure 4.30	Photo of PFD filled polypeptide capsule dispersion.....	85
Figure 4.31	AFM image (left) and height profiles (right) of PFD filled Bu-Asp <sub>40</sub> -Cys <sub>5</sub> -Phe <sub>5</sub> capsules. ....	86
Figure 4.32	AFM image (left) and height profiles (right) of PFD filled Bu-Asp <sub>7</sub> -Cys <sub>15</sub> -Phe <sub>2</sub> capsules. ....	87
Figure 4.33	AFM image (left) and height profiles (right) of PFD-filled Bu-Asp <sub>6</sub> -Cys <sub>8</sub> -Phe <sub>8</sub> capsules ....	88
Figure 4.34	AFM image (left) and height profiles (right) of PFD-filled Bu-Asp <sub>10</sub> -Cys <sub>15</sub> capsules ....	89
Figure 4.35	AFM image (left) and height profiles (right) of collapsed PFD-filled Bu-Asp <sub>10</sub> -Cys <sub>15</sub> capsules.....	90
Figure 4.36	AFM images of some capsules before and after a single compression test. (a) a completely collapsed capsule after compression test. (b) a deformed capsule after compression test.....	91
Figure 4.37	AFM image of PFD filled Bu-Cys <sub>20</sub> capsules. ....	92
Figure 4.38	Gas exchange process in a dispersion of PFD-filled triblock-peptide Bu-Asp <sub>6</sub> -Cys <sub>8</sub> -Phe <sub>8</sub> capsules as determined by the chemical shift of the <sup>19</sup> F NMR signal. ....	93
Figure 4.39	PFG-NMR echo decay plots for pure liquid PFD and the PFD in a dispersion of PFD-filled Bu-Asp <sub>7</sub> -Cys <sub>9</sub> capsules. The slopes of the decay corresponds to the self-diffusion constants of the observed nuclei. ....	94
Figure 4.40	Cytotoxic effects of PFD-filled capsules on human HK-2 cells. To determine the disruption of cellular membrane integrity, LDH analyses was performed. Control cells were incubated for 4 h (a) or 24 h (b) with DMEM/F-12 with GlutaMAX (no supplements), whereas treatment groups were incubated for 4 h or 24 h with capsules at different concentrations (0.1 %, 0.25 %, 0.5 %, 1 %, 2.5 %, 5 %), respectively. The positive control group corresponded to Lysis Buffer treatment for 45 min. Values are expressed as means ± SD (n = 12) from 4 different experiments.. ....	95
Figure 7.1	<sup>1</sup> H NMR spectrum of NPBnAsp (solvent: CDCl <sub>3</sub> ).....	101
Figure 7.2	<sup>1</sup> H NMR spectrum of NPPhe (solvent: CDCl <sub>3</sub> ).....	101
Figure 7.3	<sup>1</sup> H NMR spectrum of Bu-BnAsp <sub>40</sub> (solvent: DMSO-d <sub>6</sub> ). ....	102
Figure 7.4	<sup>1</sup> H NMR spectrum of Bu-BnAsp <sub>40</sub> -Phe <sub>5</sub> (solvent: CDCl <sub>3</sub> /TFA-d <sub>1</sub> ). ....	102
Figure 7.5	<sup>1</sup> H NMR spectrum of Bu-BnAsp <sub>40</sub> -Phe <sub>9</sub> (solvent: CDCl <sub>3</sub> /TFA-d <sub>1</sub> ). ....	103
Figure 7.6	<sup>1</sup> H NMR spectrum of Bu-BnAsp <sub>40</sub> -Phe <sub>14</sub> (solvent: CDCl <sub>3</sub> /TFA-d <sub>1</sub> ). ....	103
Figure 7.7	<sup>1</sup> H NMR spectrum of Bu-Asp <sub>40</sub> -Phe <sub>5</sub> (solvent: CDCl <sub>3</sub> /TFA-d <sub>1</sub> ).....	104
Figure 7.8	<sup>1</sup> H NMR spectrum of Bu-Asp <sub>40</sub> -Phe <sub>9</sub> (solvent: CDCl <sub>3</sub> /TFA-d <sub>1</sub> ).....	104
Figure 7.9	<sup>1</sup> H NMR spectrum of Bu-Asp <sub>40</sub> -Phe <sub>14</sub> (solvent: CDCl <sub>3</sub> /TFA-d <sub>1</sub> ). ....	105
Figure 7.10	<sup>1</sup> H-NMR spectrum of NPBnCys (solvent: CDCl <sub>3</sub> ). ....	105
Figure 7.11	<sup>1</sup> H-NMR spectrum of NPCbzCys (solvent: CDCl <sub>3</sub> ).....	106
Figure 7.12	<sup>1</sup> H-NMR spectrum of NNPCbzCys (solvent: CDCl <sub>3</sub> ). ....	106
Figure 7.13	<sup>1</sup> H NMR spectrum of Bu-BnAsp <sub>31</sub> (solvent: DMSO-d <sub>6</sub> ). ....	107

## V. List of Figures

---

Figure 7.14	$^1\text{H}$ NMR spectrum of Bu-BnAsp <sub>31</sub> -CbzCys <sub>14</sub> (solvent: DMSO-d <sub>6</sub> ). ....	107
Figure 7.15	$^1\text{H}$ NMR spectrum of Bu-BnAsp <sub>31</sub> -CbzCys <sub>6</sub> -Phe <sub>n</sub> (solvent: DMSO-d <sub>6</sub> ).....	108
Figure 7.16	$^1\text{H}$ NMR spectrum of Bu-BnAsp <sub>31</sub> -CbzCys <sub>4</sub> -Phe <sub>n</sub> (solvent: DMSO-d <sub>6</sub> ).....	108
Figure 7.17	$^1\text{H}$ NMR spectrum of Bu-Asp <sub>31</sub> -Cys <sub>4</sub> -Phe <sub>3</sub> (solvent: DMSO-d <sub>6</sub> ). ....	109
Figure 7.18	$^1\text{H}$ NMR spectrum of Bu-BnAsp <sub>40</sub> (solvent: DMSO-d <sub>6</sub> ). ....	109
Figure 7.19	$^1\text{H}$ NMR spectrum of Bu-BnAsp <sub>40</sub> -CbzCys <sub>9</sub> (solvent: DMSO-d <sub>6</sub> ).....	110
Figure 7.20	$^1\text{H}$ NMR spectrum of Bu-BnAsp <sub>40</sub> -CbzCys <sub>5</sub> -Phe <sub>n</sub> (solvent: DMSO-d <sub>6</sub> ).....	111
Figure 7.21	$^1\text{H}$ NMR spectrum of Bu-Asp <sub>40</sub> -Cys <sub>5</sub> -Phe <sub>5</sub> (solvent: DMSO-d <sub>6</sub> ). ....	111
Figure 7.22	$^1\text{H}$ NMR spectrum of Bu-BnAsp <sub>6</sub> (solvent: DMSO-d <sub>6</sub> ).....	112
Figure 7.23	$^1\text{H}$ NMR spectrum of Bu-BnAsp <sub>6</sub> -BnCys <sub>3</sub> (solvent: DMSO-d <sub>6</sub> ).....	112
Figure 7.24	$^1\text{H}$ NMR spectrum of Bu-BnAsp <sub>6</sub> -BnCys <sub>8</sub> (solvent: DMSO-d <sub>6</sub> ).....	113
Figure 7.25	$^1\text{H}$ NMR spectrum of Bu-BnAsp <sub>6</sub> -BnCys <sub>8</sub> -Phe <sub>8</sub> (solvent: TFA-d <sub>1</sub> : CDCl <sub>3</sub> = 1:1). .....	113
Figure 7.26	$^1\text{H}$ NMR spectrum of Bu-Asp <sub>6</sub> -Cys <sub>8</sub> -Phe <sub>8</sub> (solvent: TFA-d <sub>1</sub> : CDCl <sub>3</sub> = 1:1). ...	114
Figure 7.27	$^1\text{H}$ NMR spectrum of Bu-BnAsp <sub>6</sub> (solvent: DMSO-d <sub>6</sub> ).....	114
Figure 7.28	$^1\text{H}$ NMR spectrum of Bu-BnAsp <sub>6</sub> -BnCys <sub>3</sub> (solvent: DMSO-d <sub>6</sub> ).....	115
Figure 7.29	$^1\text{H}$ NMR spectrum of Bu-BnAsp <sub>13</sub> -BnCys <sub>6</sub> -Phe <sub>7</sub> (solvent: TFD-d <sub>1</sub> and CDCl <sub>3</sub> ). .....	115
Figure 7.30	$^1\text{H}$ NMR spectrum of Bu-Asp <sub>13</sub> -Cys <sub>6</sub> -Phe <sub>7</sub> (solvent: TFA-d <sub>1</sub> : CDCl <sub>3</sub> = 1:1). ...	116
Figure 7.31	$^1\text{H}$ NMR spectrum of Bu-BnAsp <sub>7</sub> (solvent: DMSO-d <sub>6</sub> ).....	116
Figure 7.32	$^1\text{H}$ NMR spectrum of Bu-BnAsp <sub>7</sub> -BnCys <sub>15</sub> (solvent: DMSO-d <sub>6</sub> ). ....	117
Figure 7.33	$^1\text{H}$ NMR spectrum of Bu-BnAsp <sub>7</sub> -BnCys <sub>15</sub> -Phe <sub>2</sub> (solvent: TFD-d <sub>1</sub> and CDCl <sub>3</sub> ). .....	117
Figure 7.34	$^1\text{H}$ NMR spectrum of Bu-Asp <sub>7</sub> -Cys <sub>15</sub> -Phe <sub>2</sub> (solvent: DMSO-d <sub>6</sub> ). ....	118
Figure 7.35	$^1\text{H}$ NMR spectrum of DBnAsp-BnAsp <sub>7</sub> (solvent: DMSO-d <sub>6</sub> ).....	118
Figure 7.36	$^1\text{H}$ NMR spectrum of DBnAsp-BnAsp <sub>7</sub> -BnCys <sub>5</sub> (solvent: DMSO-d <sub>6</sub> ). ....	119
Figure 7.37	$^1\text{H}$ NMR spectrum of DBnAsp-BnAsp <sub>7</sub> -BnCys <sub>5</sub> -Phe <sub>n</sub> (solvent: DMSO-d <sub>6</sub> ). .	119
Figure 7.38	$^1\text{H}$ NMR spectrum of Asp <sub>8</sub> -Cys <sub>5</sub> -Phe <sub>3</sub> (solvent: TFA-d <sub>1</sub> : CDCl <sub>3</sub> = 1:1).....	120

## 1 Introduction and objectives

Artificial oxygen carriers (AOCs) based on perfluorocarbons (PFCs) have been studied and developed for about half a century. Since PFCs are not dissolvable in blood, they are often emulsified [1] or encapsulated [2-4] before intravenous administration. In most cases, the administration of the above AOCs would lead to biological incompatibilities due to the emulsifier used for emulsification [1] or immune reaction due to the synthetic polymer used for encapsulation [5, 6]. Among these AOCs, the albumin-derived PFC AOC seems one of the most promising candidates because of its good biocompatibility [4].

Synthetic polypeptides, as synthetic analogues of proteins, contain the same amino acid building blocks as proteins, but allow for the adjustment of properties that are not possible with natural proteins. Therefore, using polypeptides as a shell material to encapsulate PFCs would also create AOCs with good biocompatibility and tunable properties. There are 20 naturally occurring amino acids in a human body, which can be grouped into hydrophilic amino acids and hydrophobic amino acids. The types and contents of amino acids in the polypeptide may have an impact on the size, morphology, stability, and gas permeability of the PFC AOCs.

The objectives of this thesis are synthesizing and testing suitable oligo- or polypeptides that can be used to encapsulate PFD to prepare capsules with good biocompatibility and stability. Triblock polypeptides consisting of aspartic acid, cysteine, and phenylalanine were chosen as suitable candidates for the capsule wall materials. Aspartic acid, as the hydrophilic part, can provide emulsions or capsules with both, electrostatic stabilization and steric stabilization. Phenylalanine, as hydrophobic part, may interact with the organic phase. Cysteine containing a thiol group can solidify the initially loosely associated capsule walls by forming networks of disulfide bonds.

Two main questions should be addressed before synthesizing the triblock polypeptides and preparing PFD filled capsules. The first question is, what block ratio between these three amino acids should be designed? The second question is, what the content of the free thiol groups of the central cysteine block in the synthesized peptide should be. Therefore, the ability of diblock polypeptides  $\text{Asp}_{40}\text{-Phe}_n$  with different Phe block chain length to emulsify PFD will be

studied initially, providing a solid foundation for the synthesis of tri-block peptides and their corresponding capsules. Subsequently, the polymerization efficiency and deprotection efficiency of two differently protected cysteine units will be analyzed, and the free thiol group content of their deprotection products determined as well. Finally, the triblock polypeptides should be synthesized and the effect of different cysteine contents of polypeptides on the mechanical strength of perfluorodecalin-filled polypeptide capsules investigated.

The thesis includes five chapters. Chapter 2 introduces the backgrounds of the thesis. Perfluorocarbon based artificial oxygen carriers including PFD/water emulsions (Fluosol, Oxypherol and Oxygent) and perfluorocarbon filled polymeric capsules (PLGA, PBCA, albumin, polypeptide) are introduced. Then, two kinds of activated amino acid monomers, including NCA and NPC, used to synthesize polypeptides are described. Then, the method to prepare perfluorodecalin-filled polypeptide capsules is introduced, which included formation of emulsion droplets and crosslinking of cysteine block. Therefore, polypeptide surfactants and polycysteine's properties are introduced. Finally, the basics on NMR, AFM and a video-microscopic particle tracking technique are introduced briefly.

Chapter 3 describes in detail the syntheses and characterizations of all polypeptides and capsules. Chapter 3.2 focuses on the syntheses of polypeptide surfactants, including Bu-Asp<sub>40</sub>-Phe<sub>5</sub>, Bu-Asp<sub>40</sub>-Phe<sub>9</sub>, Bu-Asp<sub>40</sub>-Phe<sub>14</sub>, as well as the syntheses of their corresponding emulsions. Chapter 3.3 describes the syntheses and polymerization of three activated protected cysteine monomers, including N-phenoxy carbonyl-S-benzyl-L-cysteine (NPBnCys), N-phenoxy carbonyl-S-carbobenzoxy-L-cysteine (NPCbzCys), and N-(4-nitrophenoxy carbonyl)-S-carbobenzoxy-L-cysteine (NNPCbzCys). Chapter 3.4 deals with the syntheses of triblock polypeptides, including Bu-Asp<sub>31</sub>-Cys<sub>5</sub>-Phe<sub>4</sub>, Bu-Asp<sub>40</sub>-Cys<sub>5</sub>-Phe<sub>5</sub> from NNPCbzCys, and Bu-Asp<sub>6</sub>-Cys<sub>8</sub>-PPhe<sub>8</sub>, Bu-Asp<sub>13</sub>-Cys<sub>6</sub>-Phe<sub>7</sub>, Asp<sub>9</sub>-Cys<sub>5</sub>-Phe<sub>2</sub> (amino acid initiator) from NPBnCys. The syntheses of their corresponding capsules are also introduced.

Chapter 4.1 compares the PFD/water emulsions from different di-block polypeptides, including Asp<sub>40</sub>-Phe<sub>5</sub>, Bu-Asp<sub>40</sub>-Phe<sub>9</sub>, Bu-Asp<sub>40</sub>-Phe<sub>14</sub>. Chapter 4.2 compares the polymerization efficiency of NNPCbzCys and NPBnCys, and introduces their structures before and after deprotection reaction. Chapter 4.3 compares the syntheses of triblock polypeptides from

NNPCbzCys and NPBnCys, and investigates some properties of perfluorodecalin-filled polypeptide capsules, including the size distribution, morphology, gas exchange rate, diffusion constant, and cytotoxicity.

Chapter 5 summarizes the whole thesis and provides some prospects for future research.

## 2 Theoretical background

### 2.1 Perfluorocarbon based artificial oxygen carriers

Currently, hundreds of thousands of people around the world receive blood and blood products every day. Blood performs many important functions in the body, including supply of nutrients and oxygen to tissues, removal of metabolites, regulation of core body temperature, transportation of messenger substances, coagulation and immunological functions, etc [7].

Red blood cell (RBC) concentrates are most frequently used in surgery or emergency medicine to maintain essential functions such as oxygen delivery. Statistical analysis prognosticates that there will be a shortage of blood and therefore a shortage of generated RBCs in the future due to demographic changes, i.e., the percentage of older people is increasing while the percentage of younger people is decreasing. Nevertheless, RBC concentrate transfusions are associated with undesired side effects, including acute transfusion reactions, transfusion-related lung injury, immune modulations, volume overload, and hemolytic reactions. Therefore, artificial oxygen carriers (AOCs) are studied in order to reduce the dependency on and the demand for RBCs [7].

There are mainly two categories of artificial oxygen carriers. One is hemoglobin-based oxygen carriers and the other is perfluorocarbon-based oxygen carriers [8]. Perfluorocarbons are mostly studied as oxygen carriers because of their relative biological inertness and good O<sub>2</sub> dissolving capacities. Perfluorocarbons (PFC) are hydrocarbons whose hydrogen atoms are fully substituted by halogen atoms, mainly fluorine atoms as shown in Figure 2.1a. Due to the high electronegativity of fluorine, the electrons are densely packed and a large electron cloud is created, which leads to a shield and thus to the particularly high stability. Because of its high stability, no toxic metabolites can be formed in the body [9]. All PFCs are capable of dissolving enormous amounts of gases due to the weak intermolecular interactions. Perfluorodecalin, for example, can dissolve 403 mL<sub>O<sub>2</sub></sub>/L<sub>PFC</sub> at 1 atm (1 bar, 713 mmHg). In contrast, water and blood can only dissolve around 10 mL<sub>O<sub>2</sub></sub>/L<sub>water</sub> and around 200 mL<sub>O<sub>2</sub></sub>/L<sub>blood</sub>, respectively. Unlike in hemoglobin, in which O<sub>2</sub> is chemically bound to the central iron atom (Figure 2.1b), O<sub>2</sub> is dissolved purely physically in cavities between the individual molecules in case of PFCs.

Therefore, no saturation of  $O_2$  occurs and PFCs are able to dissolve more oxygen with higher oxygen pressure [9].

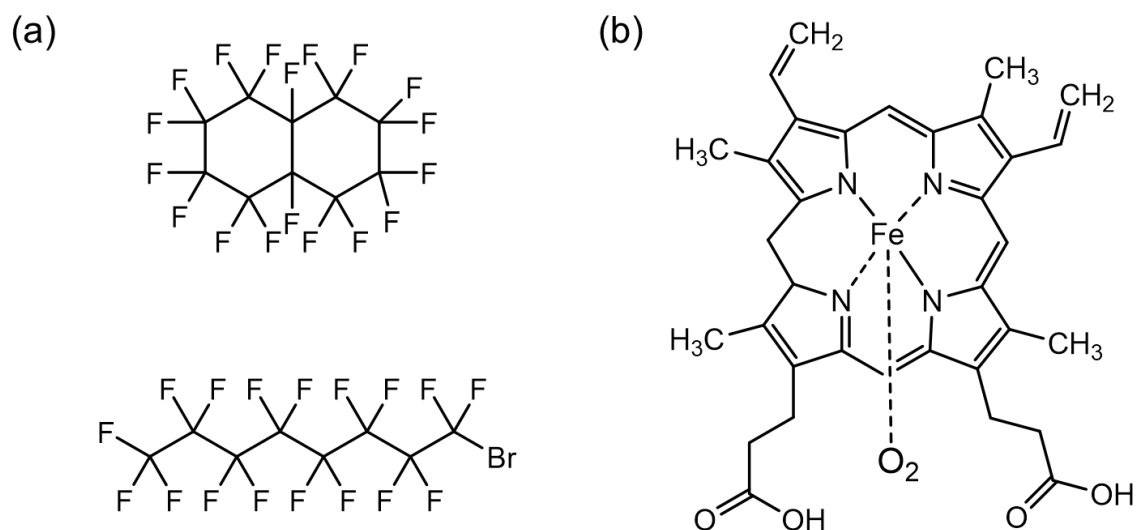


Figure 2.1 (a)The structures of two broadly used PFCs, perfluorodecalin (PFD) and perfluorooctylbromide. (b)Illustration of chemically bound of  $O_2$  to the central iron atom of hemoglobin.

Perfluorocarbons have to be emulsified or encapsulated for the use as artificial oxygen carriers due to their poor aqueous solubility. Perfluorocarbons show the unique physical property that they are both hydrophobic and lipophobic. The carbon-fluorine bond is extremely polar, but the whole PFC molecule is nonpolar because the intrinsic symmetry annuls the polarity of each carbon-fluorine bond, which lead to bad water solubility for PFCs. This extreme property prevents the formation of induced dipoles that would lead to van der Waals forces, which are essential for solubility in lipids [9]. Again, to be miscible with water, perfluorocarbons have to be emulsified or encapsulated. Therefore, both perfluorocarbon in water emulsions and perfluorocarbon filled capsules are extensively studied.

### 2.1.1 Perfluorocarbon in water emulsions

Two generations of PFC emulsions have been developed, the main differences of which include the type of emulsifier, the type of PFCs and their volume fraction [1]. The first generation emulsions include Fluosol and Oxypherol. The data were shown in Table 2.1. Toxic emulsifiers such as Pluronic-F68 was used to improve the stability of the both formulations.

Therefore, side-effects including complement activation, inhibition of leucocytes and transient hypotension were expected. Perfluorodecalin (PFD) was the main used perfluorocarbon in Fluosol, which leads to the formation of unstable emulsion due to the bad hydrophilicity and lipophilicity of perfluorodecalin. While Oxypherol was a highly stable emulsion, because perfluorotributylamine (FTBA), which has a better hydrophilicity and lipophilicity, was the only involved perfluorocarbon. The difficulties for Oxypherol were the excessively long organ retention (half-life of FTBA in the rat was about 2.5 years).

Table 2.1 Comparison between products.

Product	Formulation (%w/v PFC and %w/v surfactant)	Other additives	Mean droplet size
Fluosol	14% FDC and 6% FTPA. 2.7% Pluronic F-68, 0.4% EYP and 0.03% potassium oleate as surfactants	Sodium chloride, potassium chloride, calcium chloride, calcium bicarbonate, glycerol and dextrose	120 nm
Oxypherol	20% FTBA and Pluronic F-68 as surfactant	Krebs-Ringer bicarbonate solution	N/A
Oxygent	58% PFOB and 2% PFDB. 3.65 EYP as emulsifier	$\alpha$ -Tocopherol and EDTA, sodium chloride and a phosphate buffer	160 nm

The second generation emulsions were developed in order to overcome the difficulties in the first generation emulsions, including low stability, low oxygen carrying capacity, and side-effects from toxic emulsifiers. Oxygent is one of the famous second generation emulsions. The data were shown in Table 2.1. Egg yolk phospholipids were used as the emulsifier, which reduced the side-effects. The oxygen carrying capacity was about 4-fold larger than that of Oxypherol, because of the higher content of perfluorocarbons. The emulsions showed both good stability and acceptable organ retention because of the appropriate combination of emulsifiers and perfluorocarbon, as egg yolk phospholipids impart the emulsion electrostatic stabilization and perfluorooctyl bromide (PFOB) possessing appropriate vapor pressure can be easily exhaled.

Both generations' PFC emulsions are metastable and have a tendency to reach a complete phase separation, which is due to the fact that PFC and water are not miscible, resulting in a certain interfacial tension at the interface. Due to interfacial tension, PFC and water try to minimize the exposed interface area where they come in contact. There are two major processes which can push this decay forward [9]. The first one is coalescence, which refer to the fusion of droplets due to their contact with each other. The driving force of coalescence is the reduction of the interfacial area. Coalescence is the main reason for the poor stability of Fluosol. The possible reason is that Pluronic F68 is not sufficient to stabilize perfluorodecalin, which has very low water solubility. Charged polymeric emulsifiers may be a good choice because they can provide both electrostatic stability and steric stability for the droplets. Ostwald ripening is the other process which can lead to decay of emulsions. It happens when the PFCs has a certain solubility in water. The PFCs inside the droplet dissolves in water and transfers to larger droplets. Again, the reduction of the interfacial area in presence of surface tension is the driving force.

Encapsulating PFCs into solid capsules can avoid coalescence and Ostwald ripening, as PFC droplets are permanently encapsulated. The development of PFC filled capsules will be introduced in the following chapter.

### 2.1.2 Perfluorocarbon filled capsules

Perfluorocarbon filled capsules can also be categorized into two generations depending on the capsule wall materials. Both generations were developed by our group. Perfluorodecalin (PFD) was used as the perfluorocarbon core for both generation capsules, as it exhibits short excretion time. The data of reported perfluorodecalin filled capsules were shown in Table 2.2.

Table 2.2 Comparison between capsules filled with PFD.

Capsules	Capsule wall materials	Other additive	Mean capsule size
PLGA capsules	Poly(lactic-co-glycolic acid)	1.5 sodium cholate, or 1% PVA	1 - 8 $\mu\text{m}$
PBCA capsules	Poly(n-butyl-cyanoacrylate)	Synperonic PE/F68	200 - 400 nm
Albumin capsules	Albumin	No more additive	400 nm - 1 $\mu\text{m}$

Polypeptide capsules	Polypeptide	No more additive	100 nm – 2 $\mu$ m
----------------------	-------------	------------------	--------------------

Synthetic polymers were used as shell materials in the first generation capsules, including poly(lactic-co-glycolic acid) (PLGA) and poly(n-butyl-cyanoacrylate) (PBCA). PLGA capsule walls not only show a mechanical stability comparable to that of red blood cells, but also have sufficient permeability to allow oxygen exchange in an aqueous environment [2]. By coating with poly(ethylene glycol) PEG and stabilizing with 1% poly(vinyl alcohol) PVA, PLGA capsules exhibited a circulatory half-life of about 1 h [10]. However, severe side effects such as organ damage and hypotension occurred after intravenous infusion of large amounts of PFD-filled PLGA capsules [5]. PBCA capsules were much smaller than (150–200 nm) PLGA capsules (1-8  $\mu$ m), and their dispersions showed good oxygen carrying capacities when PFD volume reached 24%, which is about half of the capacity of human blood [3]. However, several undesired side effects were observed such as a transient decrease in systemic blood pressure, impairment in hepatic microcirculation, organ damage and elevation of plasma enzyme activities [6].

The second generation capsules were developed in order to improve the biocompatibility of the first generation capsules. Therefore, only biocompatible materials such as albumin and polypeptide were used as capsule wall materials. Albumin-derived perfluorodecalin filled nanocapsules not only showed a remarkable maximum oxygen capacity, but also were proved lacking severe side-effects after *in vivo* administration [4]. These albumin nanocapsules were also capable to protect a Langendorff heart (rat) during massive ischemia [11]. Synthetic polypeptides, as synthetic analogues of proteins, contain the same amino acid building blocks as proteins, but allow for the adjustable properties which are not possible with natural proteins. Therefore, PFD filled polypeptide capsules were studied by our group in the past three years. Those polypeptide capsules also showed a certain mechanical stability and have enough permeability to allow oxygen exchange in an aqueous environment (unpublished results). The study of PFD filled polypeptide capsules will be presented in detail in this thesis.

### 2.2 Polypeptide synthesis

Polypeptides are long chains of amino acids (normally over 20 amino acids) linked by peptide

bonds (amide bonds). The chains of less than 20 amino acids are called oligopeptides which include dipeptides, tripeptides and tetrapeptides. The specific arrangement of amino acids in polypeptide chains can be called the primary structure of polypeptide (Figure 2.2). The amide bond contains both a hydrogen bond donor (N-H) and a hydrogen bond acceptor (C=O). There is limited bond rotation in the amide bond due to resonance between the carbonyl and amine functional groups, so higher ordered secondary structures ( $\alpha$ -helix,  $\beta$ -strand, and random coil conformation) can form via H-bonds by interaction of amide bonds in a polypeptide chain (Figure 2.2). The combination of secondary structure motifs and side-chain interactions contribute to a higher tertiary structure and quaternary structure of proteins (Figure 2.2) [12].

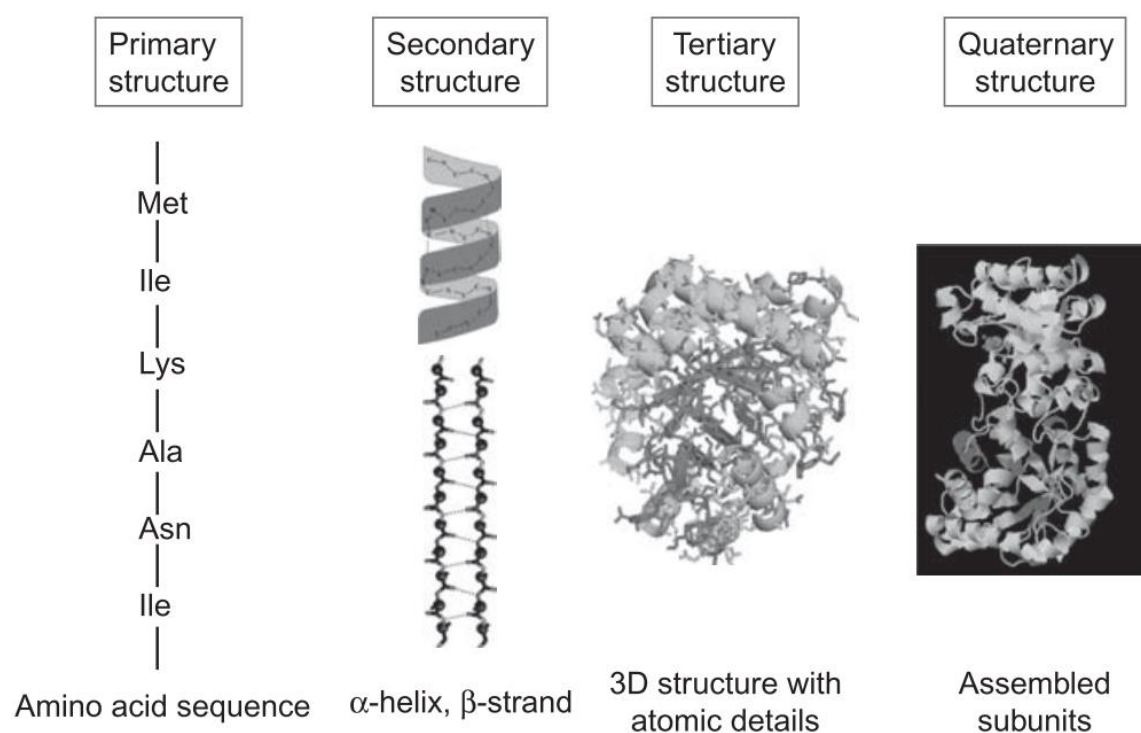
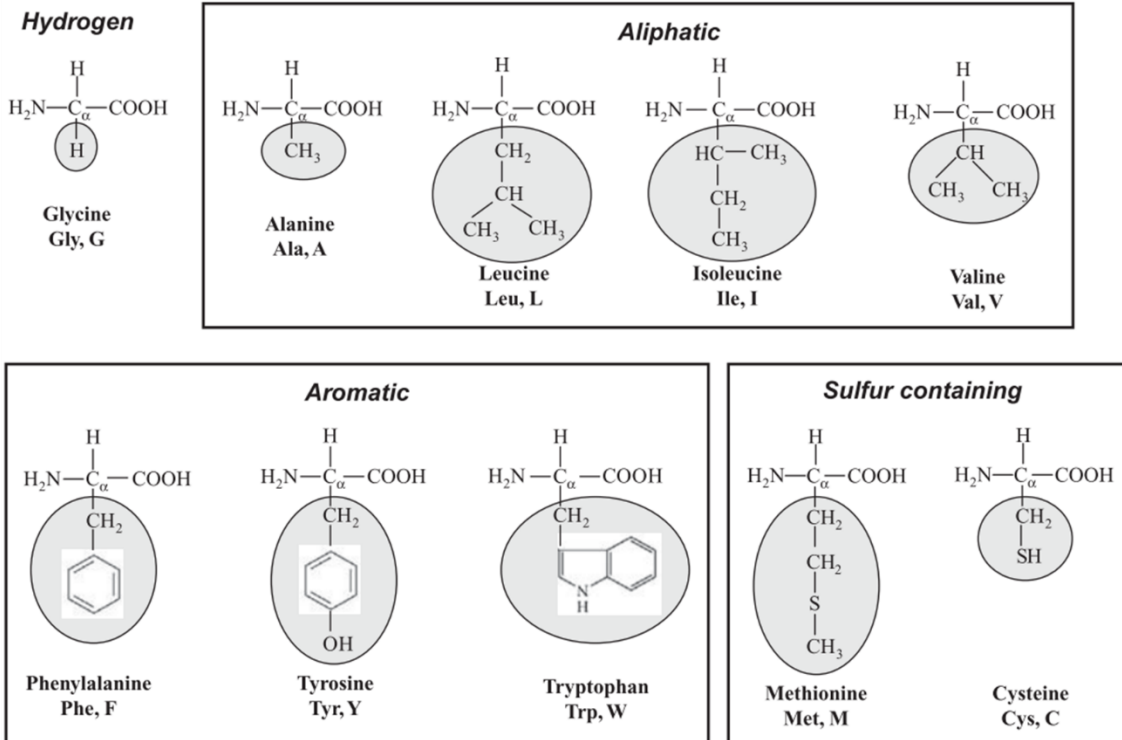


Figure 2.2 Structural organization of proteins [12].

The variable part of an amino acid which forms the side chain in the peptide is called residue. It is known that more than 500 naturally occurring amino acids constitute residues in peptides. Among these 500 amino acids, only 20 appear in human proteins, all of which are  $\alpha$ -amino acids. Except for glycine, all of the 20 natural  $\alpha$ -amino acids adopt the same stereochemistry (levorotary, L-configuration). All the 20 natural  $\alpha$ -amino acids differ from their side chains (Figure 2.3 ). Some of them can contain nonpolar and hydrophobic groups such as L-phenylalanine, while others can contain polar and hydrophilic groups such as L-aspartate and

L-cysteine. Some side chain functional group can even form covalent bond connection between each other, like cysteine and tyrosine. Many amino acids adopt specific secondary structures when they form a homopolymer. For example, poly(L-cysteine) and poly(L-glycine) adopt stable  $\beta$ -sheet conformations in the solid state. Whereas, poly( $\beta$ -benzyl-L-aspartate) and poly(L-phenylalanine) prefer to adopt  $\alpha$ -helical structures [13].

## Hydrophobic residues



## Hydrophilic residues

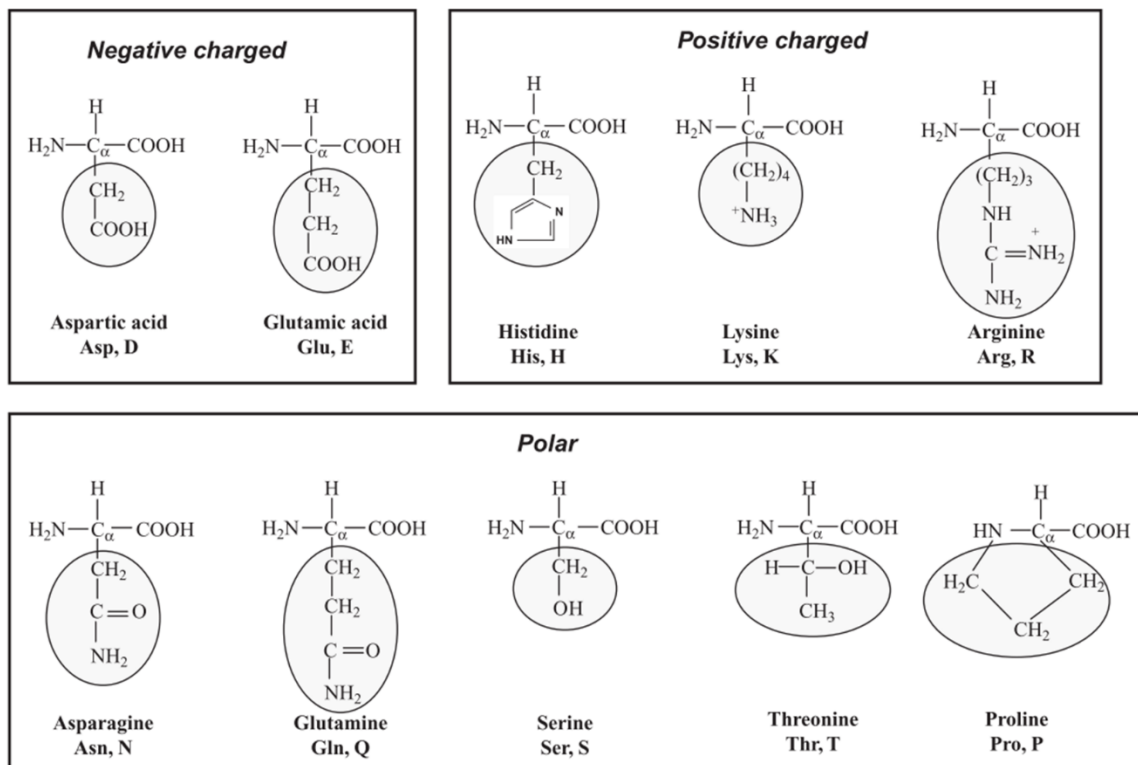


Figure 2.3 The common 20 amino acids. The three- and one-letter codes for the amino acids are also given. The amino acids are classified into hydrophobic (hydrogen,

aliphatic, aromatic, and sulfur containing) and hydrophilic (negatively charged, positively charged, and polar). The side chains are marked with oval boxes [12].

These varied structural properties of polypeptides have drawn a great deal of attention from chemists. Currently, there are mainly three types of methods for peptide synthesis: solid phase peptide synthesis (SPPS) [14], recombinant DNA methods [14], and polymerization of activated amino acid monomers [15].

The first method is solid phase peptide synthesis (SPPS) (Figure 2.4). The SPPS process starts by coupling the first  $N_\alpha$ -protected amino acid to an insoluble resin, then deprotecting the  $\alpha$ -amine protecting group with dilute acid (when Boc is used as  $\alpha$ -amine protecting group) or base (when Fmoc is used as  $\alpha$ -amine protecting group) to create a free amine end. Then the second  $N_\alpha$ -protected amino acid could be coupled to the regenerated amine and again the active free amine end can be created by deprotection of the amine-protecting group. The desired polypeptide sequence can be fully synthesized by repeating the above coupling and deprotection reaction. Finally, harsh acidic conditions such as anhydrous HF or  $\text{CF}_3\text{SO}_3\text{H}$  are used for both the resin cleavage and side-chain deprotection. Polypeptides synthesized through SPPS have controlled primary sequences and can fulfill certain functionality, but it is difficult to create high molecular weight polypeptides above 100 residues due to the inevitable side reactions [16].

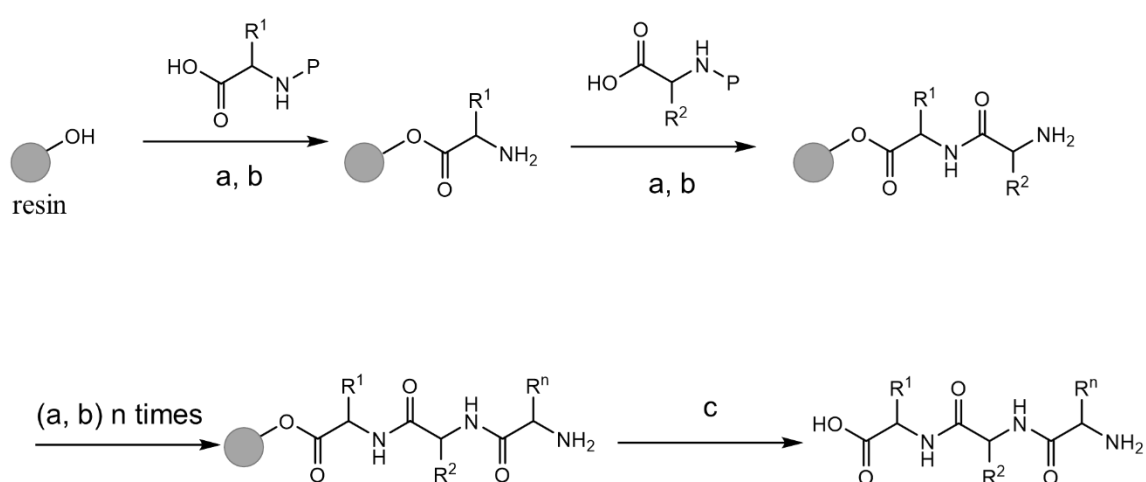


Figure 2.4 Solid-phase peptide synthesis: (a) coupling, (b) deprotection, (c) cleavage from resin. P = protecting group e.g. 9-fluorenylmethoxycarbonyl (Fmoc) or tert-butylcarbonyl (Boc).  $R_1$ ,  $R_2$ ,  $R_n$  = peptide side chains. Reproduced according to reference [14].

The second method is the so-called recombinant DNA technique (Figure 2.5). The process begins with the selection of the desired polypeptide sequence, which is then translated into a DNA sequence. The target DNA sequence is next synthesized chemically and integrated into an *Escherichia coli* plasmid vector. The complete plasmid is then transfected into *Escherichia coli* and is expressed to produce the designed polypeptide. The advantage of this method is that it can create polypeptide with specific sequences and high molecular weight. Moreover, it allows for a peptide production on a very large scale.

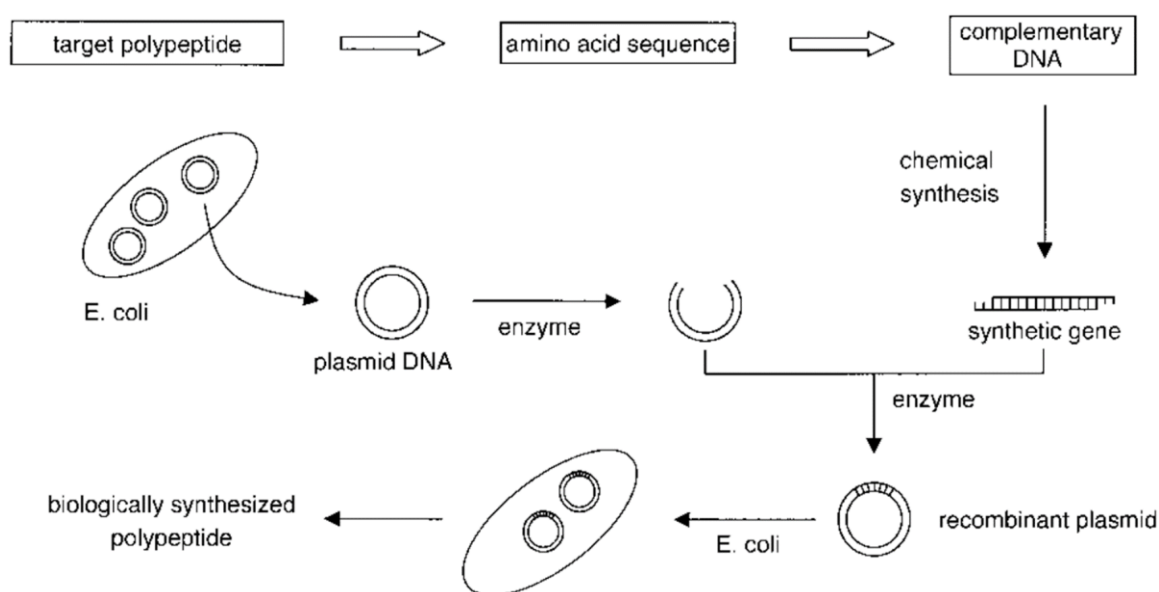


Figure 2.5 Recombinant DNA technique to synthesize polypeptides [14].

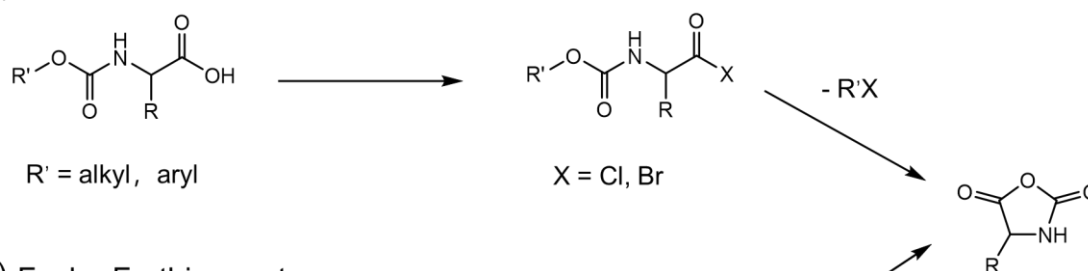
The last method is polymerization of activated amino acid monomers [17], including amino acid N-carboxyanhydrides (NCAs) [18] and N-phenoxy carbonyl amino acids (NPCs) [19]. The process begins by converting amino acids into the correspond activated monomers. Subsequently, polymerization is initiated in the presence of certain initiators. Through polymerization, one can synthesize polypeptides with large molecular weight and narrow polydispersity (PD). The specific history and mechanism of polypeptide synthesized from polymerization can be found in the following sections.

### 2.2.1 Ring-opening polymerization (ROP) of $\alpha$ -amino acid N-carboxy anhydrides (NCAs)

ROP of NCA of  $\alpha$ -amino acid is currently the most common method for the synthesis of polypeptides. During 1906 and 1908, Hermann Leuchs published three papers that described

the synthesis and properties of  $\alpha$ -amino acid N-carboxyanhydrides (NCAs; Figure 2.6a). NCAs were discovered by coincidence when Leuchs attempted purification of N-ethoxycarbonyl  $\alpha$ -amino acid chlorides. However, Leuchs changed his area of research completely from NCAs to the chemistry of strychnine alkaloids since 1907 due to the lack of proper analytical methods for NCA-polymerized products and the wrong estimation of their structure. As a result of his pioneering work, NCAs are commonly referred to as Leuchs' anhydrides [13].

(a) Leuchs route:



(b) Fuchs-Farthing route:



Figure 2.6 (a) Leuchs method to synthesize NCAs, (b) Fuchs-Farthing method to synthesize NCAs.

Presently, the most important and economical method for synthesizing NCAs is called Fuchs-Farthing method in which phosgene or its derivatives are used as a cyclizing agent (Figure 2.6b). In 1922, Friedrich Fuchs described the preparation of NCA of N-phenylglycine by phosgenation of N-phenylglycine in aqueous solution. Based on Fuchs' reaction, A. C. Farthing made some modifications and prepared some other NCAs such as NCAs of glycine, DL- $\beta$ -phenylalanine, L-leucine, etc. in 1950 [20]. Using this system, it is typical to prepare an NCA by the reaction of an  $\alpha$ -amino acid with phosgene in ethyl acetate (also tetrahydrofuran and dioxane) at elevated temperatures (60 °C) under inert atmosphere.

The ring opening polymerization (ROP) of NCAs could produce 'living' polypeptides. The expression "living polymers" was first described by M. Szwarc in 1956 when he tried to synthesize polystyrene by polymerization of styrene [21]. The term "living" mainly means that when the polymerization is terminated either by 100% conversion of the monomers, by cooling,

or by precipitation, the reactive end group responsible for chain growth remains unchanged (alive). In this way, polymers with controlled length and low polydispersity can be prepared. Moreover, it is also possible to form block copolymers by sequential addition of different monomers.

A suitable initiator is essential for polymerization of NCAs. Because of the numerous reactive sites on the five-membered NCA ring, i.e. the 2- and 5-carbonyl groups, 3-NH and 4-CH, there is a wide range of initiators available to initiate NCA polymerizations, e.g., protonic nucleophiles, nonprotonic bases, metal salts, organometallics, transition metals and their analogues of strong-bases [17, 18]. Primary amines are presently one of the most common initiators for the ROP of NCAs because of the following two reasons. Firstly, using primary amines as initiator could prepare polypeptides with a living end group (amino group). Secondly, the highly nucleophilic and sterically unhindered nature of primary amines allows them to initiate polymerization rapidly, resulting in smaller polydispersity values [13]. One possible mechanism of primary amines initiated ROP of NCAs is shown in Figure 2.7. The polymerization involves three steps of carbonyl addition, ring opening and decarboxylation. In a first step, a nucleophilic primary amine bearing a lone pair of electrons attacks the C<sub>5</sub> carbon of the NCA to initiate ring opening. This is followed by a decarboxylation step and regeneration of the amine. Finally, the regenerated amine attacks the molecule of another NCA to increase the length of the polypeptide chain. This pathway allows for the synthesis of co-polypeptides with several different blocks, with defined terminal structures and with narrow polydispersities [13].

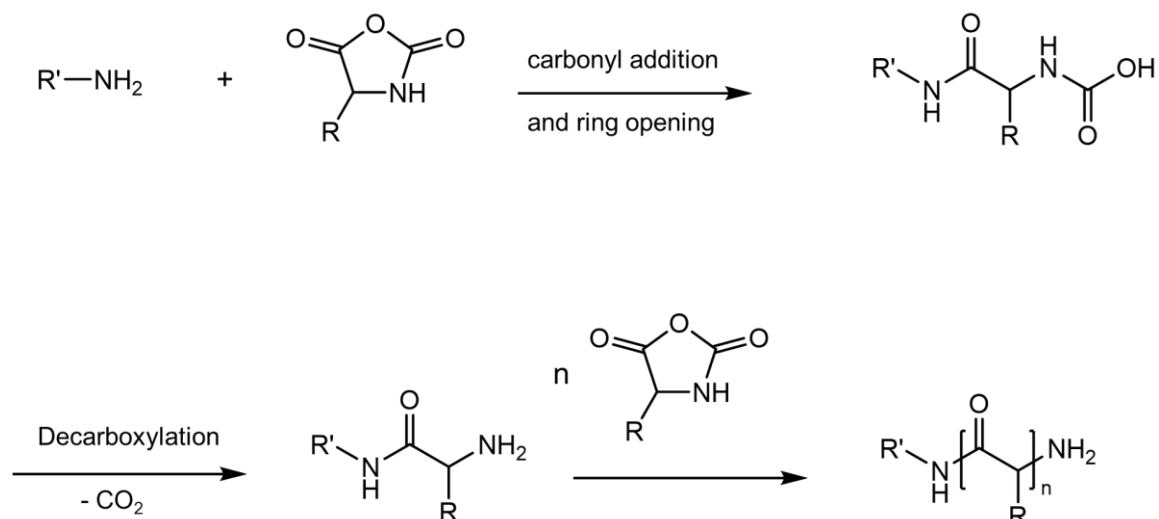


Figure 2.7 Mechanism of primary amines initiated ROP of NCAs.

However, there are two main drawbacks that limit the use of NCA on an industrial scale. Firstly, with phosgene or its derivatives, very poisonous educts are needed for the synthesis of NCA. Secondly, the storage of NCA is very difficult due to its sensitivity to moisture and heat. Thus, alternative monomers for the large scale synthesis of polypeptides have been extensively studied these years.

### 2.2.2 Polymerization of N-phenoxy carbonyl amino acid (NPCs)

NPCs are promising alternative monomers due to the fact that they are tolerant to moisture and heat and their synthesis does not require the use of phosgene derivatives [19]. Inspired by Kricheldorf's synthesis of polyamides using the monomer  $R$ -( $N$ -aryloxy carbonyl)amino- $\omega$ -carboxylalkane, in 2008, Endo et al. first synthesized several amino acid NPCs and studied their polymerization [22, 23]. NPCs are also called amino acid urethane derivatives (UDs) if hydrogens at the phenoxy group of NPC are substituted. Two routes are mainly used to prepare NPCs. One is by reaction between amino acids and phenol chloroformate. The other one is by reaction between amino acids and diphenyl carbonate (DPC) in the presence of an excess base ( $Et_3N$  or tetrabutylammonium hydroxide) (Figure 2.8). Using these two methods, Endo's group prepared a large variety of NPCs during these ten years and proved that NPCs promising alternatives for polypeptide synthesis [19].

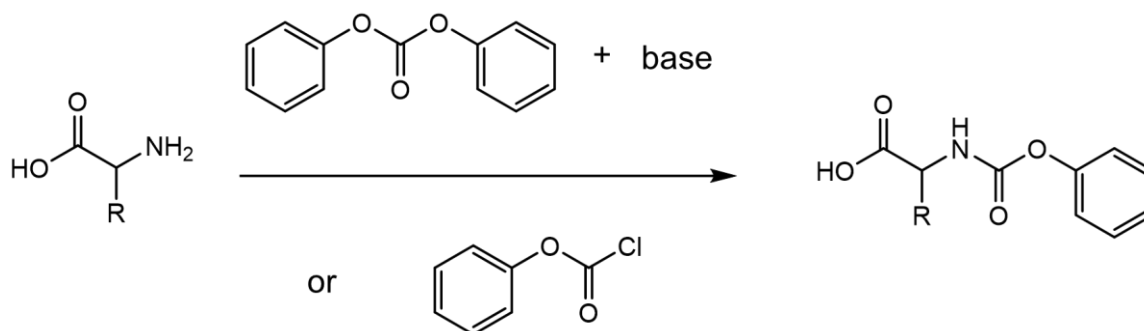


Figure 2.8 Synthetic methods to prepare NPC monomers

The controlled polymerization of these NPCs can be achieved by reaction in DMAc solution at 60°C with primary amine as initiator, which can form polypeptides with predictable MW and narrow MW distribution (less than 1.2). The described polymerization may follow the same mechanism as NCAs' polymerization because they observed the in situ formation of NCAs by  $^1\text{H}$  NMR before and during the polymerizations (Figure 2.9) [19].

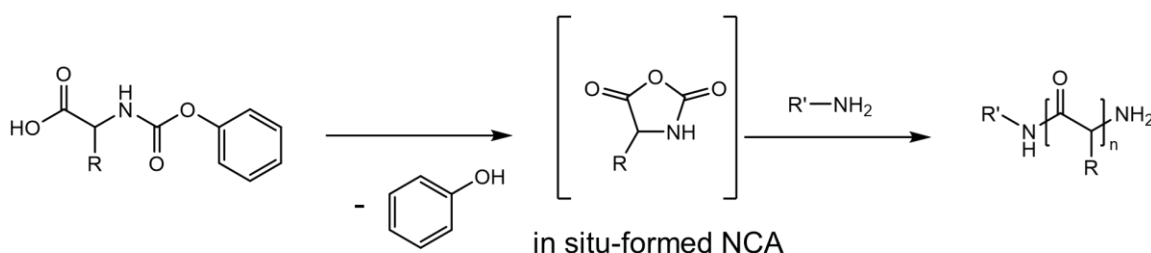


Figure 2.9 Synthesis of polypeptides by polymerization of NPCs.

### 2.3 Perfluorodecalin-filled polypeptide capsules

Micro- and nanocapsules are colloidal particles that are formed by a shell-like wall with a liquid content according to a general and widely accepted classification of nanoparticles, and they can be prepared by four principally different approaches according to a previous review: interfacial polymerization, interfacial precipitation, interfacial deposition, and self-assembly procedures [24]. The preparation of polypeptide nanocapsules can also be grouped into the above strategies [25]. The preparation of perfluorodecalin filled polypeptide capsules in this thesis consists of two stages. In the first stage, amphiphilic polypeptide molecules are accumulated at the interfaces of PFD and water to give a metastable emulsion. In the second stage, the cysteine units of polypeptides are oxidized to form disulfide bridges to solidify the

self-associated structure and to yield a solid polypeptide membrane.

The size of the capsules depends on the size of the emulsion droplets formed in the first stage, which is related to the emulsify ability of emulsifiers and input energy. The mechanical strength of the capsules depends on the amount of free thiol groups in cysteine block that can undergo cross-linking. Therefore, polypeptide emulsifier related to emulsion formation and polycysteine related to crosslink of capsule structure are introduced in detail in the follow sections.

### 2.3.1 Polypeptide surfactants

Emulsions are mixture of two or more immiscible liquids with the interface stabilized by surfactants [26]. The emulsion does not form spontaneously when the oil phase, water and surfactant are mixed together. A new interfacial area with an interfacial tension can be created by applying energy into the mixture, typically in the form of stirring or ultra-sonication. In order to create small droplets, these shear forces need to overcome the additional Laplace pressure on the surface of the original parent droplets according to the following equation.

$$P = 2\gamma/R \quad \text{Equation 2.1}$$

where  $\gamma$  is interfacial tension,  $R$  represents the droplet radius.

Surfactants can improve the stability of emulsions by reducing interfacial tension and by inhibiting droplet coalescence. Surfactants are amphiphilic molecules with a polar hydrophilic part covalently connected to a hydrophobic part. There are various types of surfactants, most of which can be categorized into small molecule surfactants and polymeric surfactants. Most small molecule surfactants consist of a long chain hydrophobic tail and hydrophilic head groups, such as phospholipids and sodium dodecyl sulfate (SDS). Polymeric surfactants are one class of amphiphilic molecules which have longer hydrophilic and hydrophobic domains than small molecule surfactants. The longer hydrophilic segments provide additional steric stabilization compared to small molecule surfactants, while the hydrophobic tails allow for better anchoring on the oil phase.

Amphiphilic block polypeptide surfactants containing hydrophilic and hydrophobic amino acid fragments are a new class of polymeric surfactants that have been intensively studied in recent

years. Hanson et al. reported polydimethyl siloxane (PDMS) in water emulsions stabilized by block copolypeptide surfactants, poly(L-lysine-HBr)<sub>60</sub>-b-poly(L-leucine)<sub>20</sub> (K<sub>60</sub>L<sub>20</sub>) [27]. Their emulsions are stable in storage for over one year, showing no sign of coalescence or Ostwald ripening. They demonstrated that high content of hydrophilic block is essential for stabilization of oil in water emulsion, as K<sub>60</sub>L<sub>20</sub> is soluble in water and therefore can be present in high concentrations in the solution to effectively stabilize the exposed oil surface formed during emulsification.

The concept of the hydrophilic-lipophilic balance (HLB) can be referred to when designing polypeptide surfactants. This parameter is a measure of the degree of hydrophilicity or lipophilicity of a surfactant and gives a better understanding of which types of emulsions can be stabilized by a particular surfactant. According to Griffin, HLB of surfactants was described as follows:

$$\text{HLB} = 20 \times \frac{M_h}{M} \quad \text{Equation 2.2}$$

where  $M_h$  is the molecular mass of the hydrophilic part of the molecule, and  $M$  is the molecular mass of the total molecule, which gives an HLB value from 0 to 20. An HLB value of 0 corresponds to a completely lipophilic molecule, and a value of 20 corresponds to a completely hydrophilic molecule. Surfactant with small HLB value between 3 and 6 has a larger percentage of lipophilicity and would be preferentially dissolved in an oil phase, stabilizing the water-in-oil (WO) emulsion. On the other hand, a surfactant with large HLB value between 10 and 16 will preferentially dissolve in the aqueous phase, which usually stabilizes the oil-in-water (OW) emulsion. Therefore, if poly(L-aspartate)<sub>m</sub>-b-poly(L-phenylalanine)<sub>n</sub> was chosen to be the surfactant to stabilize PFD in water emulsions and the number of the repeat units of hydrophilic amino acid aspartate was set to 40, we can roughly expect a range of about 8 to 30 repeat units of hydrophobic amino acid phenylalanine according to the HLB values.

### 2.3.2 Polycysteine

L-cysteine is a naturally occurring amino acid with a thiol group in the side chain. Its homopolymer [i.e., poly(L-cysteine)] exclusively forms  $\beta$ -sheet structures [13]. Peptides

containing a cysteine will form disulfide bonds in the presence of air and the oxidation is even faster under basic conditions [16]. The disulfide form of cysteine is referred to as cystine. The conversion of sulfhydryl to disulfide bonds is reversible, and the addition of a reducing agent converts the disulfide bonds to thiol groups (Figure 2.10) [16].

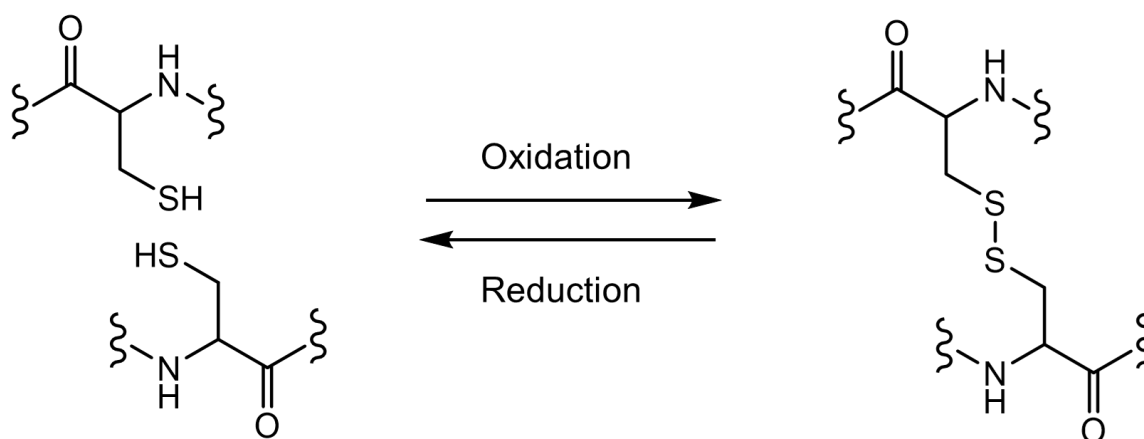


Figure 2.10 Cysteine undergoes facile oxidative dimerization to form cysteine disulfide crosslinks. Reducing conditions can readily convert cystines back into the free thiol-based cysteines [16].

Therefore, by using amphiphilic polypeptide surfactants containing cysteine units, not only oil in water emulsions can be prepared, but also capsules with certain mechanical strength can be obtained by forming disulfide bonds between polypeptide surfactants on the surface of the oil droplets. In this subsection, the main properties of polycysteine, including pH-sensitive aqueous solubility and oxidative properties, will be described in detail.

Polycysteine is soluble in alkaline aqueous solution when the pH value is over 8.0, but is insoluble in alkaline aqueous solution when the pH value is below 8.0 [28]. This is due to an equilibrium of two forms of sulfhydryl groups including thiol form (-SH) and thiolate form (-S<sup>-</sup>) which is influenced by pH value. In basic solution with pH value over 8, most of the sulfhydryl groups are present in thiolate form (-S<sup>-</sup>), which makes the polycysteine soluble in water. However, when the pH value is lower than 8, most of the sulfhydryl groups are present in thiol form, which reduces the water solubility of polycysteine.

When polycysteine is dissolved into water, an acid dissociation equilibrium occurs as shown in the following:



The acid dissociation constant ( $K_a$ ) is a measure of the degree of dissociation of an acid in solution. For thiol groups, we get:

$$K_a = \frac{[\text{H}^+] \times [\text{S}^-]}{[\text{SH}]} \quad \text{Equation 2.4}$$

Where [ ] denotes concentration in mol/dm<sup>3</sup>. The parameter  $pK_a$  is a number that indicates how strong or weak an acid is. The relationship between  $pK_a$  and  $K_a$  is given in the following equation:

$$pK_a = -\log(K_a) \quad \text{Equation 2.5}$$

Or, conversely,

$$K_a = 10^{-pK_a} \quad \text{Equation 2.6}$$

The  $pH$  scale is logarithmic and inversely indicates the concentration of hydrogen ions  $[\text{H}^+]$  in the solution. The relationship between  $pH$  and  $[\text{H}^+]$  is described by the following equation:

$$pH = -\log([\text{H}^+]) \quad \text{Equation 2.7}$$

Or, conversely,

$$[\text{H}^+] = 10^{-pH} \quad \text{Equation 2.8}$$

After combination of equation Equation 2.4, Equation 2.6, Equation 2.8 and rearrangement of them, the ratio of between thiol group ( $-\text{SH}$ ) and thiolate group ( $-\text{S}^-$ ) can be calculated as following:

$$\frac{[-S^-]}{[-SH]} = \frac{K_a}{[H^+]} = 10^{pH-pK_a} \quad \text{Equation 2.9}$$

The pKa value for the thiol group in cysteine is around 8.2. One can calculate the ratio between thiol group and thiolate group if given a pH value according to Equation 2.9. For example, if the pH value is 8.2, the concentration of thiol group and thiolate group will be same. In this case, polycysteine has both the same amount of hydrophilic thiolate groups and hydrophobic thiol groups, and this amount of thiolate groups are enough to impart the polycysteine a good water solubility. If the pH value is 9.2, the concentration of thiolate group will be ten times larger than that of thiol group. In this case, polycysteine shows very good solubility in water. If the pH value is 7.2, the concentration of thiol group will be ten times larger than that of thiolate group. In this case, the solubility of polycysteine in water will decrease, and it even becomes insoluble in water. Therefore, polycysteine solutions are pH sensitive. By adjusting the pH, we can assign polycysteine different degrees of hydrophobicity and hydrophilicity.

Polycysteine in aqueous solution is easily oxidized by hydrogen peroxide or by air in the presence of cupric ions. The oxidation product will precipitate from the basic aqueous solution and is insoluble in the common organic solvents. It presumably consists of a 3-dimensional network cross linked by disulfide bridges and its elemental composition corresponds to that of polycystine [28].

### 2.4 Studying molecules' structure and diffusion properties by nuclear magnetic resonance (NMR)

Nuclear magnetic resonance spectroscopy is suitable to study static properties of the matter (i.e. its structure) as well as dynamic properties like rotational diffusions and lateral diffusions [29] [30]. In the following section, the basics of NMR spectroscopy will be introduced because it is one of the most important method used in this thesis.

#### 2.4.1 Principle of NMR spectroscopy

The principle of NMR usually involves three sequential steps: 1) generating a net magnetic

moment in a large, constant magnetic field  $B_0$ . 2) rotating the direction of the net magnetic moment by a weak oscillating magnetic field  $B_1$ , hereby producing a transverse magnetic moment. 3) detecting and analyzing the small electromagnetic radiation induced by the precession of the transverse magnetic moment.

### 2.4.1.1 Generation of a net magnetic moment

Each atomic nucleus has four important physical properties, including mass, electric charge, magnetism and spin[31]. Among them, magnetism and spin are two physical properties that are closely related to NMR. The magnetism of a nucleus implies that the nucleus can interact with a magnetic field, like a small bar magnet. The spin of a nucleus indicates that, very loosely speaking, the atomic nucleus behaves as if it is rotating in space like a tiny planet.

The spin angular momentum  $\vec{S}$  and intrinsic magnetic moment  $\vec{\mu}$  are closely linked:

$$\vec{\mu} = g \frac{q}{2m} \vec{S} = \gamma \vec{S} \quad \text{Equation 2.10}$$

where  $\gamma$  is the gyromagnetic ratio,  $g$  is a dimensionless number called the  $g$  factor,  $q$  is the charge, and  $m$  is the mass. Both spin angular momentum and magnetic moment are vectors and they have the same or opposite direction, depending on the value of  $\gamma$ . For proton,  $\gamma$  is  $+2.67522 \times 10^8 \text{ rad s}^{-1} \text{ T}^{-1}$  and therefore the direction of the spin angular momentum is the same as the direction of the magnetic moment.

Both values and directions of spin angular momentum and magnetic moment are quantized. The values of them are determined by the spin quantum number  $I$ , and follow the following equations:

$$|\vec{S}| = \sqrt{I(I+1)} \cdot \hbar \quad \text{Equation 2.11}$$

$$|\vec{\mu}| = \gamma \cdot \sqrt{I(I+1)} \cdot \hbar \quad \text{Equation 2.12}$$

## 2 Theoretical background

---

Where  $I = 0, \frac{1}{2}, 1, \frac{3}{2}, 2 \dots 6$ , and  $\hbar$  stands for the reduced Planck constant ( $\hbar = \frac{h}{2\pi}$  and  $h = 6.6256 \cdot 10^{-34} \text{Js}$ )

The components along magnetic field of spin angular momentum and magnetic moment, which corresponds to their directions, are determined by magnetic quantum number  $m$ , and follow the following equations:

$$|\vec{S}_z| = m \cdot \hbar \quad \text{Equation 2.13}$$

$$|\vec{\mu}_z| = \gamma \cdot m \cdot \hbar \quad \text{Equation 2.14}$$

Where  $m = -I, -I + 1 \dots I - 1, I$ . In consequence, there will be  $2I + 1$  magnetic quantum numbers for one spin quantum number  $I$ .

In the following, we will combine spin angular momentum and magnetic moment together as spin for simplicity because they are always come together. For nucleus with spin quantum number  $I = \frac{1}{2}$  such as  $^1\text{H}$ ,  $^{13}\text{C}$ ,  $^{19}\text{F}$ ..., there are two possible directions of spin as shown in Figure 2.11.

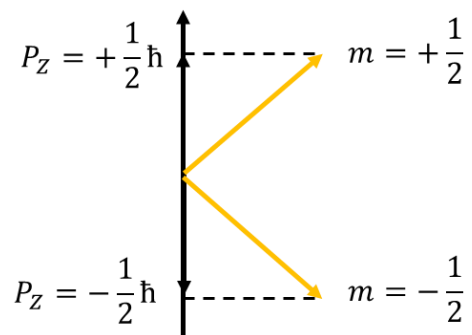


Figure 2.11 Two possible directions of spin and its z-component.

One is parallel to the magnetic field with an angle of  $54^\circ 44'$ . The other one is antiparallel to the magnetic field (with an angle of  $-54^\circ 44'$ ). The energies of these two directions of spin, which is also being called Zeeman energy levels, are shown in the following equation:

$$E_{\alpha} = -\frac{1}{2} \cdot \gamma \cdot \hbar \cdot B_0 \quad \text{and} \quad \text{Equation 2.15}$$

$$E_{\beta} = \frac{1}{2} \cdot \gamma \cdot \hbar \cdot B_0$$

Where  $E_{\alpha}$  corresponds to the energy of spin that parallels to the magnetic field, which also be called  $\alpha$  state spin.  $E_{\beta}$  corresponds to the energy of spin that antiparallels to the magnetic field, which also be called  $\beta$  state spin.  $B_0$  stands for the value of the external magnetic field. The energy difference between the two spin states is therefore equal to

$$\Delta E = \gamma \cdot \hbar \cdot B_0 \quad \text{Equation 2.16}$$

Spin exhibits two forms of motions. One is precession. Spin moves like a child's spinning top but keep a constant angle of  $54^{\circ}44'$  or  $-54^{\circ}44'$  between the spin and the field as shown in Figure 2.12a.

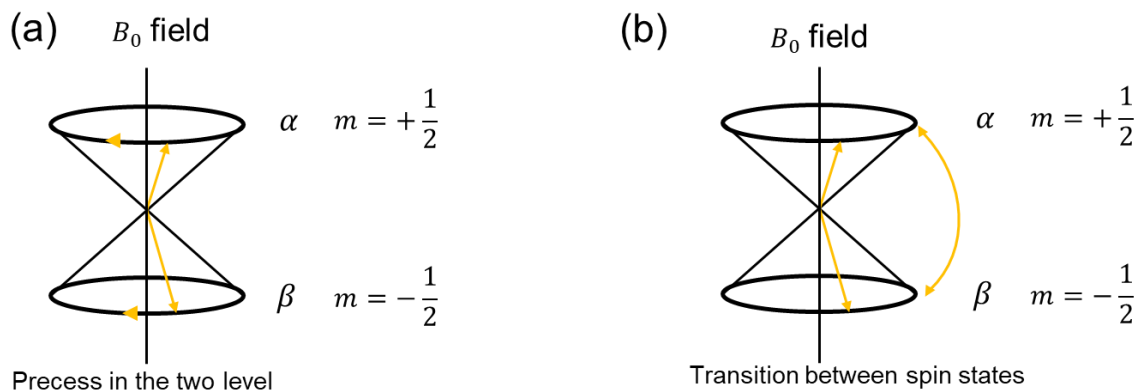


Figure 2.12 (a) Precession of spins. (b) transition between spin states.

The frequency of precession  $\omega_0$  is equal to

$$\omega_0 = \gamma B_0 \quad \text{Equation 2.17}$$

where  $\omega_0$  is the angular frequency.

The other form of motion of the spin is flipping. The spin can undergo transitions between the two states as shown in Figure 2.12b. The transition of spins from  $\alpha$  state to called  $\beta$  state will absorb energy from the surrounding environment, and transition of spins from  $\beta$  state to  $\alpha$  state will release energy to the surrounding environment. Initially, the numbers of the spins at different states are the same. Later, spins at  $\alpha$  state will exceed spins at  $\beta$  state when the spin system reach to a thermal equilibrium, because the transition rates from one state to another state are different. The number distribution of spins at the two different states satisfies Boltzmann distribution:

$$\frac{N_\alpha}{N_\beta} = e^{-\frac{\Delta E}{k_B T}} \approx 1 - \frac{\Delta E}{k_B T} = 1 - \frac{\gamma \hbar B_0}{k_B T} \quad \text{Equation 2.18}$$

Where  $k_B$  is Boltzmann constant and  $T$  is the temperature.

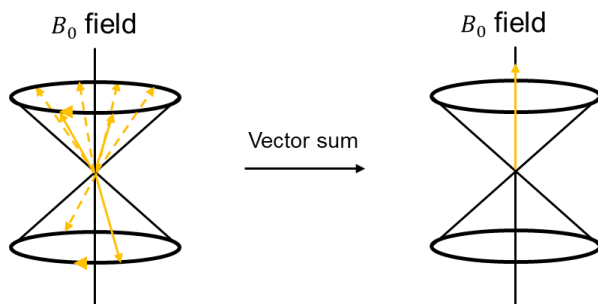


Figure 2.13 Thermal equilibrium.

The small excess of  $\alpha$  state spins contribute to a net magnetic moment ( $\vec{M}_{eq}$ ) along the magnetic field. This net magnetic moment can be used for the observation of NMR signals (Figure 2.13). The energies of spins are released to the surrounding environment during the formation of the net magnetic moment. Therefore, this process is also being called spin-lattice relaxation, longitudinal relaxation or  $T_1$  relaxation.

#### 2.4.1.2 Production and precession of transverse magnetic moment

$\vec{M}_{eq}$  can be progressively tipping away from its initial alignment with  $\vec{B}_0$ , if an oscillating magnetic field  $B_1$  perpendicular to  $\vec{B}_0$  with a frequency equal to the Larmor frequency of the precession of the spin is applied to the sample. This temporary  $B_1$  field is called a radio

frequency (r.f.) pulse.  $\vec{M}_{eq}$  can be rotated by  $22^\circ$ ,  $90^\circ$ ,  $361^\circ$ ,  $521^\circ$ , or any other amount. After every  $360^\circ$  rotation,  $\vec{M}_{eq}$  returns to its initial alignment with  $\vec{B}_0$ . In the following, let's take a look at the influence of  $90^\circ$  pulse on the individual spins for an example.

When a  $90^\circ$  pulse is applied to the sample, the direction of  $\vec{M}_{eq}$  is transferred from a direction along z-axis ( $\vec{B}_0$  direction) to a direction along the  $-y$ -axis as shown in Figure 2.14 a. Two changes of the individual spins take place after the  $90^\circ$  pulse as shown in Figure 2.14 b. One is that more spins at  $\alpha$  state will absorb energy to transition into  $\beta$  state, which leads to an equal distribution between the two states. The other change is that spins at both states will experience the same phase. These two changes together contribute to the net transverse magnetic moment.

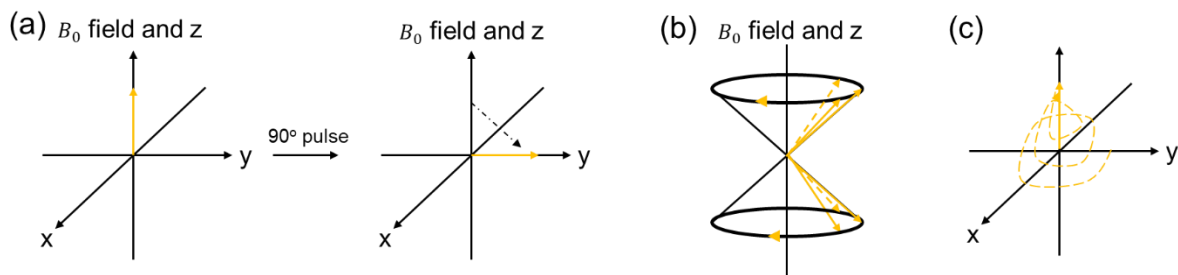


Figure 2.14 (a) Direction of  $M_{eq}$  after a pulse. (b) Direction of every one nuclear spin after a pulse. (c) Precession of the transverse magnetization.

When the  $90^\circ$  pulse is turned off,  $\vec{M}_{eq}$  will progressively recover to z-axis from  $-y$ -axis. This is achieved by two separated relaxation process which is just the opposite way of producing net transverse magnetic moment as shown in Figure 2.14 c. One is the longitudinal relaxation due to the flipping of spins from  $\beta$  state to  $\alpha$  state. The other one is the transverse relaxation. Spins gradually get out of phase with each other due to slightly fluctuating microscopic magnetic fields in the sample.

The transverse magnetic moment at a time  $t$  after the pulse has the form

$$M_y = -M_{eq} \cos(\omega_0 t) \cdot e^{-t/T_2} \quad \text{Equation 2.19}$$

$$M_x = M_{eq} \sin(\omega_0 t) \cdot e^{-t/T_2}$$

where  $T_2$  denotes the so-called transverse relaxation time, or spin-spin relaxation time. The transverse magnetic moment precesses at the nuclear Larmor frequency  $\omega_0$ , slowly decaying at the same time according to the spin-spin or transverse relaxation as shown in Figure 2.15.

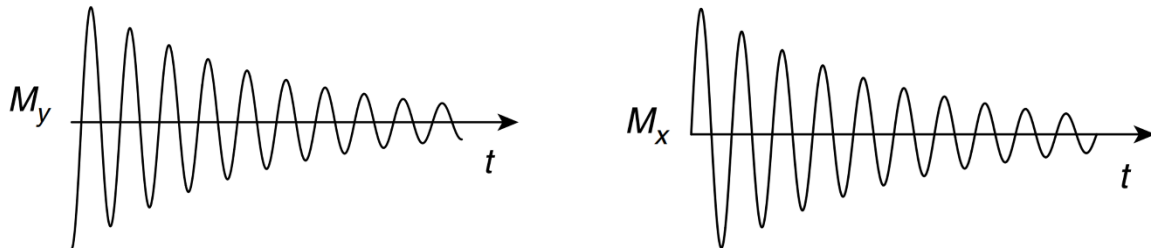


Figure 2.15 Decay and oscillation of the transverse magnetic moment [32].

#### 2.4.1.3 Detection and analysis of the small oscillating electric currents induced by the precession of the transverse magnetic moment

The acquisition of the NMR signal is closely related to the transverse magnetic moment as described above. A rotating magnetic moment generates a rotating magnetic field. Through Maxwell's equations, a changing magnetic field is associated with an electric field. If a wire coil is near the sample, then the electric field sets the electrons in the wire in motion, i.e. an oscillating electric current flows in the wire. It is possible to detect this small oscillating current by using a sensitive r.f. detector as shown in Figure 2.16. The oscillating electric current induced by the precessing nuclear transverse magnetization is called the NMR signal or free-induction decay (FID).

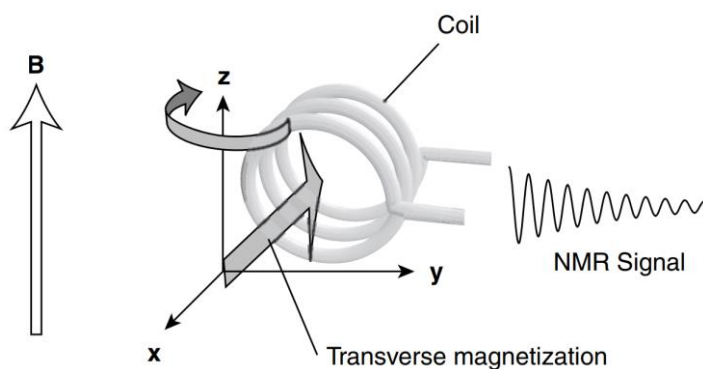


Figure 2.16 The induction of an NMR signal [32].

The NMR signals described above have the same form as in Equation 2.19 and are functions of time. The signals need to be converted into a function of frequency through various mathematical operations including the numerical calculation called Fourier transformation (FT) as shown in Figure 2.17.

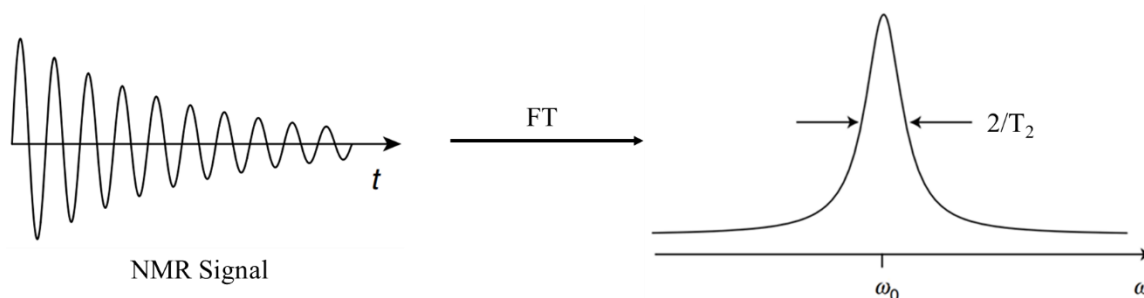


Figure 2.17 NMR signals and its Fourier transformed frequency spectrum [32].

The horizontal axis is an angular frequency axis, marked by the symbol  $\omega$ . The center of the peak is placed at the Larmor frequency of the spins, equal to  $\omega_0$ . The peak width at half-height, measured in  $\text{rad s}^{-1}$ , is equal to  $2/T_2$ , in units of radians per second. The faster the NMR signals oscillates, the larger the Larmor frequency  $\omega_0$ . The more slowly the signals decay, the larger the decay time constant  $T_2$ , also called the spin-spin relaxation time, the narrower the spectral peak.

#### 2.4.2 Spin interactions in molecules

The chemical structural information arises from the interaction of a nuclear spin with internal local fields. The interaction of spins with external static magnetic field  $\vec{B}_0$  is known as the Zeeman interaction, which is the strongest interaction but contains no relevant structural information. The internal interactions include chemical shift interaction, dipole-dipole interaction, J-coupling and quadrupole interaction. Chemical shift interaction involves an induced magnetic field from  $\vec{B}_0$  field by precessing electron clouds, which gives rise to a shift in resonance frequency. Dipole-dipole interaction arises from the fact that one nuclear spin will experience a local dipolar field of the other. Scalar or J-coupling between nuclei is mediated by chemical bonds, which gives rise to multiplets in the spectrum, and is therefore very useful in establishing which nuclei are close to one another on the bonding framework [33].

Quadrupole interaction is the interaction between nuclear electric quadrupole moment and electric field gradients, which only exists for spins with spin quantum number larger than  $\frac{1}{2}$ . Since dipole-dipole interaction is averaged to zero due to the fast tumbling movement of molecules in solution NMR and can be eliminated by decoupling irradiation, and quadrupole interaction only appear for nucleus with a spin quantum number larger than  $\frac{1}{2}$ , these two interactions will not be further discussed.

### 2.4.2.1 Chemical shift interaction

In a magnetic field the electron clouds which precess around a nucleus will produce a local magnetic field. This induced magnetic field gives rise to a frequency shift in NMR spectrum. Therefore, this interaction is usually called the chemical shift interaction. The chemical shift Hamiltonian of a spin  $\vec{I}$  is expressed by:

$$H_{CS} = \gamma_i \vec{I} \vec{\sigma} \vec{B}_0 \quad \text{Equation 2.20}$$

The chemical shift interaction is an anisotropic interaction which is represented by a second rank tensor  $\vec{\sigma}$ . As a result of the anisotropy of the chemical shift, the resonance frequency of a nuclear spin depends on the orientation of the nucleus or molecule relative to  $\vec{B}_0$  [34].

In principal axis systems (PAS) which is fixed to the molecular axes and is different for each nucleus, the chemical shift tensor is diagonal and is given in the following:

$$\vec{\sigma}^{PAS} = \begin{bmatrix} \sigma_{11} & 0 & 0 \\ 0 & \sigma_{22} & 0 \\ 0 & 0 & \sigma_{33} \end{bmatrix} \quad \text{Equation 2.21}$$

Where  $\sigma_{11}$ ,  $\sigma_{22}$  and  $\sigma_{33}$  are the principal elements of the tensor, and  $\sigma_{11}$  is the least shielded element (shifted to down field) and  $\sigma_{33}$  is the most shielded element (shifted to up field) [34].

Viewed from the principal axis system, the direction of  $\vec{B}_0$  field is defined by the polar angles  $\theta$  and  $\varphi$ , as shown in Figure 2.18. It can be easily derived that the Larmor frequency of a spin

with chemical shift interaction in a static magnetic field  $\vec{B}_0$  is given by:

$$\omega = \gamma B_0 (\sin^2 \theta \cos^2 \varphi \sigma_{11} + \sin^2 \theta \sin^2 \varphi \sigma_{22} + \cos^2 \theta \sigma_{33}) - \gamma B_0 \quad \text{Equation 2.22}$$

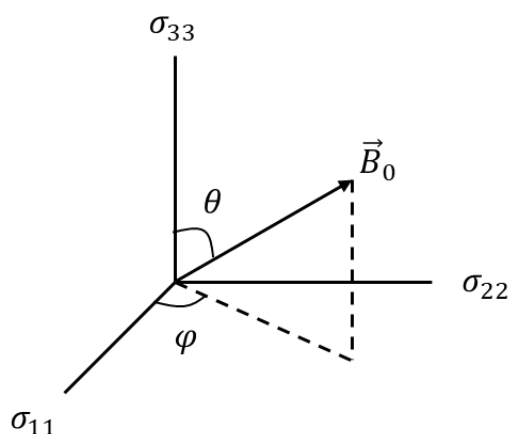


Figure 2.18 Orientation of  $\vec{B}_0$  in the principal axis system as defined by the polar angles  $\theta$  and  $\varphi$ .

In a solution, where the molecules rotate randomly at fast rates, the chemical shift interaction tensor is averaged to its isotropic value,  $\sigma_{iso}$ . Therefore, the Larmor frequency of a spin is given by

$$\omega_{iso} = \gamma B_0 \sigma_{iso} - \gamma B_0 \quad \text{Equation 2.23}$$

Commonly, the horizontal axis in the NMR spectrum is the chemical shift  $\delta$ . The expression for the chemical shift  $\delta$  is

$$\delta = \frac{\omega_{iso} - \omega_{TMS}}{\omega_{TMS}} \cdot 10^6 \text{ ppm} \quad \text{Equation 2.24}$$

where  $\omega_{iso}$  is the Larmor frequency of a particular nucleus, and  $\omega_{TMS}$  is the Larmor frequency of the same isotope in a reference compound such as tetramethylsilan (TMS) which is exposed to the same applied field. If the applied field  $B_0$  is increased, then both quantities  $\omega_{iso}$  and  $\omega_{TMS}$  increase in the same proportion, so the ratio  $\delta$  remains constant.

2.4.2.2 *J-coupling*

*J*-coupling, which is also called scalar coupling, is an indirect interaction between two nuclear spins that arises from hyperfine interactions between the nuclei and the local electrons. In NMR spectroscopy, *J*-coupling contains information about relative bond angles and bond distances. It is responsible for the splitting of resonance lines in the NMR spectra of molecules.

'Tree' diagrams can be used to predict the form of the multiplets [33]. For example, if a spin-half nucleus is coupled with a second spin-half nucleus, the resonance from the spin splits symmetrically about the chemical shift into two lines, called a doublet. (Figure 2.19a) The amount of the splitting of doublet is referred to as the coupling constant, *J*. It is found that the values of coupling constants are independent of the field strength, so they are always state in Hz. If a third spin also has a coupling to the first spin of size  $J_{13}$ , another layer of branching to the tree diagram can be added as shown in Figure 2.19b. To construct the second layer, each line from the first layer is split symmetrically into two with the splitting being  $J_{13}$ , which leads to a four-line-multiplet which is called a doublet of doublets. If the two constants,  $J_{13}$  and  $J_{12}$ , are equal, the two peaks in the middle will overlap with each other, which will produce a triplet with a ratio of integral as 1: 2: 1.

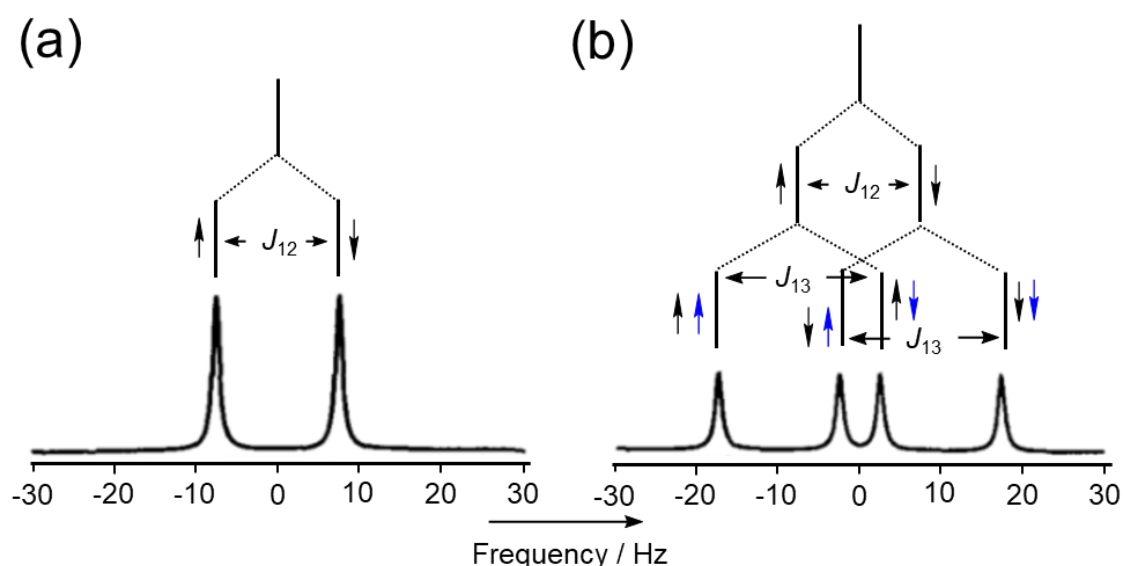


Figure 2.19 Illustration of how multiplets are built up as a result of scalar coupling.

Scalar coupling arises between different protons through electron clouds, and it is not affected

by the orientations of molecules in a magnetic field. Equivalent protons, such as protons in a methyl group (fast single bond rotation) and protons in ethylene (symmetry), wouldn't induce scalar coupling.

### 2.4.3 Study diffusion properties of molecules

Dissolved molecules in a fluid medium undergo two distinct type of diffusive motions. One is lateral self-diffusion which is also known as Brownian motion. The other one is rotational diffusion. In this section, we will introduce some basis on studying diffusive motions of molecules by NMR.

#### 2.4.3.1 Lateral diffusion of molecules

Pulse field gradient (PFG) NMR is a very powerful experimental technique for the direct observation of lateral diffusion of molecules. A PFG NMR experiment normally uses an echo pulse sequence combined with a pair of gradient pulses with a certain spacing  $\Delta$ . (Figure 2.20)

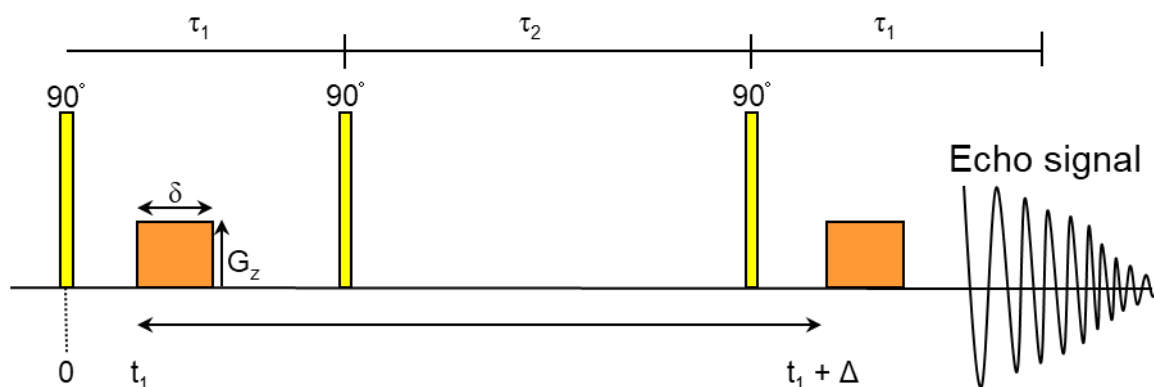


Figure 2.20 Pulse sequence in PFG NMR experiment [35].

Simulated echo sequence is used because the echo decay is determined by spin-lattice relaxation which always have time constants in the range of seconds for both small and large molecules. It consists of three successive 90° pulses. The first 90° pulse create transverse magnetization. The second 90° pulse transfers isochromats of the transverse magnetization into  $-z$ -direction. The third 90° pulse refocused the transverse magnetization. The pulse gradients with a gradient strength  $G$  and duration  $\delta$  are applied between the first and second and immediately after the third 90° pulse [30].

Then, it measures the echo intensity  $I$ . The larger distance a molecule moves during the gradient pulse spacing  $\Delta$ , the smaller the intensities of echo signals will be. The data obtained from the experiment are plotted in a Stejskal-Tanner plot, which represents the echo intensity with respect to the original value  $I_0$  (for  $G = 0$ ) at increasing gradient strengths (Figure 2.21). The Stejskal-Tanner plot was first introduced by E. O. Stejskal and J. E. Tanner in 1965 [36]. The slope of the plot provides information about the diffusion coefficient of the molecules under different conditions, such as free diffusion and restricted diffusion.

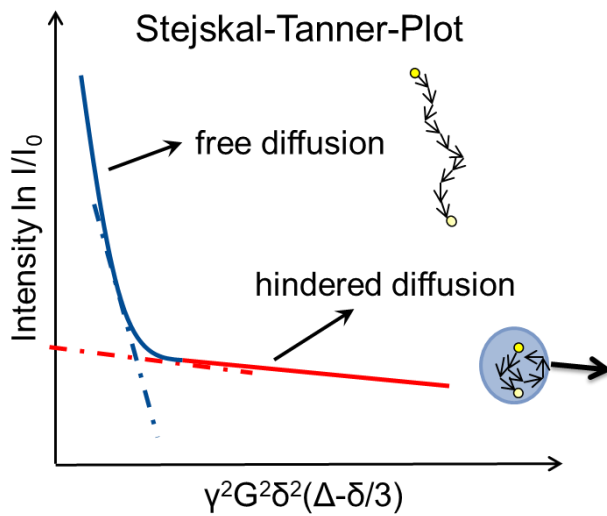


Figure 2.21 Stejskal Tanner plot [35].

In the case of free diffusion with a diffusion coefficient  $D$ , the decay of echo signal satisfies the following equation,

$$\frac{I}{I_0} = I_{rel} = \exp \left[ -\gamma^2 \delta^2 G^2 D \left( \Delta - \frac{\delta}{3} \right) \right] \quad \text{Equation 2.25}$$

Therefore, the slope of the decay curve corresponds to the diffusion coefficient  $D$  of molecules.

If molecules were partly encapsulated by capsules or vesicles, the situation becomes more complicated. In the case of very small capsules or vesicles with diameters significantly below  $1 \mu\text{m}$ , the diffusion constant of encapsulated molecules is dominated by the Brownian motion of capsules if large gradient pulse spacing is applied. Therefore, the decay curve consists of two sections. The large slope of the first section of the curve corresponds to a self-diffusion constant of free dissolved molecules. The small slope of the final sections of the decay curves

corresponds to the diffusion constant of Brownian motion of capsules or vesicles [37].

#### 2.4.3.2 Rotational diffusion of molecules

Rotational correlation time  $\tau_c$  is defined to quantify the rotation rate of a molecule, which is the average time it takes for a molecule to end up at an orientation about 1 radian from its starting position. The rotation of a molecule is a source of relaxation because it will result in the modulation of the local fields due to both the dipolar interaction and the chemical shift anisotropy (CAS). A plot of the rate constants for longitudinal ( $R_{xy}$ ) and transverse ( $R_z$ ) relaxation as a function of the correlation time is shown in Figure 2.22. The fast motion limit, in which the two rate constants are equal, is seen when  $\tau_c$  is small. As the correlation time increases, the longitudinal relaxation rate constant eventually reaches a maximum when  $\omega_0\tau_c = 1$ . As the correlation time increases further,  $R_z$  falls off steadily. While the transverse relaxation rate constant goes on increasing with  $\tau_c$  [33].

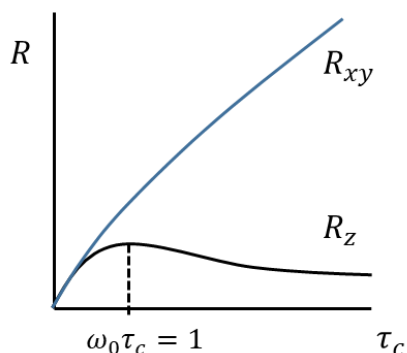


Figure 2.22 Plot of the rate constants for longitudinal and transverse relaxation, caused by random fields, as a function of the correlation time,  $\tau_c$ .

The practical consequence of these observations is that for large molecules, which tumble slowly and so have long correlation times, transverse magnetization decays away to zero much more quickly than the z-magnetization recovers to equilibrium.

Fast rotation of a dissolved molecule with  $\tau_c < 100 \text{ ms}$  will lead to both longer  $T_2$  relaxation times and narrow line in the spectrum due to almost complete averaging of all angular dependent contributions including dipolar interaction and the chemical shift anisotropy. (Figure 2.23a) If a molecule formed nanoparticle dispersion, its correlation time  $\tau_c$  would increase dramatically due to the reduced rotational diffusion of the particles, which will lead to both

shorter  $T_2$  relaxation times and broad line in the spectrum. (Figure 2.23b) Therefore, NMR spectra line shape can be used to differentiate between all solid constituents from those in the liquid phase [29]. The correlation time of molecules which formed a nanoparticle can be approximately determined by comparison between the experimental spectrum and the simulated reference line shapes [30].

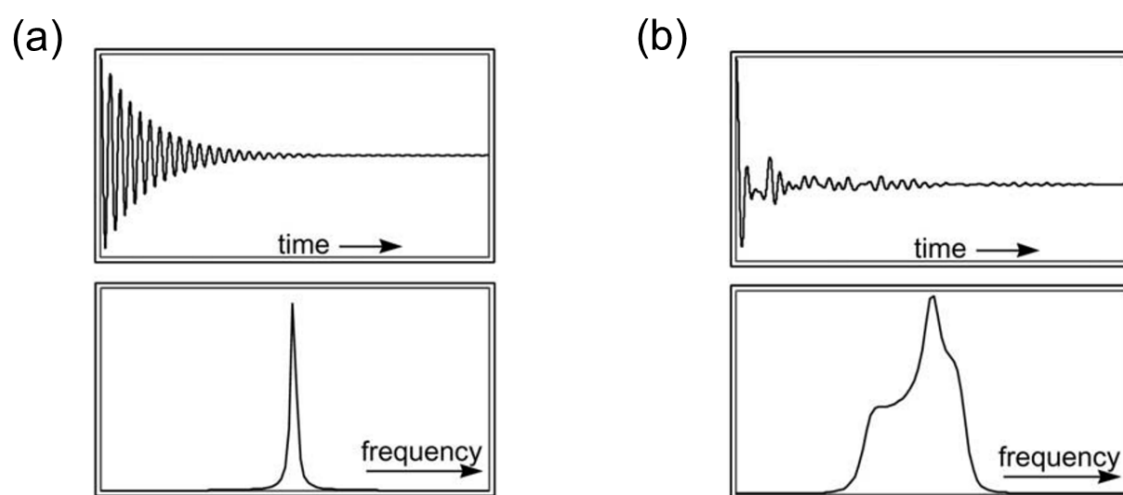


Figure 2.23 Graphic representation of the dependence of NMR time signal after  $90^\circ$  pulse and the corresponding frequency spectrum on molecules with (a) extremely fast rotational diffusion and (b) extremely slow rotational diffusion [30].

### 2.5 Studying nano-capsules

The size distribution and morphology are two important parameters that influence the performance of capsules. Therefore, two important methods including video microscopic particle tracking and atomic force microscopy were introduced in this chapter.

#### 2.5.1 Determination of capsule size distribution by video microscopic particle tracking

The size and size distribution of nanocapsules were determined by video microscopic particle tracking. The principle of this method is based on Einstein's Brownian motion equation of nanoparticles. The instrumentation includes a transmitted dark field microscope together with a CCD camera and a particle tracking program. The particle tracking program can determine mean square displacement of every nanoparticle under the given room temperature and viscosity with respect to a given time interval  $\Delta$ , and then assign individual particle sizes

according to Einstein's Brownian motion equation. We will introduce this method in detail in the following subsections.

### 2.5.1.1 Brownian motion and Einstein's theory

British botanist Robert Brown first reported the phenomenon that tiny particles from plant pollen would move irregularly in water in 1827. In 1905, theoretical physicist Albert Einstein published a paper where he attributed the irregular motion of pollen particles to the random collision of water molecules, and he derived an equation for particles Brownian motion as following [38]:

$$R_H = \frac{R \cdot T \cdot \Delta}{3 \cdot \pi \cdot \eta \cdot N_A \cdot \overline{x^2}} \quad \text{Equation 2.26}$$

Where  $R_H$  stands for hydrodynamic radius of particles,  $R$  stands for universal gas constant,  $N_A$  stands for Avogadro constant,  $T$  stands for temperature,  $\Delta$  stands for time interval for the movement,  $\eta$  stands for viscosity of fluid medium,  $\overline{x^2}$  stands for mean square displacement of individual nanoparticle during  $\Delta$ .

There are two parts to Einstein's theory. The first part consists in the formulation of a diffusion equation for Brownian particles, which relates the diffusion coefficient of particles to the statistical mean square displacement of the particles and a given time interval  $\Delta$ . In this part, Einstein firstly lets  $f = f(x, t)$  be the probability density that a Brownian particle is at  $x$  at time  $t$  in an one dimensional space. Then, making certain probabilistic assumptions, he derived that  $f$  satisfies the diffusion equation:

$$\frac{\partial f}{\partial t} = D \frac{\partial^2 f}{\partial x^2} \quad \text{Equation 2.27}$$

Where  $D$  is a positive constant, called the coefficient of diffusion. Assuming that  $N$  particles start from the origin at the initial time  $t = 0$ , the diffusion equation has the solution:

$$f(x, t) = \frac{N}{\sqrt{4\pi Dt}} e^{-\frac{x^2}{4Dt}} \quad \text{Equation 2.28}$$

Thus the average value of the squares of displacements ( $\overline{x^2}$ ) of a Brownian particle, in a time

interval  $t = \Delta$  is Equation 2.29, which is also called Einstein-Smoluchowski Equation:

$$\overline{x^2} = 2D\Delta \quad \text{Equation 2.29}$$

The second part consists in relating the diffusion coefficient to measurable physical quantities, such as particle size, temperature, viscosity of continuous phase liquid. In this part, Einstein derived that the diffusion constant of a spherical particle in a fluid medium satisfies the following equation, which is also being called the Stokes -Einstein equation:

$$D = \frac{RT}{6\pi\eta N_A R_H} \quad \text{Equation 2.30}$$

The initial Equation 2.26, which is Einstein's Brownian motion equation, can be obtained by eliminating the diffusion coefficient  $D$  in Equation 2.29 and Equation 2.30.

### 2.5.1.2 *Dark-field microscopy*

A dark-field microscope is an optical microscope that differs from a bright-field microscope only in the light path between the light source and the objective lens. For bright-field microscope, the light is focused onto the sample by condenser lens, and the directly transmitted light enters the objective lens. For dark-field microscope, light is focused onto the sample by a special dark-field condenser lens, but the directly transmitted light simply misses the objective lens, and only the scattered light enters the objective lens (Figure 2.24).

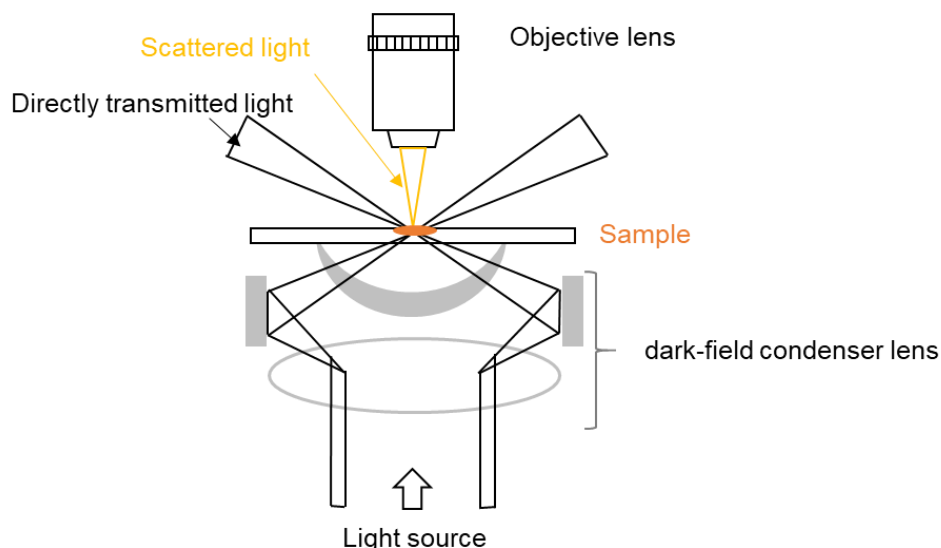


Figure 2.24 Light path of dark-field microscopy.

If a colloidal dispersion is now observed in the bright-field microscope, we can see a dark object on a bright background, because some of the light is absorbed by the particles. In contrast, a dark-field microscope displays white pixels on a dark background, because the particles scatter the incident light according to the Tyndall effect, whereby a certain proportion of the scattered radiation is directed into the objective.

One advantage of dark-field microscope is that it has a very high contrast between the light intensity of the background and the object, as the following equation illustrates [39]:

$$K = \frac{I_{\text{background}} - I_{\text{object}}}{I_{\text{background}} + I_{\text{object}}} \quad \text{Equation 2.31}$$

Where  $K$  represents contrast, and  $I$  represents intensity.

When the intensity of the background tends toward 0, the contrast tends toward -1. This denotes optimal contrast and means that perceptibility is determined only by the intensity of the light scattered from the object.

Another advantage is that this method is not limited by the resolution according to Abbe (Equation 2.32), which determines the resolution of the bright-field microscope:

$$d = k \cdot \frac{\lambda}{n \cdot \sin(\theta)} \quad \text{Equation 2.32}$$

Where  $d$  represents dissolution,  $k$  is constant (mostly 0.3 – 1.1),  $\lambda$  represents wavelength of the irradiated light,  $n$  represents refractive index of the medium,  $\sin(\theta)$  represents half the aperture angle of the entering light.

The limitation of dark field microscopy is the scattering intensity of the observed particles, which depends on both the particle diameter  $d$  and the wavelength  $\lambda$  of the irradiated light as described by Rayleigh in Equation 2.33:

$$I \sim \frac{d^6}{\lambda^4} \quad \text{Equation 2.33}$$

### 2.5.1.3 Particle tracking system

Particle tracking is performed using a combination of dark field microscopy with a CCD camera (Charged-Couple-Device) and the program "Advanced Nanoparticle Tracking" (ANT). The determination of the particle size distribution consists of several steps, including data acquisition, image restoration, particle detection and tracking, and finally the calculation of individual particle sizes and their compilation into histograms [39] [40]. In 'data acquisition' step, the program controls the CCD camera and store the image data in the RAM. The aim of 'image restoration' is to remove digitization errors and static elements of the image background as well as the continuous background noise. In 'particle detection and tracking' step, the particles undergoing Brownian motion are identified and their trajectories are tracked. Then, the average of the squared displacements of each particle under Brownian motion and the time required are inserted into Einstein's Brownian motion equation (Equation 2.26) and a hydrodynamic particle radius of each particle is calculated. In the final step, all calculated particle radii are saved within a continuous table. A size histogram is then created from this table by determining the number of particles per 10 nm wide size range.

The advantage of this method over other particle size measurement methods is that an absolute measurement of all particles in the field of view can be performed. Because this

method is particle by particle, the resultant size distribution is of high resolution. The reliability of the particle size results is related to the accuracy of the Brownian motion trajectory of the particles obtained by the program. Therefore, there are three requirements in sample preparation. First, the sample needs to be optimally diluted, otherwise the program may obtain incorrect trajectories due to the overlapping of each particle in the field of view. Second, slides and cover glasses with hydrophobic surfaces are to be used to reduce the surface tension between the liquid and the glass surface as well as minimize the attractive interactions between the particles and the two glass surfaces. Lastly, the edges of cover glasses need to be sealed with wax in case that external influences such as convection have some effects on the trajectories. In addition, the light source used in our dark field microscope is green light because green light does not tend to raise the samples' temperature, which have an effect on the results as well.

### 2.5.2 Determination of capsule morphology and strength by atomic force microscopy

The morphology and mechanical strength of the capsules are characterized by atomic force microscopy. In this subsection we will describe this technique of scanning atomic force microscopy. The atomic force microscope (AFM) is one type of scanning probe microscopy (SPM), which can be used to study topography, mechanical properties and composition of a wide range of samples, including atoms, molecules, molecular aggregates, and cells. The advantages of AFM are that the sample preparation is easy and the measurement can be operated in a number of environments, including ambient air, ultra-high vacuum (UHV), and even liquids [41].

A normal AFM consists basically of three parts. One is the AFM head, which is where all the scanners, lasers and detectors are. Another one is the controller, which controls all the movement of the cantilever in the head. The last one is PC with the graphical unit interface for users to easily control the AFM system. Since the AFM system is very sensitive and all vibrations might disturb the measurements, it is usually mounted on an active damping table as shown in Figure 2.25.

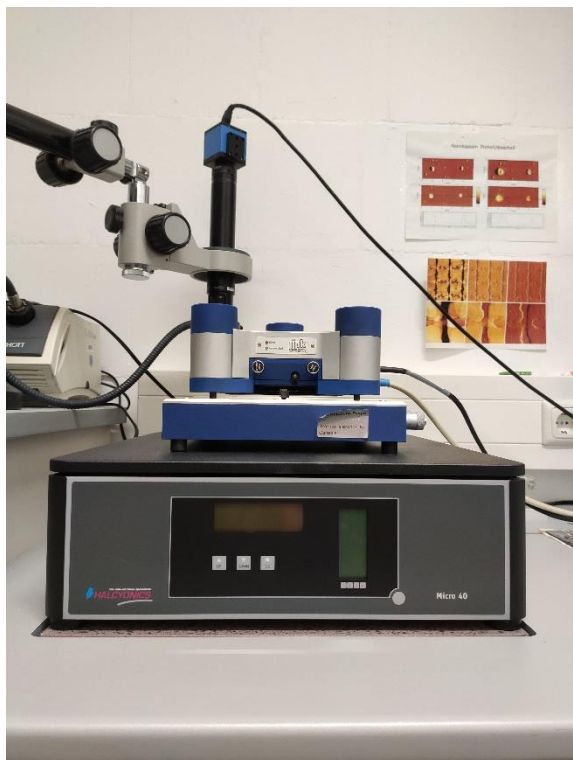


Figure 2.25 Picture of an AFM system on an active damping table.

The basic principle of AFM is that the local attractive or repulsive force between the tip and the sample is converted into a deflection of the cantilever. (Figure 2.26) Cantilever is a critical part of AFM head, which is a plate spring and is fixed at one end. At the other end it supports a pointed tip, which will have an interaction with sample surface when it gets close to the sample. If the interaction between the tip and sample surface is attractive, the cantilever will deflect towards the surface. If it is repulsive, the cantilever will deflect away from the surface.

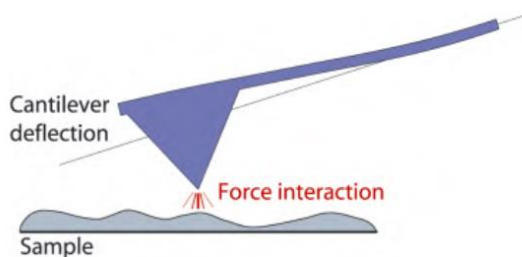


Figure 2.26 Cantilever deflection due to force interaction between cantilever and sample [42].

The most common way to detect the deflection of the cantilever is the beam deflection method. The schematic representation of this approach is shown in Figure 2.27. A detection laser is

focused on the end of the cantilever and is then reflected onto a photodiode array. Most photodiode arrays contain four quadrants that allow for a precise measure of the displacement of the laser spot as the tip position changes during an image scan. As the tip makes contact with the surface and scans over features, the cantilever bends back and forth, causing the laser position on the photodiode to shift. These signals from individual photodiode quadrants of the detector are compared to calculate the deflection signal. The vertical deflection of the cantilever can be determined by comparing the signals from the 'top' and 'bottom' halves of the detector. The lateral deflection of the cantilever can also be calculated by comparing the signals from the 'left' and 'right' halves of the detector.

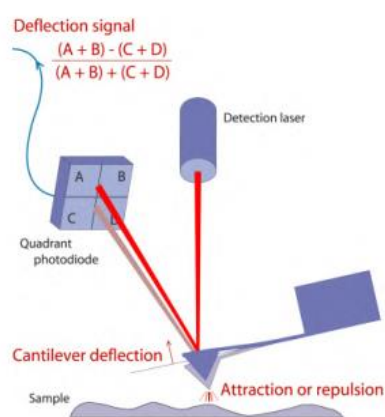


Figure 2.27 Detection of cantilever deflection by beam deflection method [42].

One possible way to obtain the sample surface image is scanning laterally over the surface without changing the height of the cantilever and just measuring the deflection signals. This is known as 'constant height' imaging, but it is not the most common way. The most common procedure to obtain the sample surface image is to use some form of feedback loop to monitor the cantilever response, and adjust the height of the cantilever accordingly to take account of the changes in surface height. In this case, the base of the cantilever is moved up and down over higher or lower parts of the sample.

'Contact mode' and 'tapping mode' are two most common imaging modes, in which two different forms of cantilever response are used as the feedback signal. In contact mode, a value of the cantilever deflection (set point) is selected for the feedback system. The feedback system

adjusts the height of the cantilever to keep this deflection constant as the tip moves over the surface. In contact mode, deflection of cantilever varies with the change of repulsive force between tip and sample, which depends on the distance between tip and sample, and this leads to beam position changes on the photodiode. The tip bends more when the repulsive force gets bigger. The scan procedure of contact mode is as follows. First, a set point (deflection degree) is made for the system. Second, the tip start approaching to the sample surfaces until the cantilever reaches the set point (deflection degree). Third, the tip start scan and during the scanning, feedback moves Z scanner up and down to maintain the constant deflection degree of the cantilever, and finally a topography information of the sample surface will be obtained. The disadvantage of contact mode is that some deformation may happen on the sample surface due to the very short distance between the tip and sample surface.

In tapping mode, the cantilever is driven to oscillate near the resonance frequency by a piezo crystal, a value of oscillation amplitude (set point) is selected for the feedback system. The feedback system adjusts the height of the cantilever to keep this oscillation amplitude constant as the tip moves over the surface. Before the approaching of the cantilever to the sample surface, the amplitude of the oscillation is related to the driven frequency. The closer of the driven frequency to the resonance frequency, the larger the amplitude of the oscillation. After a certain driven frequency is choose and the approaching of the cantilever to the sample surface, the attractive or repulsive force will have an influence to the amplitude of the oscillation at that choose driven frequency. The larger the attractive or repulsive force in between the tip and sample surface, the smaller the amplitude of the oscillation. A driven frequency near the resonance frequency is usually used for the oscillation, and the amplitude for the set point is usually smaller than that for the free oscillation (70% amplitude of the free oscillation). The scan procedure of tapping mode is the same as that of contact mode except that the amplitude of the oscillation is used for the feedback. The feedback maintains the amplitude of the oscillation constant by moving the Z scanner. Apart from that, the height image could be obtained, a phase image which gives information about the mechanical properties of the sample surfaces can be obtained as well because the changes of different materials can influence the phase of the oscillation of the cantilever.

### 3 Materials and methods

#### 3.1 Chemicals used

The chemicals used in this thesis are all listed in Table 3.1. All chemicals were used as they were received.

Table 3.1 Chemicals used.

Chemical	Short name	CAS-RN	Provider	Purity
β-Benzyl-L-aspartate	BnAsp	2177-63-1	TCI Deutschland GmbH	>98%
			BLD Pharmatech GmbH	97%
S-Benzyl-L-cysteine	BnCys	3054-01-1	Alfa Aesar	99%
S-Carbobenzyloxy-L-cysteine	CbzCys	1625-72-5	BLD Pharmatech GmbH	95%
L-Phenylalanin	Phe	63-91-2	Carl Roth GmbH + Co. KG	≥99%
Phenyl chloroformate	PCF	1885-14-9	Alfa Aesar	99%
4-Nitrophenyl chloroformate	NPCF	7693-46-1	TCI Deutschland GmbH	>98%
n-Butylamine	n-BuNH <sub>2</sub>	109-73-9	Alfa Aesar	99%
Chloroform	CHCl <sub>3</sub>	67-66-3	Thermo Fisher Scientific Inc.	99.97%
Deuterated chloroform	CDCl <sub>3</sub>	865-49-6	Deutero GmbH	99.8%
Deuterated dimethyl sulfoxide	DMSO-d <sub>6</sub>	67-68-5	Deutero GmbH	99.8%
Diethyl ether	DEE	60-29-7	Thermo Fisher Scientific Inc.	99.5%
N,N-Dimethylacetamide	DMAc	127-19-5	Acros Organics B.V.B.A.	99.5%, with molecular sieve
Dithiothreitol	DTT	3483-12-3	TCI Deutschland GmbH	>98.0%
Ethyl acetate	EA	141-78-6	Thermo Fisher Scientific Inc.	≥99.8%
n-Hexane	n-Hex	110-54-3	Thermo Fisher Scientific Inc.	≥95%
Hydrobromic acid	HBr	10035-10-6	Thermo Fisher Scientific Inc.	33% HBr in acetic acid
Hydrogen peroxide	H <sub>2</sub> O <sub>2</sub>	7722-84-1	Alfa Aesar	35%

				aqueous solution
Magnesium sulfate	MgSO <sub>4</sub>	7487-88-9	Carl Roth GmbH + Co. KG	≥99%
Perfluorodecalin	PFD	306-94-5	J&K Scientific Ltd.	95%
Sodium chloride	NaCl	7647-14-5	Thermo Fisher Scientific Inc.	≥99.5%
Sodium hydroxide	NaOH	1310-73-2	Bernd Kraft GmbH	1 M
Sodium sulfate	Na <sub>2</sub> SO <sub>4</sub>	7757-82-6	VWR International, LLC	≥98.0%
Trifluoroacetic acid	TFA	76-05-1	TCI Deutschland GmbH	>99%
Trifluoromethanesulfonic acid	TFMSA	1493-13-6	TCI Deutschland GmbH	>98%

### 3.2 Syntheses of PFD in water emulsions stabilized by diblock polypeptide surfactants

#### 3.2.1 Syntheses of activated amino acid monomers

##### 3.2.1.1 Synthesis of *N*-phenoxy carbonyl- $\beta$ -Benzyl *L*-aspartate (NPBnAsp)

NPBnAsp was synthesized following the procedure of Kamei et al. [43] Briefly,  $\beta$ -benzyl-*L*-aspartate (12.8 g, MM = 223.23 g/mol, 57.3 mmol) was dispersed in 100 mL of ethyl acetate, and then phenyl chloroformate (10.5 g, MM = 156.57 g/mol, 67.1 mmol) was added into the reaction system under nitrogen atmosphere. The reaction mixture was stirred at 45 °C for 48 h. The reaction mixture was washed twice with distilled water and saturated aqueous NaCl solution, dried over anhydrous Na<sub>2</sub>SO<sub>4</sub>, filtered, concentrated by a rotary evaporator. After recrystallization with ethyl acetate/*n*-hexane, the product was obtained as white powder (8.1 g, MM = 343.34 g/mol, 23.6 mmol, yield: 41.2 %).

##### 3.2.1.2 Synthesis of *N*-phenoxy carbonyl-*L*-Phenylalanine (NPPhe)

NPPhe was synthesized as reported by Yamada et al. [44] *L*-Phenylalanine (2.2 g, MM = 165 g/mol, 13.3 mmol) was dispersed in 20 mL of methanol, and then 40 % tetrabutylammonium hydroxide in methanol (9.5 mL, 1.4 mmol/mL, 13.3 mmol) was slowly added at room temperature. After stirring for 1 h, the solvent was removed using a rotary evaporator. The resulting residues were dispersed in 20 mL of acetonitrile and then added to a stirred solution of DPC (2.9 g, MM = 214.22 g/mol, 13.4 mmol) in 20 mL of acetonitrile. After the reaction

mixture was stirred at room temperature for 3 h, 10 mL of water was added to the above system to stop the reaction. After the mixture was acidified to pH 2 using 1 M HCl, it was extracted with 30 mL ethyl acetate. The organic fractions were washed with saturated NaCl aqueous solution, dried over anhydrous Na<sub>2</sub>SO<sub>4</sub>, filtered, and concentrated by a rotary evaporator to give a yellowish oil. The oil was purified by column chromatography (ethyl acetate : n-hexane = 3:7), and then recrystallized with the same ethyl acetate/n-hexane mix to give the product as white powder. (1.3 g, MM = 285 g/mol, 4.4 mmol, yield: 33.2 %)

#### 3.2.2 Synthesis of polypeptide through polymerization of activated amino acid monomers

##### 3.2.2.1 polymerization of NPBnAsp

NPBnAsp (8 g, MM = 338 g/mol, 23.7 mmol, 50 eq) was dissolved in anhydrous DMAc, and then n-Butylamine (47.4  $\mu$ L, 0.01 mmol/ $\mu$ L, 0.474 mmol, 1 eq), was added into the above solution under the protection of nitrogen. The reaction was allowed to proceed for 48 h at 60 °C. Subsequently, the reaction mixture was precipitated into a large amount of diethyl ether, filtered, washed with diethyl ether, and dried under vacuum for 24 h to get the final product as a white solid (3.85 g, M<sub>n</sub> = 8250 g/mol, 0.47 mmol). The given number average of MM (M<sub>n</sub> = 8250 g/mol) was calculated from the <sup>1</sup>H NMR spectrum of the resulting Bu-BnAsp<sub>m</sub>. It corresponds to an average chain length of m = 40 units.

##### 3.2.2.2 Polymerization of NPPhe using Bu-BnAsp<sub>40</sub> as macromolecule initiator

Bu-BnAsp<sub>40</sub> was dissolved in anhydrous DMAc, and then NPPhe (variable equivalents to the initiator) was added into the above solution under the protection of nitrogen. The reaction was allowed to proceed for 2 d at 60 °C. Subsequently, the reaction mixture was precipitated into a large amount of diethyl ether, filtered, washed with diethyl ether, and dried under vacuum for 24 h to get the final product as a yellowish solid.

The syntheses of protected polypeptide are summarized in Table 3.2.

Table 3.2 Summarized syntheses of Bu-BnAsp<sub>40</sub>-Phe<sub>n</sub>.

Syntheses	initiator	monomer	Product	Quantity	Yield
1	Butylamine (34.7 mg, 73.14, 0.474 mmol)	NPBnAsp (8 g, 338, 23.7 mmol, 50 eq.)	Bu-BnAsp <sub>40</sub>	3.85 g	79.3 %
2	Bu-BnAsp <sub>40</sub> (496 mg, 8250, 0.06 mmol)	NPPhe (119 mg, 285, 0.42 mmol, 7 eq.)	Bu-BnAsp <sub>40</sub> - Phe <sub>5</sub>	481 mg	86.3 %
3	Bu-BnAsp <sub>40</sub> (504 mg, 8250, 0.06 mmol)	NPPhe (240 mg, 285, 0.84 mmol, 14 eq.)	Bu-BnAsp <sub>40</sub> - Phe <sub>9</sub>	550 mg	87.6 %
4	Bu-BnAsp <sub>40</sub> (500 mg, 8250, 0.06 mmol)	NPPhe (500 mg, 285, 1.75 mmol, 29 eq.)	Bu-BnAsp <sub>40</sub> - Phe <sub>14</sub>	690 mg	91.0 %

### 3.2.2.3 De-protection of Bu-BnAsp<sub>40</sub>-Phe<sub>n</sub>

Bu-PBnAsp<sub>40</sub>-PPhe<sub>n</sub> was dispersed in trifluoroacetic acid (TFA), then 33% HBr in acetic acid (10 equiv. of HBr per protecting group) was added into the above solution under the protection of nitrogen. The reaction was allowed to proceed for about 5 h at room temperature. Subsequently, the reaction mixture was precipitated into a large amount of diethyl ether and washed with diethyl ether. Finally, it was dried under vacuum to get the raw product as a yellow solid.

The De-protection reactions of di-block peptide are summarized in Table 3.3.

Table 3.3 Summarized de-protection reactions of Bu-BnAsp<sub>40</sub>-Phe<sub>n</sub>.

Syntheses	Protected peptide	TFA	33% HBr/ CH <sub>3</sub> COOH	Product	Quantity
1	Bu-BnAsp <sub>40</sub> -Phe <sub>5</sub> (400 mg, 9000, 44 μmol)	4 mL	2 mL	Bu-Asp <sub>40</sub> -Phe <sub>5</sub>	270 mg, 5400, 50 μmol
2	Bu-BnAsp <sub>40</sub> -Phe <sub>9</sub> (408 mg, 9600, 42.5 μmol)	4 mL	2 mL	Bu-Asp <sub>40</sub> -Phe <sub>9</sub>	303.4 mg, 6000, 50.6 μmol
3	Bu-BnAsp <sub>40</sub> -Phe <sub>14</sub> (300 mg, 10300, 29 μmol)	3 mL	1.5 mL	Bu-Asp <sub>40</sub> - Phe <sub>14</sub>	224.7 mg, 6700, 33.5 μmol

#### 3.2.3 Preparation of PFD/water emulsion stabilized by diblock peptide emulsifier

100 mg peptide was dispersed in 10 mL water and a few drops of sodium hydroxide aqueous solution (1 M) was added into it under stirring. Peptide sodium hydroxide aqueous solution with a concentration about 10 mg mL<sup>-1</sup> could be obtained after several minutes of stirring. A few drops of hydrogen chloride aqueous solution (1 M) were added to adjust the pH value to around pH 7.

2.5 mL previously prepared polypeptide aqueous solution was diluted to 10 mL, and 100- 500 µL of PFD was added into it. The mixture was treated with ultrasonication (50- 70% power) for 2-5 min to obtain the emulsions.

### 3.3 Syntheses of oligo- and polycysteines

#### 3.3.1 Synthesis of activated amino acid monomers

##### 3.3.1.1 Synthesis of *N*-phenoxycarbonyl-*S*-benzyl-*L*-cysteine (NPBnCys)

NPBnCys was synthesized as reported by Yamada et al. [45] S-Benzyl-*L*-cysteine (3.86 g, MM = 211.28 g/mol, 18.3 mmol) was dispersed in 20 mL of methanol, and then 40 % tetrabutylammonium hydroxide in methanol (13.1 mL, 1.4 mmol/mL, 18.3 mmol) was slowly added at room temperature. After stirring for 1 h, the solvent was removed using a rotary evaporator. The resulting residues were dispersed in 20 mL of acetonitrile and then added to a stirred solution of DPC (4.0 g, MM = 214.22 g/mol, 18.6 mmol) in 20 mL of acetonitrile. After the reaction mixture was stirred at room temperature for 3 h, 10 mL of water was added to the above system to stop the reaction. After the mixture was acidified to pH 2 using 1 M HCl, it was extracted with 30 mL ethyl acetate. The organic fractions were washed with saturated NaCl aqueous solution, dried over anhydrous Na<sub>2</sub>SO<sub>4</sub>, filtered, and concentrated by a rotary evaporator to give a yellowish oil. The oil was purified by column chromatography (ethyl acetate: n-hexane = 3:7), and then recrystallized with the same ethyl acetate/n-hexane mix to give the product as white powder. (2.07 g, MM = 331 g/mol, 6.3 mmol, yield: 34.2 %).

#### 3.3.1.2 Synthesis of *N*-phenoxycarbonyl-*S*-Carbobenzoxy-*L*-cysteine (NPCbzCys)

*S*-Carbobenzoxy-*L*-cysteine (4.7 g, MM = 255.29 g/mol, 18.4 mmol) was dispersed in 30 mL of ethyl acetate, and then phenyl chloroformate (3.2 mL, MM = 156.57 g/mol, 8 mmol/mL, 25.6 mmol) was added into the reaction system under nitrogen atmosphere. The reaction mixture was stirred at 45 °C for 24 h. The reaction mixture was washed twice with distilled water and saturated aqueous NaCl solution, dried over anhydrous Na<sub>2</sub>SO<sub>4</sub>, filtered, concentrated by a rotary evaporator. After recrystallization with ethyl acetate/*n*-hexane, the product was obtained as white solid (2.1 g, MM = 375.4 g/mol, 5.6 mmol, yield: 30.4 %).

#### 3.3.1.3 Synthesis of *N*-(4-nitrophenoxycarbonyl)-*S*-Carbobenzoxy-*L*-cysteine (NNPCbzCys)

*S*-Carbobenzoxy-*L*-cysteine (3.7 g, MM = 255.29 g/mol, 14.5 mmol) was dispersed in 50 mL of ethyl acetate, and then 4-nitrophenyl chloroformate (2 g, MM = 201.56 g/mol, 9.9 mmol) was added into the reaction system under nitrogen atmosphere. The reaction mixture was stirred at 45 °C for 24 h. The reaction mixture was washed twice with distilled water and saturated aqueous NaCl solution, dried over anhydrous Na<sub>2</sub>SO<sub>4</sub>, filtered, concentrated by a rotary evaporator. After recrystallization with ethyl acetate/*n*-hexane, the product was obtained as white powder (2.13 g, MM = 420 g/mol, 5.1 mmol, yield: 35.2 %).

### 3.3.2 Synthesis of peptide through polymerization of activated amino acid monomers

#### 3.3.2.1 Polymerization of NPBnCys

NPBnCys (variable equivalents to the initiator) was dissolved in anhydrous DMAc, and then *n*-butylamine was added into the above solution under the protection of nitrogen. The reaction was allowed to proceed for 24 h at 60 °C. Subsequently, the reaction mixture was precipitated into a large amount of diethyl ether, filtered, washed with diethyl ether, and dried under vacuum for 24 h to get the final product as a white solid.

#### 3.3.2.2 Polymerization of NPCbzCys

NPCbzCys (0.98 g, MM = 375.4 g/mol, 2.66 mmol) was dissolved in 3 mL of anhydrous DMAc, and then *n*-butylamine (17.8 μL, 0.01 mmol/μL, 0.178 mmol), was added into the above

solution under the protection of nitrogen. The reaction was allowed to proceed for 48 h at 60 °C. Subsequently, the reaction mixture was precipitated into a large amount of diethyl ether, filtered, washed with diethyl ether, and dried under vacuum for 24 h to get the final product as a brown solid (25 mg). This given, the yield is considered to be too small.

### 3.3.2.3 Polymerization of NNPCbzCys

NNPCbzCys (variable equivalents to the initiator) was dissolved in anhydrous DMAc, and then n-butylamine was added into the above solution under the protection of nitrogen. The reaction was allowed to proceed for 48 h at 60 °C. Subsequently, the reaction mixture was precipitated into a large amount of diethyl ether, filtered, washed with diethyl ether, and dried under vacuum for 24 h to get the final product as a yellow solid.

Polymerization reaction conditions and their results are summarized in Table 3.4.

Table 3.4 Summarized synthesis of Bu-BnCys<sub>c</sub> or Bu-CbzCys<sub>c</sub>.

Synthesis	initiator	monomer	temperature	time	Product	Quantity	Yield
1	Butylamine (7.31 mg, 73.14, 100 μmol)	NPBnCys (1 g, 331, 3 mmol, 30 eq.)	60 °C	24 h	Bu-BnCys <sub>20</sub>	460 mg	78.9 %
2	Butylamine (43.88 mg, 73.14, 600 μmol)	NPBnCys (1 g, 331, 3 mmol, 5 eq.)	60 °C	24 h	Bu-BnCys <sub>6</sub>	402 mg	69.0 %
3	Butylamine (13.02 mg, 73.14, 178 μmol)	NPCbzCys (0.98 g, 375, 2.60 mmol, 15 eq.)	60 °C	48 h	-	trace	0%
4	Butylamine (5.78 mg, 73.14, 79 μmol)	NNPCbzCys (1 g, 420, 2.38 mmol, 30 eq.)	60 °C	30 h	Bu-CbzCys <sub>5</sub>	100.8 mg	17.9 %
5	Butylamine (3.44 mg, 73.14, 47 μmol)	NNPCbzCys (1 g, 420, 2.38 mmol, 50 eq.)	60 °C	48 h	Bu-CbzCys <sub>18</sub>	196.3 mg	34.8 %
6	Butylamine	NNPCbzCys	30 °C	48 h	Bu-	264.7	25.8

	(10.53 mg, 73.14, 144 $\mu$ mol)	(1.818 g, 420, 4.33 mmol, 30 eq.)			CbzCys <sub>17</sub>	mg	%
7	Butylamine (1.83 mg, 73.14, 25 $\mu$ mol)	NNPCbzCys (520 mg, 420, 1.24 mmol, 50 eq.)	30 °C	48 h	Bu-CbzCys <sub>18</sub>	67.3 mg	23.0 %

### 3.3.3 Deprotection of protected peptides

#### 3.3.3.1 Deprotection of Bu-BnCys<sub>c</sub>

Bu-BnCys<sub>c</sub> was dispersed in CF<sub>3</sub>COOH, then triflic acid (10 eq. of the benzyl groups) was added into the above solution under the protection of nitrogen. The reaction was allowed to proceed for 5- 20 h at 40 °C. Subsequently, the reaction mixture was precipitated into a large amount of diethyl ether and washed with diethyl ether. Finally, it was dried under vacuum to get the raw product as a brown solid.

#### 3.3.3.2 De-protection of Bu-CbzCys<sub>c</sub>

Bu-CbzCys<sub>c</sub> was dispersed in CF<sub>3</sub>COOH, then 33% HBr/CF<sub>3</sub>COOH (10 eq. of the Cbz groups) was added into the above solution under the protection of nitrogen. The reaction was allowed to proceed for 3 h at 20 °C. Subsequently, the reaction mixture was precipitated into a large amount of diethyl ether and washed with diethyl ether. Finally, it was dried under vacuum to get the raw product as a brown solid.

The synthesis of Bu-Cys<sub>c</sub> is summarized in Table 3.5.

Table 3.5 Summarized de-protection reaction of Bu-BnCys<sub>c</sub> or Bu-CbzCys<sub>c</sub>.

Syntheses	Protected peptide	TFA	Acid	Time and temperature	Product	Quantity
1	Bu-BnCys <sub>20</sub> (300 mg, 3930, 76.3 $\mu$ mol)	3 mL	triflic acid (1.38 mL, 15.5 mmol, 10 eq of Bn)	5 h, 40 °C	Bu-Cys <sub>20</sub>	356 mg
2	Bu-BnCys <sub>6</sub> (184 mg,	3	triflic acid	19 h, 40 °C	Bu-	186.7 mg

	1230, 76.3 $\mu\text{mol}$ )	mL	(1.38 mL, 15.5 mmol, 10 eq of Bn)		Cys <sub>6</sub>	
3	Bu-CbzCys <sub>17</sub> (100 mg, 4100, 24.4 $\mu\text{mol}$ )	1 mL	33% HBr/ CH <sub>3</sub> COOH (0.74 mL, 4.22 mmol, 10 eq of Cbz)	2.5 h, 25 °C	Bu- Cys <sub>17</sub>	60.2 mg
4	Bu-CbzCys <sub>18</sub> (176 mg, 4330, 40.6 $\mu\text{mol}$ )	2 mL	33% HBr/ CH <sub>3</sub> COOH (1 mL, 5.70 mmol, 10 eq of Cbz)	3 h, 25 °C	Bu- Cys <sub>18</sub>	88.5 mg
5	Bu-CbzCys <sub>18</sub> (56 mg, 4330, 12.9 $\mu\text{mol}$ )	1 mL	33% HBr/ CH <sub>3</sub> COOH (0.5 mL, 2.85 mmol, 10 eq of Cbz)	3 h, 25 °C	Bu- Cys <sub>18</sub>	30.0 mg

### 3.4 Syntheses of PFD filled triblock polypeptide capsules

#### 3.4.1 Synthesis of the homopolymers, the diblock-peptide, and the triblock-peptide

##### 3.4.1.1 Synthesis of Bu-BnAsp<sub>m</sub>

NPBnAsp (variable equivalents to the initiator) was dissolved in anhydrous DMAc, and then n-butylamine, was added into the above solution under the protection of nitrogen. The reaction was allowed to proceed for 1-3 d at 60 °C. Subsequently, the reaction mixture was precipitated into a large amount of diethyl ether, filtered, washed with diethyl ether, and dried under vacuum for 24 h to get the final product as a white solid.

##### 3.4.1.2 Synthesis of Bu-BnAsp<sub>m</sub>-CbzCys<sub>c</sub> or Bu-BnAsp<sub>m</sub>-BnCys<sub>c</sub>

Bu-BnAsp<sub>m</sub> was dissolved in anhydrous DMAc, and then NPBnCys or NNPCBzCys (variable equivalents to the initiator), was added into the above solution under the protection of nitrogen. The reaction was allowed to proceed for 1-3 d at 60 °C. Subsequently, the reaction mixture was precipitated into a large amount of diethyl ether, filtered, washed with diethyl ether, and

dried under vacuum for 24 h to get the final product as yellow solid.

### 3.4.1.3 Synthesis of Bu-BnAsp<sub>m</sub>-CbzCys<sub>c</sub>-Phe<sub>n</sub> or Bu-BnAsp<sub>m</sub>-BnCys<sub>c</sub>-Phe<sub>n</sub>

Bu-BnAsp<sub>m</sub>-CBzCys<sub>c</sub> or Bu-BnAsp<sub>m</sub>-BnCys<sub>c</sub> was dissolved in anhydrous DMAc, and then NPPhe (variable equivalents to the initiator), was added into the above solution under the protection of nitrogen. The reaction was allowed to proceed for 1-3 d at 60 °C. Subsequently, the reaction mixture was precipitated into a large amount of diethyl ether, filtered, washed with diethyl ether, and dried under vacuum for 24 h to get the final product as white.

Table 3.6 Summarized syntheses of Bu-BnAsp<sub>m</sub>-CbzCys<sub>c</sub>-Phe<sub>n</sub>.

Synthesis	Initiator	Monomer	Temperature	Product	Quantity	Yield
1.1	Butylamine (13.1 mg, 73.14, 0.179 mmol)	NPBnAsp (3.03 g, 338, 8.96 mmol, 50 eq.)	60 °C	Bu-BnAsp <sub>31</sub>	1.02 g	55.5 %
1.2	Bu-BnAsp <sub>31</sub> (500 mg, 6400, 0.078 mmol)	NNPCBzCys (1.35 g, 420, 2.5 mmol, 32 eq.)	60 °C	Bu-BnAsp <sub>31</sub> -CbzCys <sub>5</sub>	700 mg	55.6 %
1.3.1	Bu-BnAsp <sub>31</sub> -CbzCys <sub>5</sub> (300 mg, 7600, 0.039 mmol)	NPPhe (111.1 mg, 285, 0.39 mmol, 10 eq.)	60 °C	Bu-BnAsp <sub>31</sub> -CbzCys <sub>5</sub>	230 mg	64.4 %
1.3.2	Bu-BnAsp <sub>31</sub> -CbzCys <sub>5</sub> (200 mg, 7600, 0.026 mmol)	NPPhe (300 mg, 285, 1.05 mmol, 40 eq.)	60 °C	Bu-BnAsp <sub>31</sub> -CbzCys <sub>5</sub> -Phe <sub>4</sub>	230 mg	64.8 %
2.1	Butylamine (34.7 mg, 73.14, 0.474 mmol)	NPBnAsp (8 g, 338, 23.7 mmol, 50 eq.)	60 °C	Bu-BnAsp <sub>40</sub>	3.85 g	79.3 %
2.2	Bu-BnAsp <sub>40</sub> (514 mg, 8250, 0.062 mmol)	NNPCbzCys (840 mg, 420, 2 mmol, 33 eq.)	30 °C	Bu-BnAsp <sub>40</sub> -CbzCys <sub>10</sub>	688 mg	68.9 %
2.3	Bu-BnAsp <sub>40</sub> -CbzCys <sub>10</sub> (305 mg, 10600, 0.029 mmol)	NNPPhe (280 mg, 330, 0.85 mmol, 28 eq.)	30 °C	Bu-BnAsp <sub>40</sub> -CbzCys <sub>10</sub> -Phe <sub>5</sub>	330 mg	76.7 %

Table 3.7 Summarized syntheses of Bu-BnAsp<sub>m</sub>-BnCys<sub>c</sub>-Phe<sub>n</sub>.

Synthesis	Initiator	Monomer	Time	Product	Quantity	Yield
1.1	Butylamine (21.9 mg, 73.14, 0.3 mmol)	NNPBnAsp (1.23g, 388, 3.17 mmol, 10.6 eq.)	1 d	Bu-BnAsp <sub>6</sub>	350 mg	53%
1.2	Bu-BnAsp <sub>6</sub> (307 mg, 1300, 0.24 mmol)	NPBnCys (888 mg, 331, 2.7 mmol, 11.3 eq.)	1 d	Bu-BnAsp <sub>6</sub> -BnCys <sub>3</sub>	400 mg	48.5 %
1.3	Bu-BnAsp <sub>6</sub> -BnCys <sub>3</sub> (386.7 mg, 1880, 0.206 mmol)	NPBnCys (773 mg, 331, 2.3 mmol, 11.3 eq.)	3 d	Bu-BnAsp <sub>6</sub> -BnCys <sub>8</sub>	582 mg	69.5 %
1.4	Bu-BnAsp <sub>6</sub> -BnCys <sub>8</sub> (520 mg, 2850, 0.182 mmol)	NPPhe (627 mg, 285, 2.2 mmol, 11 eq.)	3 d	Bu-BnAsp <sub>6</sub> -BnCys <sub>8</sub> -PPhe <sub>8</sub>	740 mg	87.8 %
2.1	Butylamine (28.7 mg, 73.14, 0.393 mmol)	NNPBnAsp (3.05 g, 388, 7.86 mmol, 20 eq.)	1 d	Bu-BnAsp <sub>13</sub>	857 mg	53.2 %
2.2	Bu-BnAsp <sub>13</sub> (400 mg, 2740, 0.146 mmol)	NPBnCys (520 mg, 331, 1.57 mmol, 10.8 eq.)	1 d	Bu-BnAsp <sub>13</sub> -BnCys <sub>6</sub>	520 mg	74.0 %
2.3	Bu-BnAsp <sub>13</sub> -BnCys <sub>6</sub> (490 mg, 3900, 0.126 mmol)	NPPhe (378 mg, 285, 1.33 mmol, 10.6 eq.)	1 d	Bu-BnAsp <sub>13</sub> -BnCys <sub>6</sub> -Phe <sub>7</sub>	605 mg	88.3 %
3.1	Butylamine (34.5 mg, 73.14, 0.472 mmol)	NPBnAsp (2 g, 338, 5.9 mmol, 12.5 eq.)	3 d	Bu-BnAsp <sub>7</sub>	861.4 mg	71.0 %
3.2	Bu-BnAsp <sub>7</sub> (230 mg, 1500, 0.147 mmol)	NPBnCys (730 mg, 331, 2.2 mmol, 15 eq.)	2 d	Bu-BnAsp <sub>7</sub> -BnCys <sub>15</sub>	465 mg	70.8 %
3.3	Bu-BnAsp <sub>7</sub> -BnCys <sub>15</sub> (370 mg, 4400, 0.084 mmol)	NPPhe (65 mg, 285, 0.23 mmol, 2.7 eq.)	2 d	Bu-BnAsp <sub>7</sub> -BnCys <sub>15</sub> -Phe <sub>2</sub>	330 mg	81.7 %

Table 3.8 Summarized syntheses of DBnAsp-BnAsp<sub>m</sub>-BnCys<sub>c</sub>-Phe<sub>n</sub>.

Synthesis	Initiator	Monomer	Time	Product	Quantity	Yield
1	DBnAsp (135 mg, 313, 0.43 mmol)	NNPBnAsp (2.56 g, 388 g/mol, 6.6 mmol, 15 eq.)	2 d	DBnAsp-BnAsp <sub>7</sub>	550 mg	40.7 %
2	DBnAsp-BnAsp <sub>7</sub> (514 mg, 1940, 0.265 mmol)	NPBnCys (508 mg, 331, 1.53 mmol, 5.8 eq.)	1 d	DBnAsp – BnAsp <sub>7</sub> -BnCys <sub>5</sub>	650 mg	80.2 %
3	DBnAsp-BnAsp <sub>7</sub> -BnCys <sub>5</sub> (500 mg, 2900, 0.172 mmol)	NPPhe (198 mg, 285, 0.69 mmol, 4 eq.)	1 d	DBnAsp-BnAsp <sub>7</sub> -BnCys <sub>5</sub> -Phe <sub>2</sub>	510 mg	84.7 %

#### 3.4.1.4 Synthesis of Asp<sub>m</sub>-Cys<sub>c</sub>-Phe<sub>n</sub> or Bu-Asp<sub>m</sub>-Cys<sub>c</sub>-Phe<sub>n</sub>

Bu-BnAsp<sub>m</sub>-CbzCys<sub>c</sub>-Phe<sub>n</sub> was dispersed in 3 mL of CF<sub>3</sub>COOH, then triflic acid or 33% HBr/CF<sub>3</sub>COOH (10 eq. of the protecting groups) was added into the above solution under the protection of nitrogen. The reaction was allowed to proceed for 6 h at 25 °C. Subsequently, the reaction mixture was precipitated into a large amount of diethyl ether and washed with diethyl ether. Finally, it was dried under vacuum to get the raw product as a brown solid.

Table 3.9 Summarized de-protection reaction of triblock polypeptide.

Syntheses	Protected peptide	Solvent	Acid	Product	Quantity
1	Bu-BnAsp <sub>31</sub> -CbzCys <sub>5</sub> -Phe <sub>4</sub> (140 mg, 8200, 17 μmol)	3 mL TFA	1 mL 33% HBr/CH <sub>3</sub> COOH	Bu-Asp <sub>31</sub> -Cys <sub>5</sub> -Phe <sub>4</sub>	100 mg, 4700, 21 μmol
2	Bu-BnAsp <sub>40</sub> -CbzCys <sub>5</sub> -Phe <sub>5</sub> (195 mg, 10200, 19.1 μmol)	2 mL TFA	1 mL 33% HBr/CH <sub>3</sub> COOH	Bu-Asp <sub>40</sub> -Cys <sub>10</sub> -Phe <sub>5</sub>	-
3	Bu-BnAsp <sub>6</sub> -BnCys <sub>8</sub> -Phe <sub>8</sub> (66 mg, 4000, 16.5 μmol)	5 mL CH <sub>2</sub> Cl <sub>2</sub>	CF <sub>3</sub> SO <sub>3</sub> H (1 mL, 11.3 mmol/mL, 11.3 mmol)	Bu-Asp <sub>6</sub> -Cys <sub>8</sub> -Phe <sub>8</sub>	43 mg, 2670, 16 μmol
4	Bu-BnAsp <sub>13</sub> -BnCys <sub>6</sub> -Phe <sub>7</sub> (191.9 mg, 4920, 0.039 mmol)	5 mL CH <sub>2</sub> Cl <sub>2</sub>	CF <sub>3</sub> SO <sub>3</sub> H (1 mL, 11.3 mmol/mL, 11.3 mmol)	Bu-Asp <sub>13</sub> -Cys <sub>6</sub> -Phe <sub>7</sub>	140 mg, 3210, 43 μmol
5	Bu-BnAsp <sub>7</sub> -BnCys <sub>15</sub> -	3 mL	CF <sub>3</sub> SO <sub>3</sub> H (1	Bu-Asp <sub>7</sub> -Cys <sub>15</sub> -	280 mg,

	Phe <sub>2</sub> (250 mg, 4700, 0.053 mmol)	TFA	mL, 11.3 mmol/mL, 11.3 mmol)	Phe <sub>2</sub>	2700, 104 μmol
6	DBnAsp-BnAsp <sub>8</sub> -BnCys <sub>5</sub> -Phe <sub>2</sub> (120 mg, 3200, 0.0375 mmol)	5 mL CH <sub>2</sub> Cl <sub>2</sub>	CF <sub>3</sub> SO <sub>3</sub> H (1 mL, 11.3 mmol/mL, 11.3 mmol)	Asp <sub>8</sub> -Cys <sub>5</sub> -Phe <sub>2</sub>	100 mg, 1840, 54 μmol

#### 3.4.2 Synthesis of nanocapsules

10-30 mg polypeptide was dispersed in 10 mL water and a few drops of sodium hydroxide aqueous solution (1 M) was added into it under stirring. 3 eq. of DTT was added to the above solution or dispersion and the mixture was stirred for half hour to fully reduce all disulfide bridges into free thiol groups. Then 50-200 μL PFD was added to the above mixture and the mixture was treated with ultrasonication (60% power) for 3 min to obtain the emulsion. The above obtained emulsion was treated with 5-10 eq. of 35% hydrogen peroxide aqueous solution under stirring for 30 min for crosslinking of cysteine residue to solidify the capsules. Finally, the capsules were prepared after dialysis against water over night.

### 3.5 Devices used

#### 3.5.1 Nuclear magnetic resonance spectroscopy

The DRX500 spectrometer from Bruker was used for the measurements of <sup>1</sup>H NMR spectra to study the structure of the synthesized monomer and the oligomers. Some of the measurements were helped by Dr. Torsten Schaller from the working group of Prof. Dr. Schrader.

The Avance 500 spectrometer from Bruker was used for the measurements of <sup>19</sup>F NMR and <sup>19</sup>F PFG NMR to study the gas exchange rate of capsules and diffusion constant of capsules. All the measurements were conducted by Dr. Juergen Linders from the working group of Prof. Dr. Mayer.

#### 3.5.2 UV-vis spectroscopy

UV-1900i UV-Vis spectrophotometer from Shimadzu was used for the measurement of UV-vis spectra to test the thiol group content of oligo- or poly-peptides.

#### 3.5.3 MALD-TOF Mass spectroscopy

The Bruker Autoflex speed from Bruker was used for the measurements of molecular mass and molecular mass distribution of oligo- or poly-peptides. All the measurements were conducted by Dr. Florian Uteschil from the working group of Prof. Dr. Schmitz.

#### 3.5.4 Gel permeation chromatography

The GPC system (with column from polymer standards service (PSS), pump PU 2008 Plus from Jasco, detector ETA-2020 from WGE) was used for the measurements of molecular weight distribution of oligo- or poly-peptides. All the measurements were conducted by Mr. Sebastian Buchholz from the working group of Prof. Dr. Ulbricht.

#### 3.5.5 Atomic force microscopy

NanoWizard AFM from JPK Instruments (Berlin, Germany) was used for the measurements of the morphology of capsules. All samples were prepared by drying a drop of the capsule dispersion on a normal glass. All measurements were conducted under noncontact mode with noncontact mode cantilevers from NanoWorld (Neuchatel, Switzerland).

#### 3.5.6 Dark-field microscopy

Dark-field microscope combined with a Phytec FCAM-011H camera and a nanoparticle tracking program was used for the measurements of the size distribution of capsules.

## 4 Results and discussion

### 4.1 Investigation of PFD in water emulsions stabilized by di-block polypeptides

#### 4.1.1 Discussion of activated monomers and polymers

The synthesis route of di-block peptide is shown in Figure 4.1.

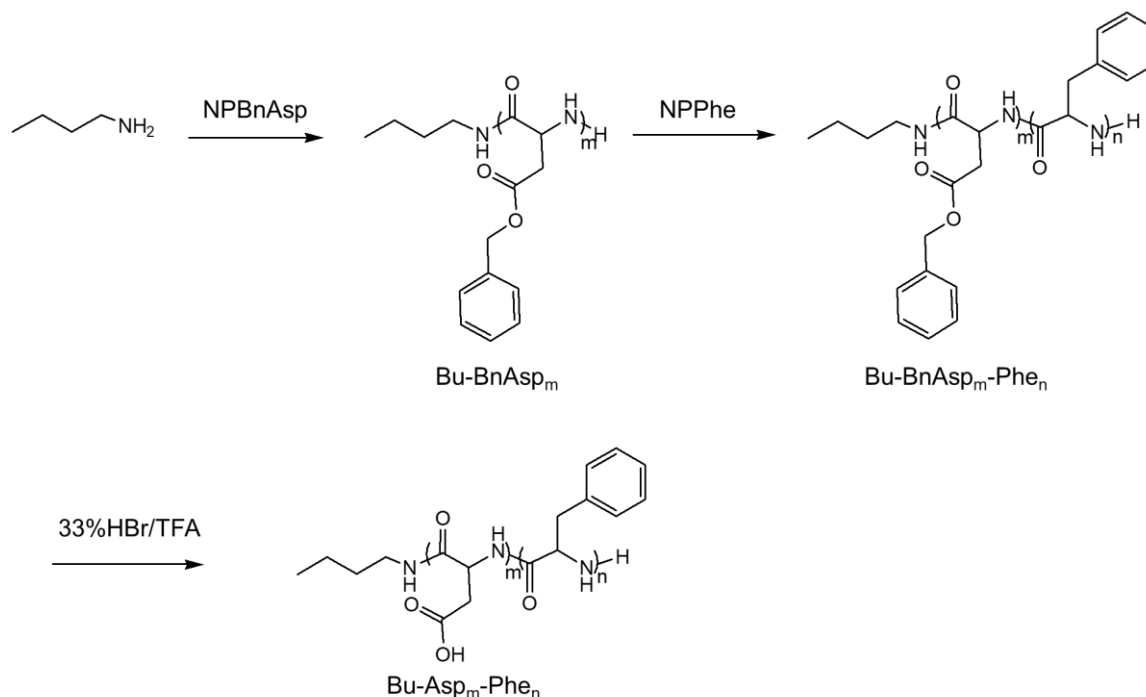


Figure 4.1 Synthetic route for di-block peptide.

The  $^1\text{H}$  NMR spectra of monomers, protected polypeptides and deprotected polypeptides are shown in the appendices (Figure 7.1- Figure 7.9).

During the synthesis of Bu-BnAsp<sub>40</sub>, no precipitation or gelation was observed and the reaction solvent remains clear, because Bu-BnAsp<sub>40</sub> is well soluble in DMAc. During the synthesis of three di-block peptide, Bu-BnAsp<sub>40</sub>-Phe<sub>5</sub>, Bu-BnAsp<sub>40</sub>-Phe<sub>9</sub>, Bu-BnAsp<sub>40</sub>-Phe<sub>14</sub>, the solvent became more and more turbid with the increase of the hydrophobic block Phe content (Figure 4.2). This turbidity phenomenon is due to the formation of Phe block in a  $\beta$ -sheet structure which are generally insoluble in DMAc [44], which reduced the solubility of the peptide in DMAc.

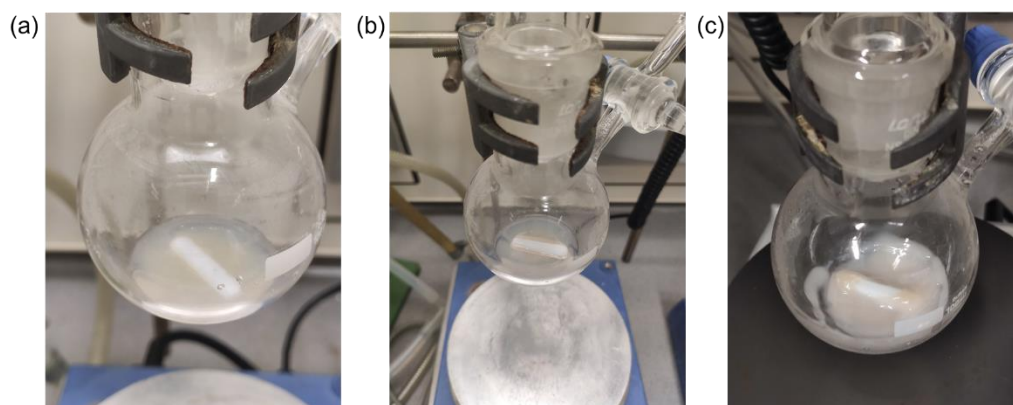


Figure 4.2 Photos of the reaction DMAC solution after two days' reaction of di-block peptides. (a) Bu-BnAsp<sub>40</sub>-Phe<sub>5</sub>. (b) Bu-BnAsp<sub>40</sub>-Phe<sub>9</sub>. (c) Bu-BnAsp<sub>40</sub>-Phe<sub>14</sub>.

After de-protection reaction, we tested the water solubility of each di-block peptide. The water solubility of deprotected di-block peptides, Asp<sub>40</sub>-Phe<sub>5</sub>, Asp<sub>40</sub>-Phe<sub>9</sub>, Asp<sub>40</sub>-Phe<sub>14</sub>, also decreases with the increase of the hydrophobic block Phe content. After removal of benzyl groups of BnAsp block, each di-block peptide was dispersed into 0.1 M NaOH aqueous solution to prepare peptide solution or dispersion with a concentration of 10 mg/mL (Figure 4.3). The solution of Asp<sub>40</sub>-Phe<sub>5</sub> is almost clear, very close to Bu-Asp<sub>40</sub> solution. For Asp<sub>40</sub>-Phe<sub>9</sub>, the solution looks a little bit unclear but the peptide is well dispersed. For Asp<sub>40</sub>-Phe<sub>14</sub>, the solution looks very turbid and many peptides still remain undispersed at the bottom of the bottle.

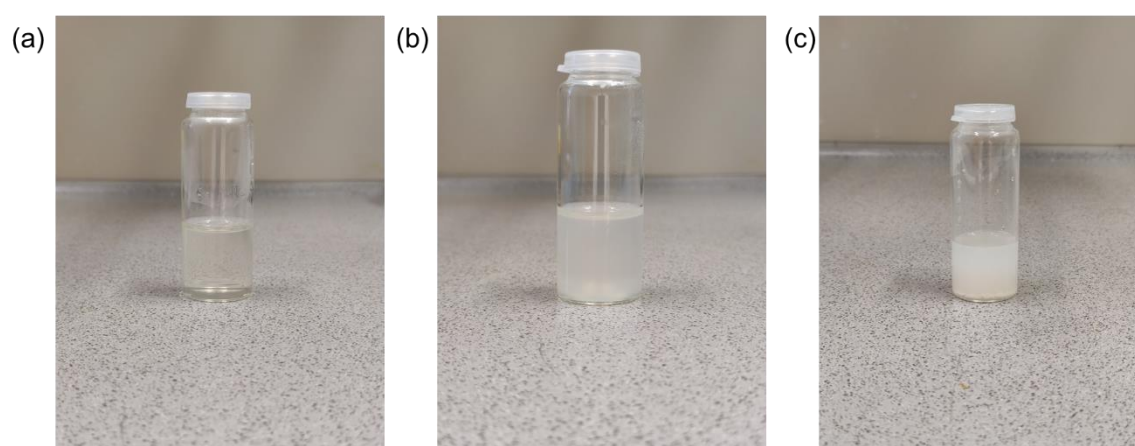


Figure 4.3 Photos of the di-block peptide 0.1 M NaOH aqueous solution or dispersion. (a) Bu-Asp<sub>40</sub>-Phe<sub>5</sub>. (b) Bu-Asp<sub>40</sub>-Phe<sub>9</sub>. (c) Bu-Asp<sub>40</sub>-Phe<sub>14</sub>. (NaOH is used to help the Asp block be soluble in water)

### 4.1.2 Discussion of PFD in water emulsions

The emulsification properties of three di-block peptides were studied. 500  $\mu\text{L}$  of PFD was added to 10 mL peptide aqueous solution or dispersion containing 25 mg peptide and 10 mg NaOH. After the PFD/peptide/water mixture was treated with ultra-sonication (60 % power) in an ice bath for 2 min, the PFD in water emulsion was prepared. The emulsions stabilized by the three di-block peptides, Bu-Asp<sub>40</sub>-Phe<sub>5</sub> and Bu-Asp<sub>40</sub>-Phe<sub>9</sub>, Bu-Asp<sub>40</sub>-Phe<sub>14</sub> were all well dispersed and the PFD droplets would settle down slowly after 1 d due to the density differences between PFD and water. The emulsion can be re-dispersed easily by shaking the bottle gently. The photos of the emulsions stabilized by the three di-block peptide was shown in Figure 4.4.

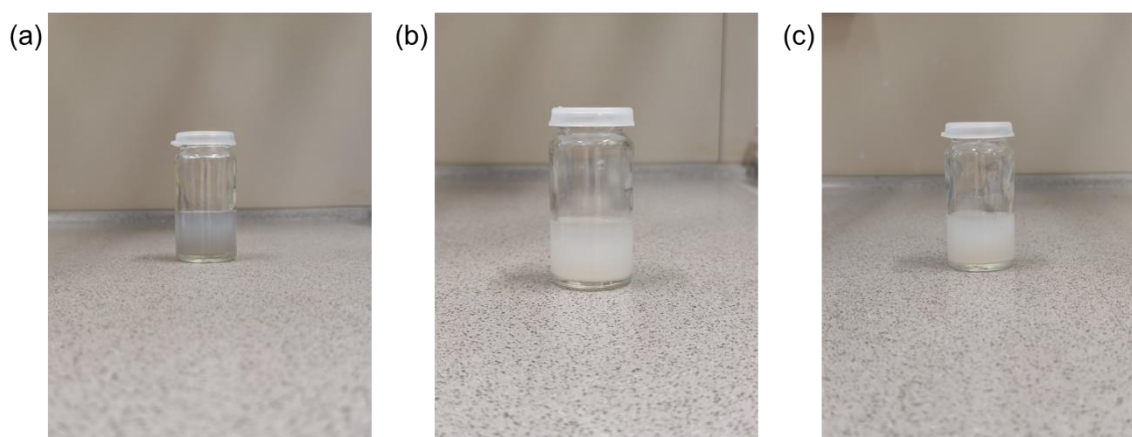


Figure 4.4 Photos of the PFD emulsions stabilized by different di-block peptide. (a) Bu-Asp<sub>40</sub>-Phe<sub>5</sub>. (b) Bu-Asp<sub>40</sub>-Phe<sub>9</sub>. (c) Bu-Asp<sub>40</sub>-Phe<sub>14</sub>. PFD volume fraction is 5%.

All the emulsions were observed using dark-field microscopy (DM). Taking PFD emulsions stabilized by Bu-Asp<sub>40</sub>-Phe<sub>14</sub> as an example, the emulsion was diluted 100-fold with water and was observed using DM. Only 1 or 2 nanoparticles (bright dots) were observed doing Brownian motion and nothing else can be found in the dark background. However, many dark dots were found doing Brownian motion when we brightened the background as shown in Figure 4.5. These dark dots should be the PFD droplets which may have a diameter in the micrometer scale. These results indicate that DM may be not suitable for the detection of emulsion droplets, as these droplets couldn't efficiently deflect light into the microscope.

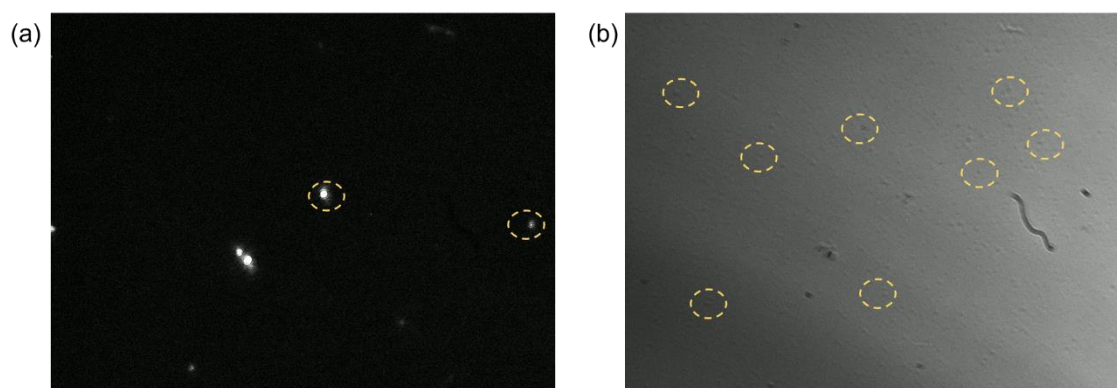


Figure 4.5 Dilute PFD in water emulsions stabilized by Bu-Asp<sub>40</sub>-Phe<sub>14</sub> under dark-field (a) and bright-field (b) conditions. Yellow circles are some examples.

Increasing the input energy into the emulsion can decrease the size of emulsion droplets. Therefore, two strategies, including extending ultra-sonication period (60% power for 5 min) and increasing ultra-sonication power (70% power for 2 min), were used to input more energy into the emulsion. However, the PFD droplets were still detectable under bright field conditions, which may indicate a diameter of droplets that is in the micrometer scale. Increasing the input energy doesn't work when the emulsifier is not sufficient to cover all the interfaces between oil droplets and water. Therefore, emulsion containing the same peptide concentration but small PFD volume fraction (1%) was prepared. However, still many dark dots under bright field conditions were observed, which indicate a large number of droplets with diameter in a micrometer scale.

Then all emulsions (1% PFD volume fraction) were investigated by AFM. Figure 4.6 shows the dilute PFD filled Asp<sub>40</sub>-Phe<sub>5</sub> emulsions. Most emulsion structures are collapsed, and the diameter of them ranges from around 400 nm (K3) to 1100 nm (K1).

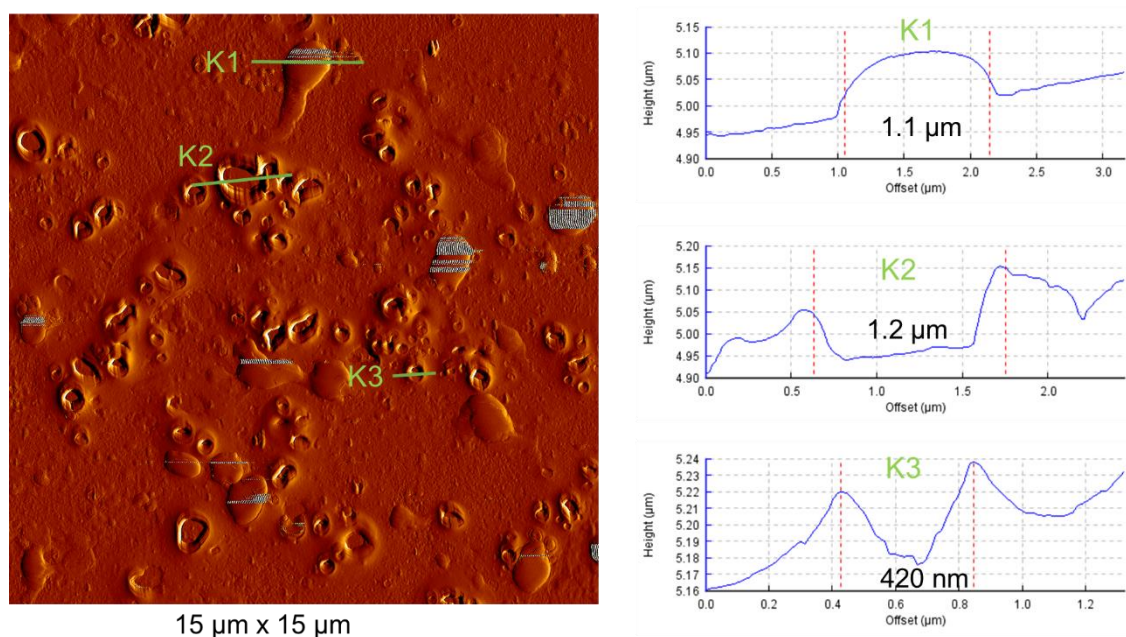


Figure 4.6 AFM image of a diluted sample of a PFD-filled Asp<sub>40</sub>-Phe<sub>5</sub> emulsion.

Figure 4.7 shows the diluted PFD-filled Asp<sub>40</sub>-Phe<sub>14</sub> emulsions. Apart from many collapsed structures with diameter ranging from around 550 nm to 1200 nm, many self-assembled polypeptide micelles, which are well dispersed around PFD droplets, are observed as well.

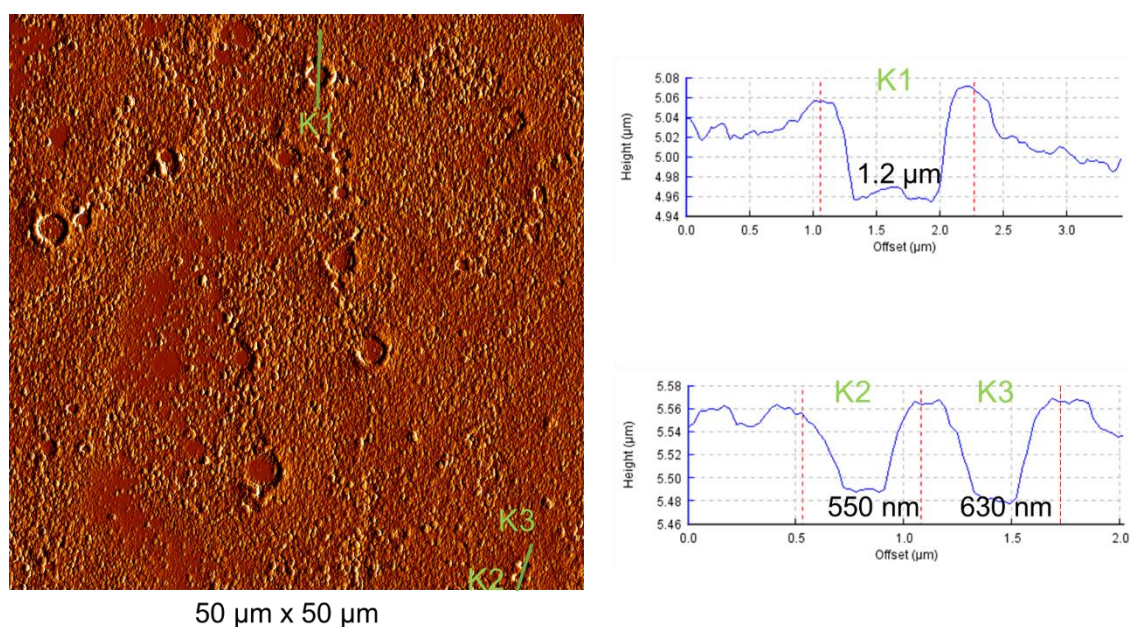


Figure 4.7 AFM image of a diluted PFD filled Asp<sub>40</sub>-Phe<sub>14</sub> emulsion.

Because Asp<sub>40</sub>-Phe<sub>14</sub> has large content of Phe unit, they can self-assembled into micelles.

Therefore, Asp<sub>40</sub>-Phe<sub>14</sub> micelles were prepared by ultra-sonication of Asp<sub>40</sub>-Phe<sub>14</sub> into water. Figure 4.8 shows the diluted Asp<sub>40</sub>-Phe<sub>14</sub> micelles. Many micelles are observed and they have diameters ranging from around 75 nm to 300 nm. Therefore, the nanoparticles observed in Figure 4.7 may be Asp<sub>40</sub>-Phe<sub>14</sub> micelles instead of PFD filled capsules.

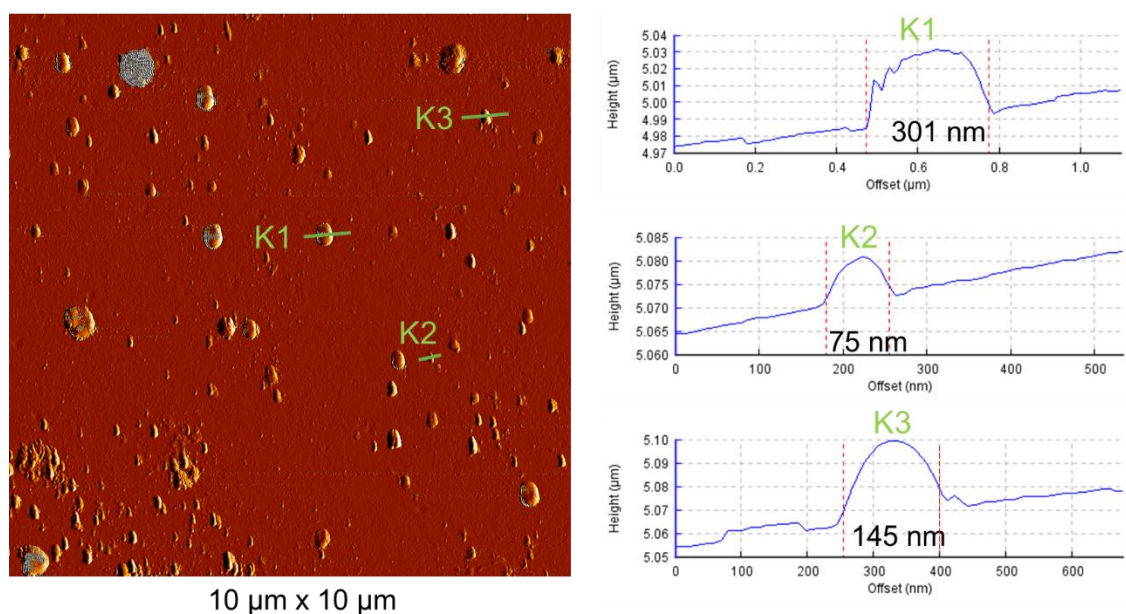


Figure 4.8 AFM image of diluted Asp<sub>40</sub>-Phe<sub>14</sub> micelles.

## 4.2 Comparison of polycysteine synthesized from differently protected cysteines

### 4.2.1 Discussion of activated monomers

The synthesis routes for the three monomers are shown in Figure 4.9.

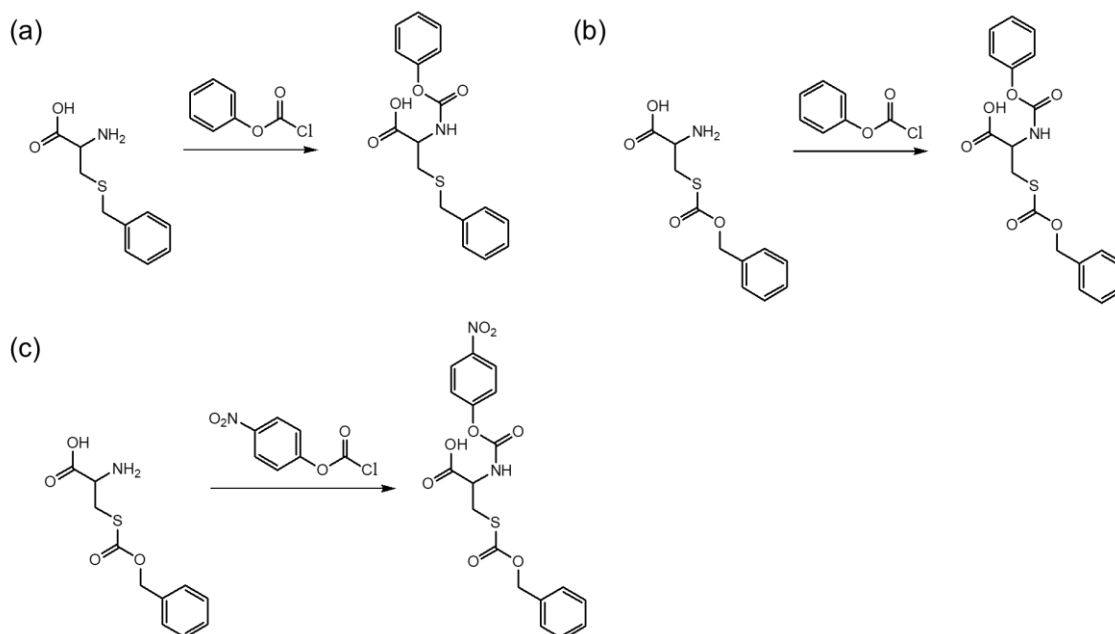


Figure 4.9 Synthesis route of activated protected cysteines, including (a) NPBnCys, (b) NPCbzCys, and (c) NNPCbzCys.

The syntheses of the three monomers are successful and their corresponding  $^1\text{H}$  NMR spectra are shown in the appendices (Figure 7.10- Figure 7.12).

#### 4.2.2 Discussion of polymerization of each monomer

The polymerization of the three monomers is shown in Figure 4.10.

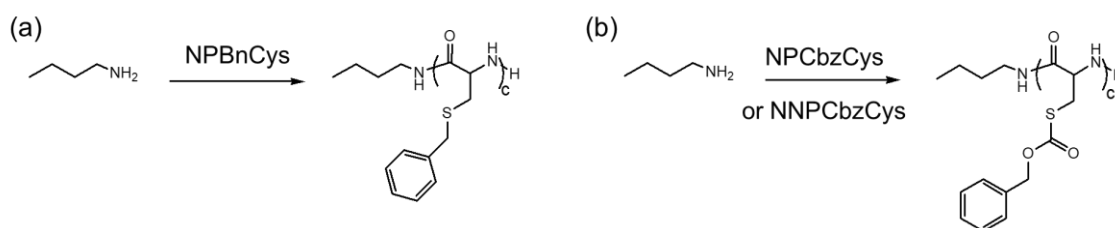


Figure 4.10 Syntheses of protected oligo- or poly-cysteine, including (a) oligo- or poly-BnCys and (b) oligo- or poly-CbzCys.

Monomer N-phenoxycarbonyl-S-carbobenzyloxy-L-cysteine (NPCbzCys) was unable to polymerize at all, possibly due to its inefficiency of conversion to NCA, as reported by Endo et al [46]. N-(4-nitrophenoxycarbonyl)-S-carbobenzyloxy-L-cysteine (NNPCbzCys) has a more



Figure 4.12 shows the  $^1\text{H}$  NMR spectrum of Bu-CbzCys<sub>c</sub> obtained at 60 °C. The average degree of polymerization (DP) was calculated as around 8 according to the integrals of the signals a and h. While the average DP was calculated as around 5 according to the yield (17.9 %) and feed ratio between monomer and initiator (30). The higher DP of the product than that calculated from the yield may also due to the dissolution of some oligomers with lower DP in ether.

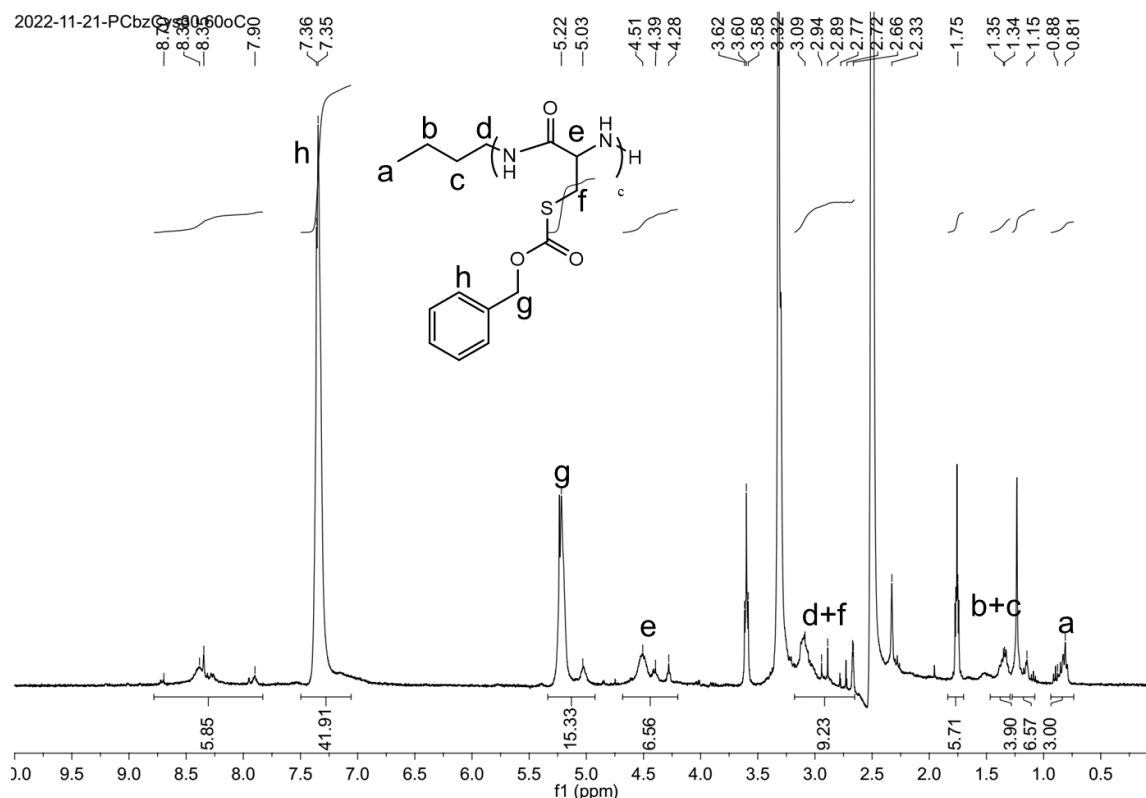


Figure 4.12  $^1\text{H}$  NMR spectrum of Bu-CbzCys<sub>c</sub> obtained at 60 °C (solvent: DMSO- $d_6$ ).

Figure 4.13 shows the  $^1\text{H}$  NMR spectrum of Bu-BnCys<sub>c</sub> obtained at 60 °C. The average DP was calculated as around 20 according to the integrals of the signals a and h. While the average DP was calculated as around 24 according to the yield (78.9%) and feed ratio between monomer and initiator (30). The DP calculated from the NMR results is lower than the DP calculated from the yield, which may be due to some loss of NMR signal caused by the incomplete dissolution of PBnCys in DMSO- $d_6$ . Therefore, the actual DP of PBnCys may be larger than 20.

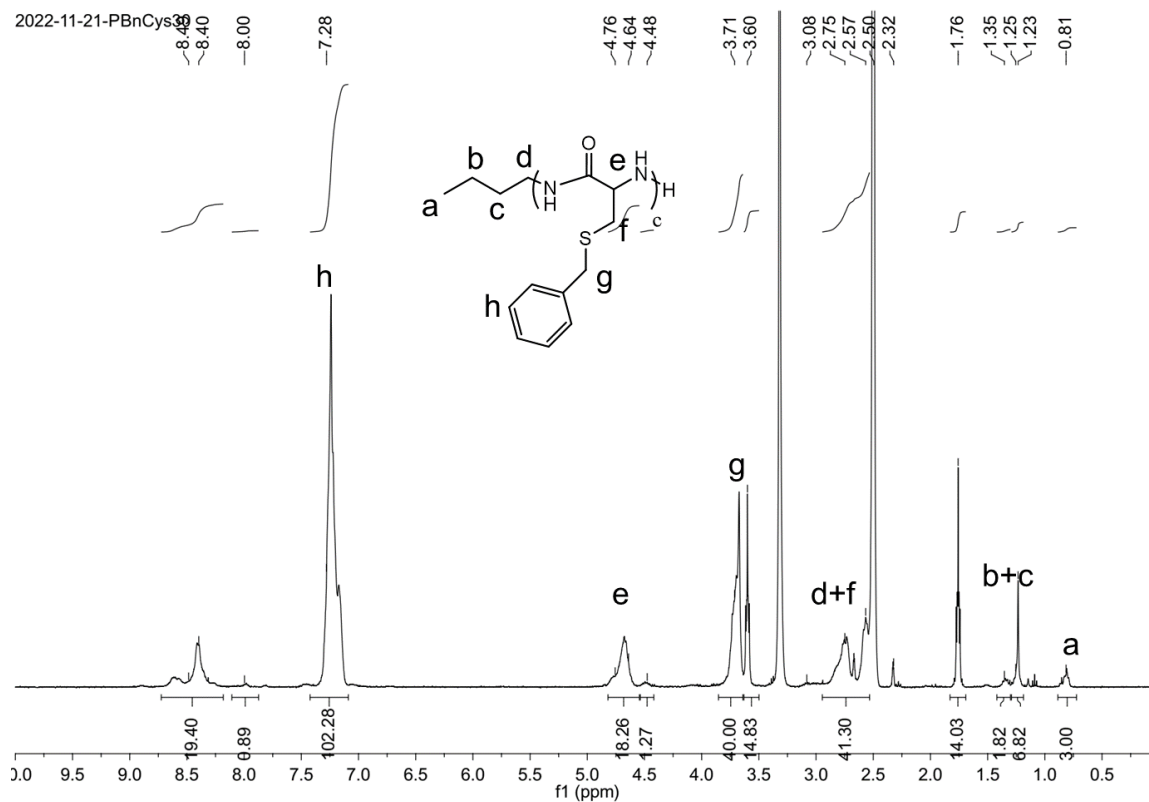
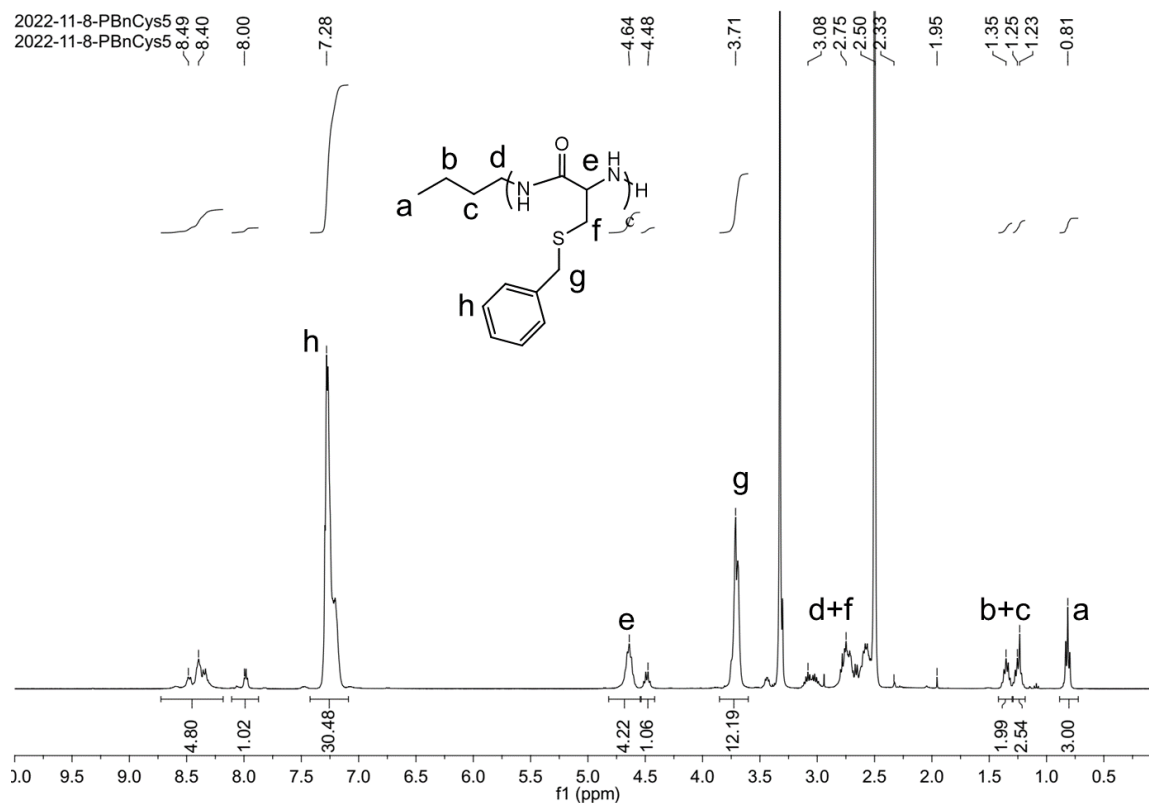
Figure 4.13 <sup>1</sup>H NMR spectrum of Bu-BnCys<sub>c</sub> obtained at 60 °C (solvent: DMSO-d<sub>6</sub>).Figure 4.14 <sup>1</sup>H NMR spectrum of Bu-BnCys<sub>c</sub> obtained at 60 °C (solvent: DMSO-d<sub>6</sub>).

Figure 4.14 shows the  $^1\text{H}$  NMR spectrum of Bu-BnCys<sub>c</sub> obtained at 60 °C with lower monomer to initiator ratio. The average DP was calculated as around 6 according to the integrals of the signals a and h. While the average DP was calculated as around 3.5 according to the yield (69%) and feed ratio between monomer and initiator (5). The higher DP of the product than that calculated from the yield may due to the dissolution of some oligomers with lower DP in ether.

The molecular size distribution of the two Bu-CbzCys<sub>c</sub> was analyzed by SEC. Bu-CbzCys<sub>c</sub> obtained at 30 °C showed an average Mw of 4284 and PDI of 1.52, and Bu-CbzCys<sub>c</sub> obtained at 60 °C showed an average Mw of 1102 and PDI of 1.82. The Mw of both Bu-CbzCys<sub>c</sub> obtained from SEC was consistent with that from  $^1\text{H}$  NMR spectra. Bu-BnCys<sub>c</sub> was not analyzed with SEC because it was partially soluble in DMAc, which are not allowed for SEC test. The PDI of Bu-BnCys<sub>c</sub> was estimated around 1.2 according to the report from Endo et al [45].

The terminal structure of the three protected oligo- or poly-cysteine were characterized by MALDI-TOF MS. Figure 4.15 showed the MALDI-TOF mass spectrum of Bu-BnCys<sub>c</sub> with a feed ratio between monomer and initiator 30: 1. Only one series of signals which is marked as series-A was observed in the spectrum, and it corresponds to polymers with mass values of around 2416, 2608, 2802, 2996, 3189 and 3382. These signals are regularly located with a spacing of about 193 Da, which is equal to the formula mass of the repeating unit of Bu-BnCys<sub>c</sub>. The molecular weight of peptide terminal was calculated as around 70. These mass values are consistent with the polymer structure which has a butylamine-derived initiating end and an amino group at the propagating end.

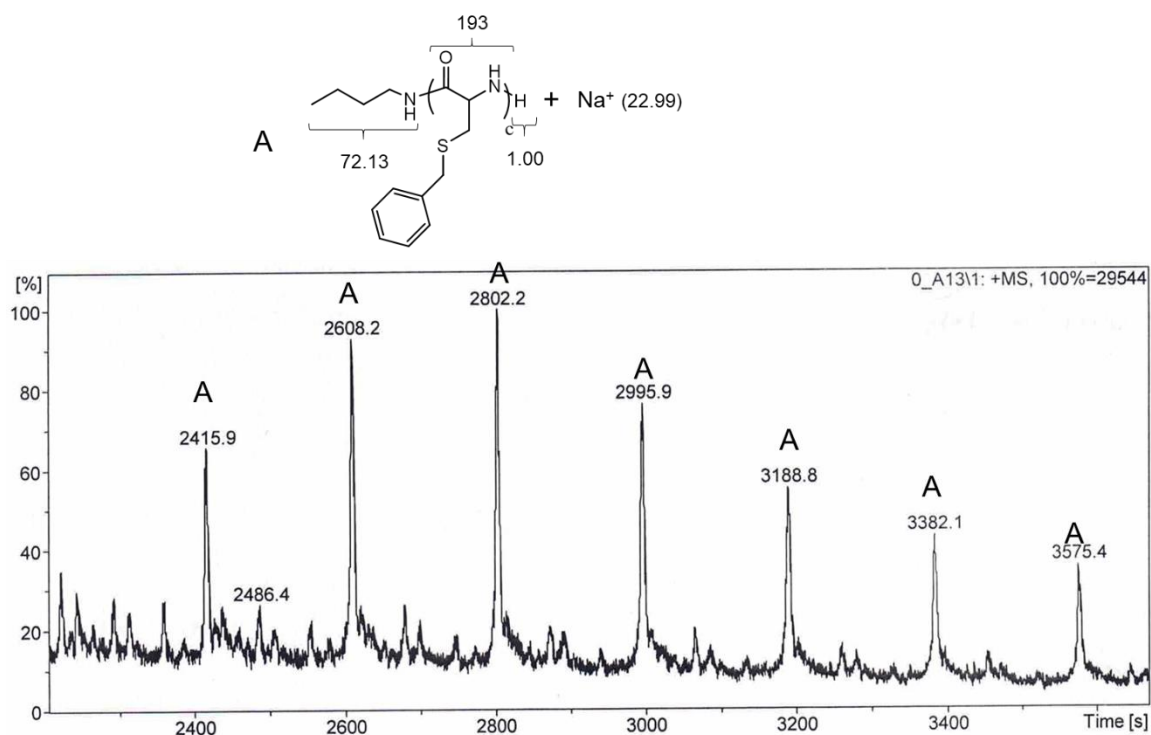


Figure 4.15 MALDI-TOF mass spectrum of Bu-BnCys<sub>c</sub>.

Figure 4.16 shows the MALDI-TOF mass spectrum of Bu-CbzCys<sub>c</sub> reacted at 60 °C. It seemed like there are several series of signals in the spectrum, and series-A signals was much stronger than the other series of signals. Series-A signals correspond to polymers with mass values of about 1353, 1591, 1828, 2065 and 2303. These signals are regularly located with a spacing of around 237 Da, which is equal to the formula mass of the repeating unit of Bu-CbzCys<sub>c</sub>. If there is no cleavage between protecting groups and amino acid residues, the molecular weight of peptide terminal (series-A) was calculated as around 45 or around 282, which is not in agreement with the two possible terminal structure (B and C) as shown in Figure 4.16. If one protecting group was removed during the measurement, the molecular weight of peptide terminal (series-A) was calculated as around 180 or around 417, which is still not in agreement with the two possible terminal structure (B and C) as shown in Figure 4.16. Some unknown intramolecular termination reaction may occur in this case.

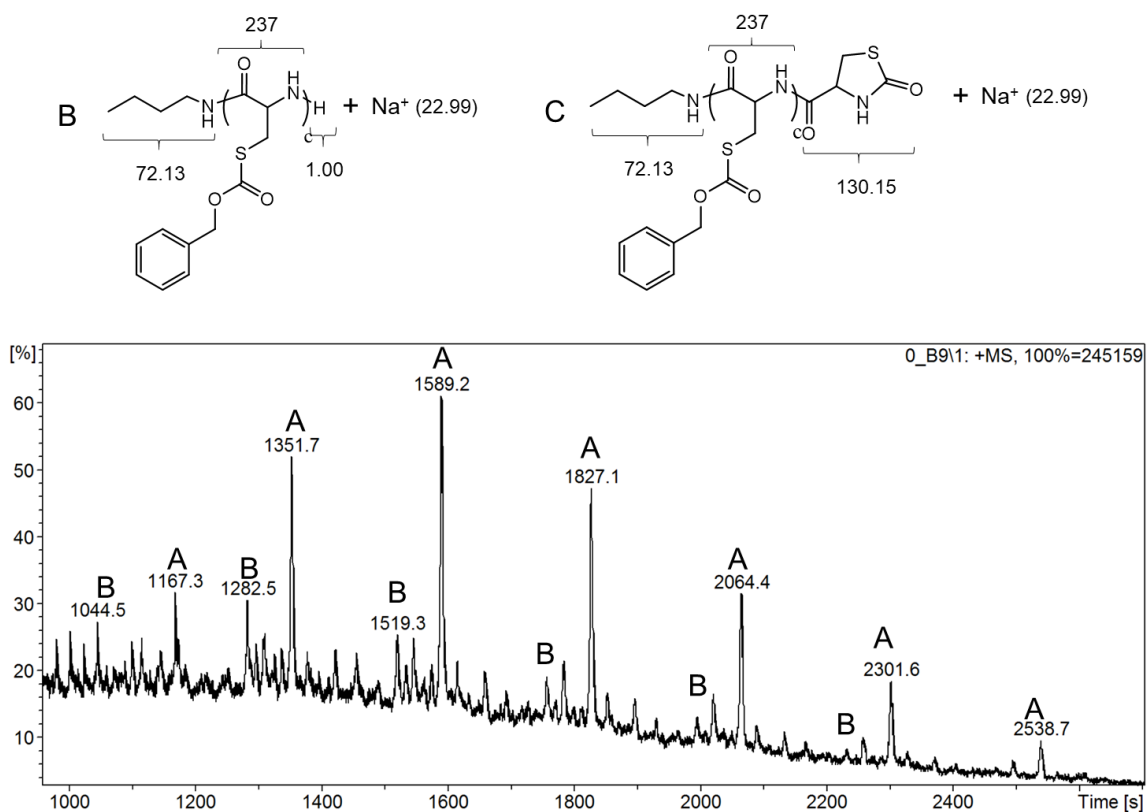


Figure 4.16 MALDI-TOF mass spectrum of Bu-CbzCys<sub>c</sub>.

Figure 4.17 shows the MALDI-TOF mass spectrum of Bu-CbzCys<sub>c</sub> reacted at 30 °C. The spectrum looked very nearly the same as that of Bu-CbzCys<sub>c</sub> reacted at 60 °C. Therefore, this spectrum will not be further discussed.

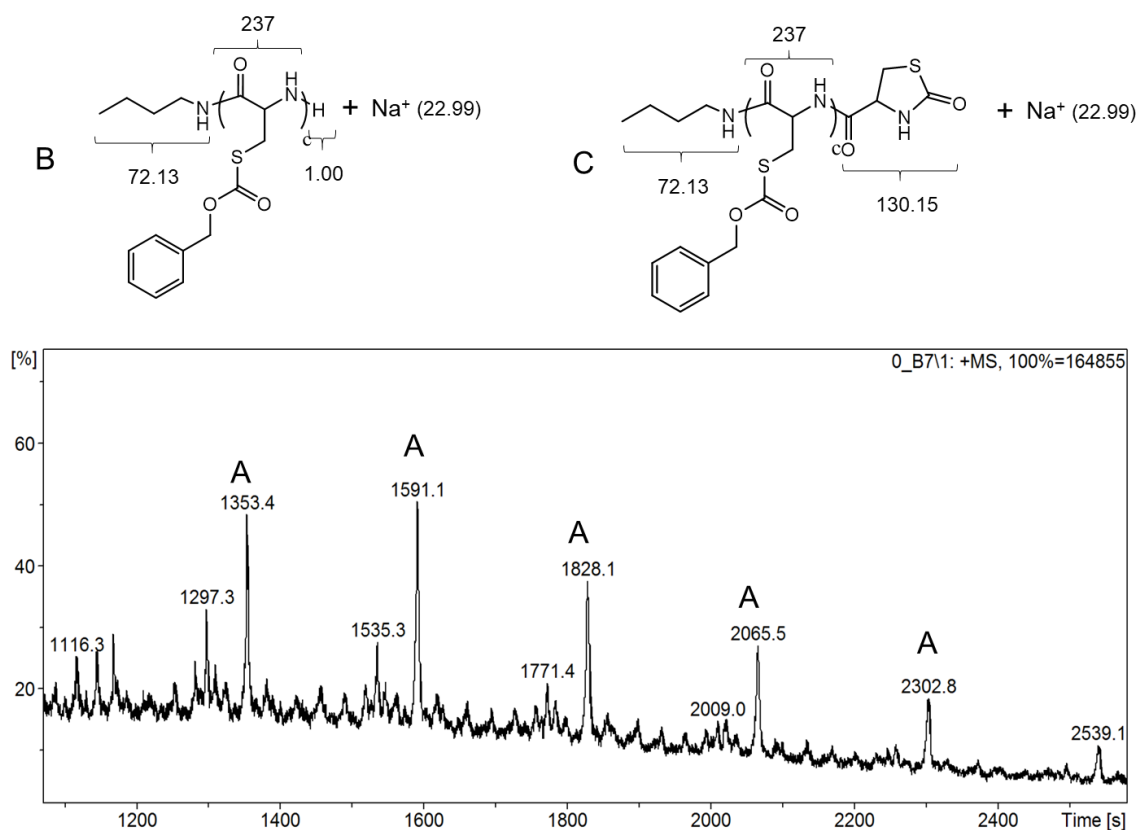


Figure 4.17 MALDI-TOF mass spectrum of Bu-CbzCys<sub>c</sub> reacted at 30 °C.

However, we were not sure when the intramolecular termination reaction occurs. It may take place before we precipitated the polymerization reaction mixture out of ether. It may also occur during the sample preparation for MALDI-TOF MS. Endo et al. studied the polymerization of *N*-(4-Nitrophenoxycarbonyl)- $\gamma$ -benzyl-L-glutamate in the presence of butylamine at 30 °C and they analyzed the terminal structure of the resulting poly- $\gamma$ -benzyl-L-glutamate by MALDI-TOF MS. They observed that if the reaction mixture was measured by MALDI-TOF MS, all poly- $\gamma$ -benzyl-L-glutamate had an amino terminal. However, when the formed poly- $\gamma$ -benzyl-L-glutamate was isolated by precipitation from ether and then analyzed by MALDI-TOF MS, the amino terminal was totally converted into the lactam moiety [23].

#### 4.2.3 Discussion of deprotection of polycysteine

The <sup>1</sup>H NMR spectra of each deprotected oligo- or poly-cysteine were shown in Figure 4.18 and Figure 4.19.

Figure 4.18 shows the <sup>1</sup>H NMR spectrum of Bu-Cys<sub>17</sub>. Only around 2.5 Cbz groups remain in

## 4 Results and discussion

each polymer chain according to the integrals of the signals a and h, which indicated that around 85% of Cbz groups was removed.

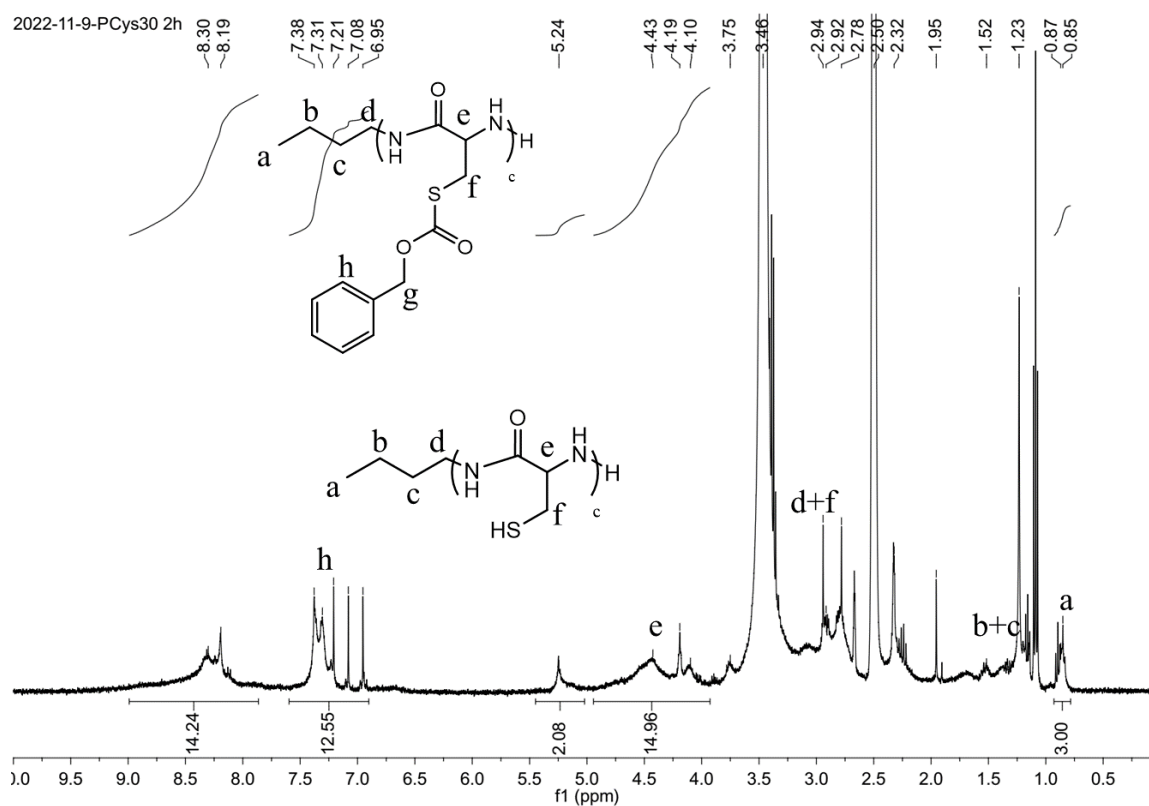


Figure 4.18  $^1\text{H}$  NMR spectrum of Bu-Cys<sub>17</sub> (solvent: DMSO- $d_6$ ).

Figure 4.19 shows the  $^1\text{H}$  NMR spectrum of Bu-Cys<sub>20</sub>. Only around 3 Bn groups remain in each polymer chain according to the integrals of the signals a and h, which indicated that around 85% of Bn groups was removed.

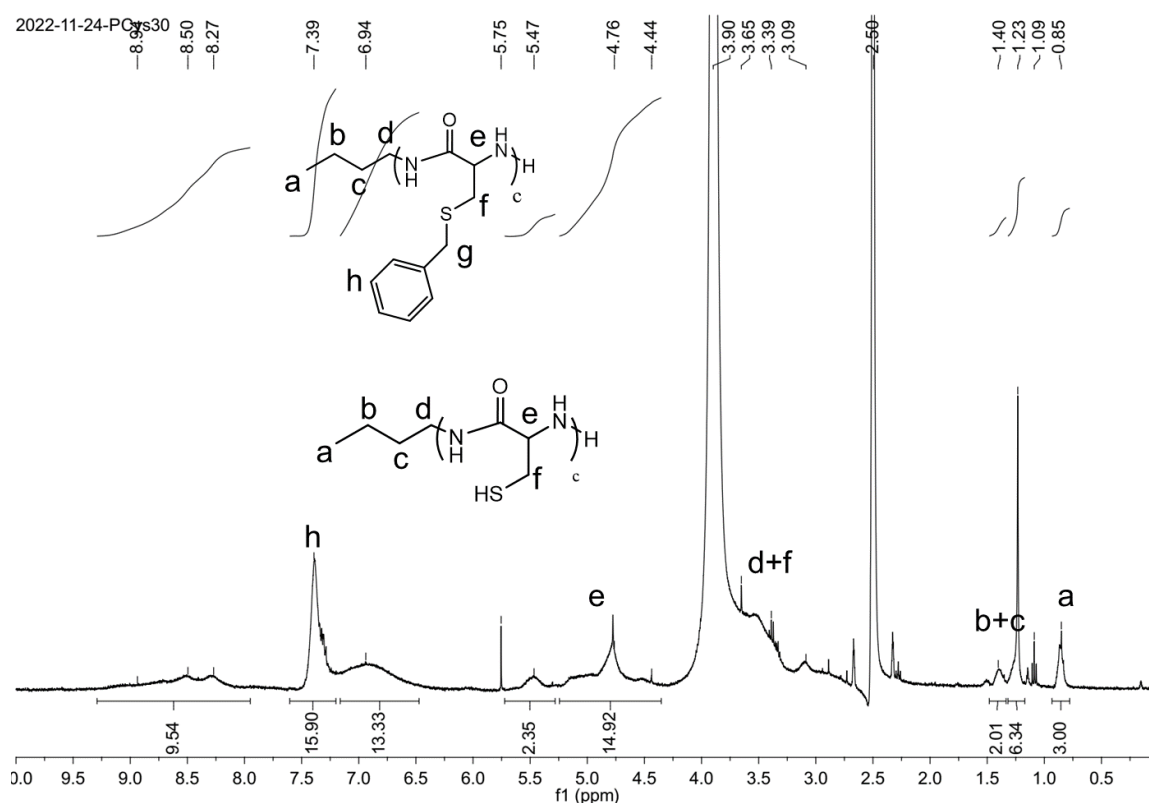


Figure 4.19  $^1\text{H}$  NMR spectrum of Bu-Cys<sub>20</sub> (solvent: DMSO- $d_6$ ).

All the  $^1\text{H}$  NMR spectra of deprotected oligo- or poly-cysteine showed wide peak shape for methine proton of cysteine residues (Peak e), which may be due to two possible reasons. One is the restricted motion of methine proton due to formation of disulfide bridges. The formation of disulfide bridges between different polymer chain may lead to larger molecules or even nanoparticles, which will reduce the rotational motion of methine proton in the cysteine residues. The chemical shift anisotropy and dipolar coupling couldn't be averaged, which leads to broad peak. Another possible reason may be attribute to a tautomerism in analogy to the well known amide-iminole-tautomerism of peptide groups as shown in Figure 4.20. This exchange may well be a consequence of the -I effect from the SH-group and depend on the pH of the solution. Fast exchange rate will lead to one narrow peak. Slow exchange rate will lead to two narrow peaks. If the exchange rate is in the region of NMR frequency, one broad peak will be observed in the spectrum.

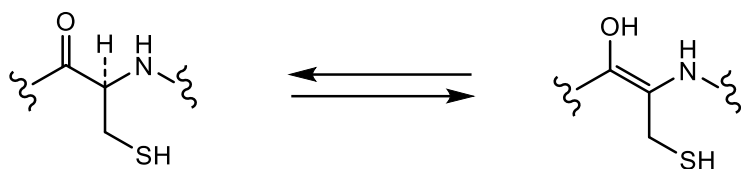


Figure 4.20 Possible amide-iminole-tautomerism.

When triflic acid was used as deprotecting reagent, the resulting deprotected peptide was always heavier than the protected peptide, which may be due to the formation of salts between triflic acids and cysteine residues, and the triflic acid can be removed by dialysis. The  $^{19}\text{F}$  NMR spectrum indicates that there are both TFA and triflic acid in the peptide structure and the ratio between these two acids is around 1: 4.17 (Figure 4.21a). Around 30% (w/w) of the deprotected products were derived from these two acids according to the calculation of the integral of the  $^{19}\text{F}$  NMR spectrum of products with the addition of a known amount of TFA as a reference. (Figure 4.21b)

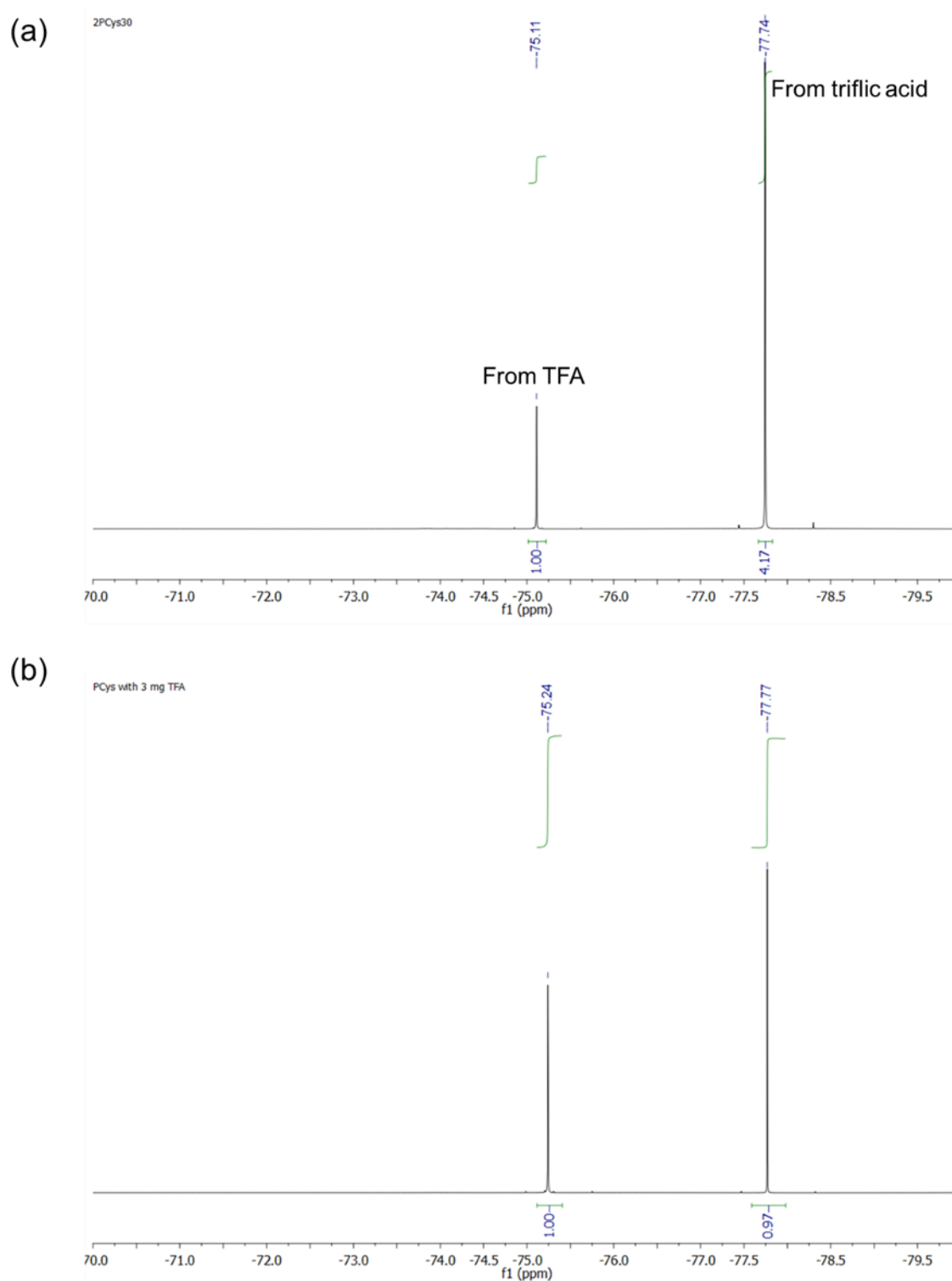


Figure 4.21 (a) <sup>19</sup>F NMR of Bu-Cys<sub>20</sub> (solvent: DMSO-d<sub>6</sub>). (b) <sup>19</sup>F NMR of 20 mg Bu-Cys<sub>20</sub> with 3 mg of TFA as a reference (solvent: DMSO-d<sub>6</sub>)

PFG NMR was conducted in order to check if the two acids were connected with the peptides, the result was shown in Figure 4.22. The diffusion constant of peptide, triflic acid, and TFA was calculated according to PFG <sup>1</sup>H NMR and PFG <sup>19</sup>F NMR separately. From the result we can

see diffusion constants of the two acids are one magnitude larger than that of peptides, which indicates that these two acids are not covalently bonded with the peptide.

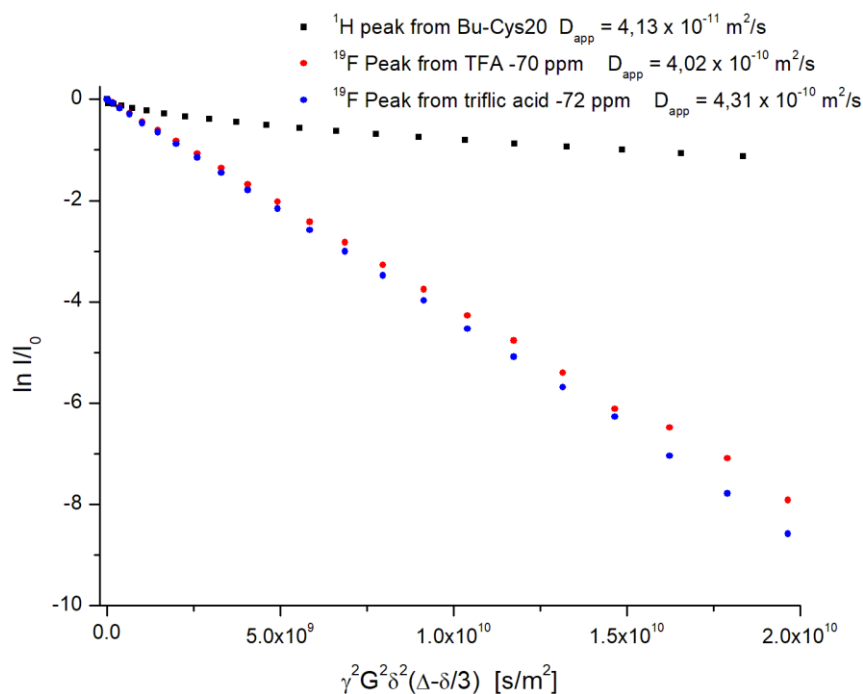


Figure 4.22 PFG-NMR echo decay plots for peptide and the two acids. The slopes of the decay corresponds to the self-diffusion constants of the observed nuclei.

Di-block peptide Bu-BnAsp<sub>11</sub>-BnCys<sub>15</sub> was synthesized to be used to study the deprotection efficiency and free thiol group content in acidolytic deprotection as well, because the peptide used for capsule formation consists of aspartate, cysteine, and phenoalanine block, and phenoalanine block will decrease the solubility of the triblock polypeptide in DMSO and water, which isn't suitable for the following  $^1\text{H}$ -NMR and UV test. The structure of the di-block polypeptide Bu-BnAsp<sub>11</sub>-BnCys<sub>15</sub> was confirmed by  $^1\text{H}$ -NMR as shown in Figure 4.23.

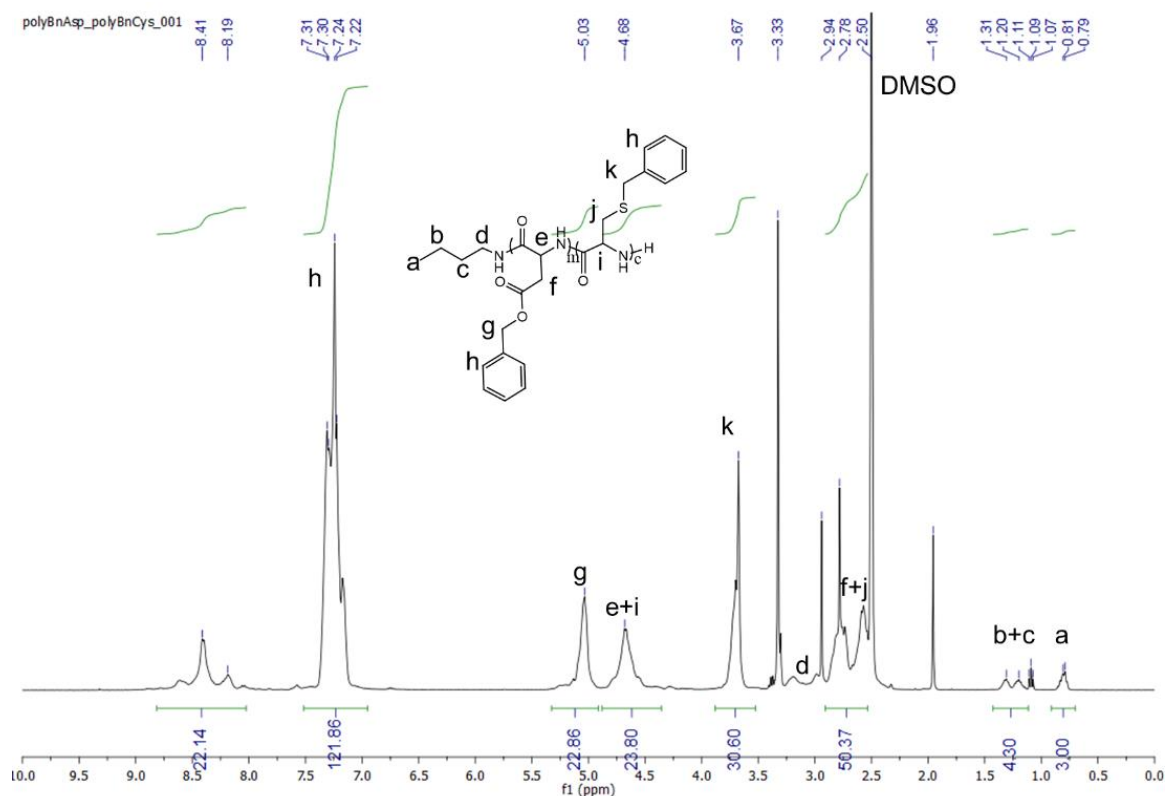


Figure 4.23  $^1\text{H}$  NMR spectrum of Bu-BnAsp<sub>11</sub>-BnCys<sub>15</sub> (solvent: DMSO-*d*<sub>6</sub>).

Reaction of Bu-BnAsp<sub>11</sub>-BnCys<sub>15</sub> with triflic acid at 40 °C for 3 h removes 85% of protecting groups according to calculation of signal integral (a and h) in  $^1\text{H}$ -NMR as shown in Figure 4.24, the deprotection efficiency is similar to that of mono-block Bu-BnCys<sub>20</sub>. However only around 20% of free thiol groups were detected according to Ellman's reagent test. The lower thiol group content may be due to the formation of disulfide bridges during the reaction. The broadening of the NMR lines is usually due to restricted rotational diffusion [30], which may be caused by the formation of nanoparticles due to cross-linking of cysteine residues.

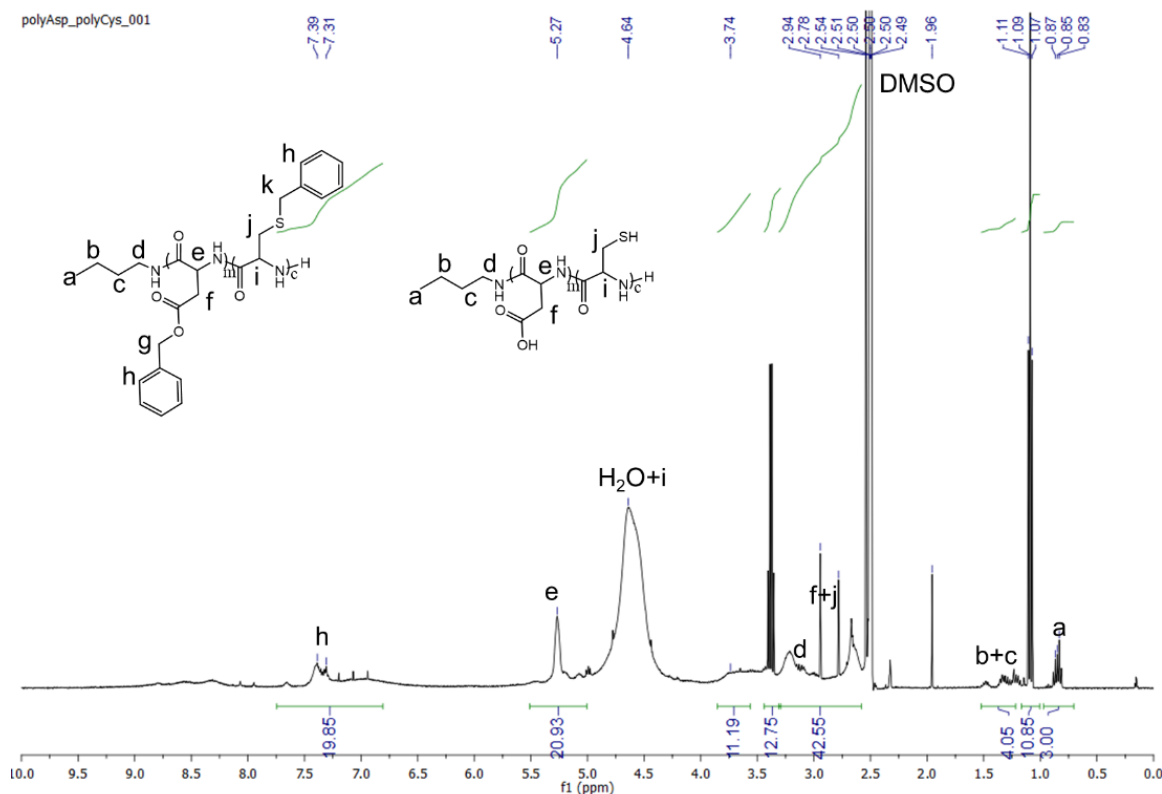


Figure 4.24  $^1\text{H}$  NMR spectrum of Bu-Asp<sub>11</sub>-Cys<sub>15</sub> (solvent: DMSO- $d_6$ ).

Another possible side reaction during the acidolytic deprotection of cysteine containing peptide is re-benzylation of thiol group [47]. Carbocation scavengers, such as anisole, have been reported to prevent the re-benzylation of nucleophilic free thiol groups with benzyl cations formed during the acidolytic deprotection [48]. Another carbocation scavenger 1,2-ethandithiol can not only prevent re-benzylation of thiol groups but also prevent the crosslink of cysteine residues. Therefore, we also conducted the acidolytic deprotection with anisole and 1,2-ethandithiol as carbocation scavengers. However, there are still around 15 Bn groups remain in each polymer chain according to the integrals of the signals a and h in Figure 4.25, which indicated that only around 42% of Bn groups was removed. Most of the protecting groups are probably derived from anisole, which can be a source of methylating agents when strong acids such as triflic acid are present [49].



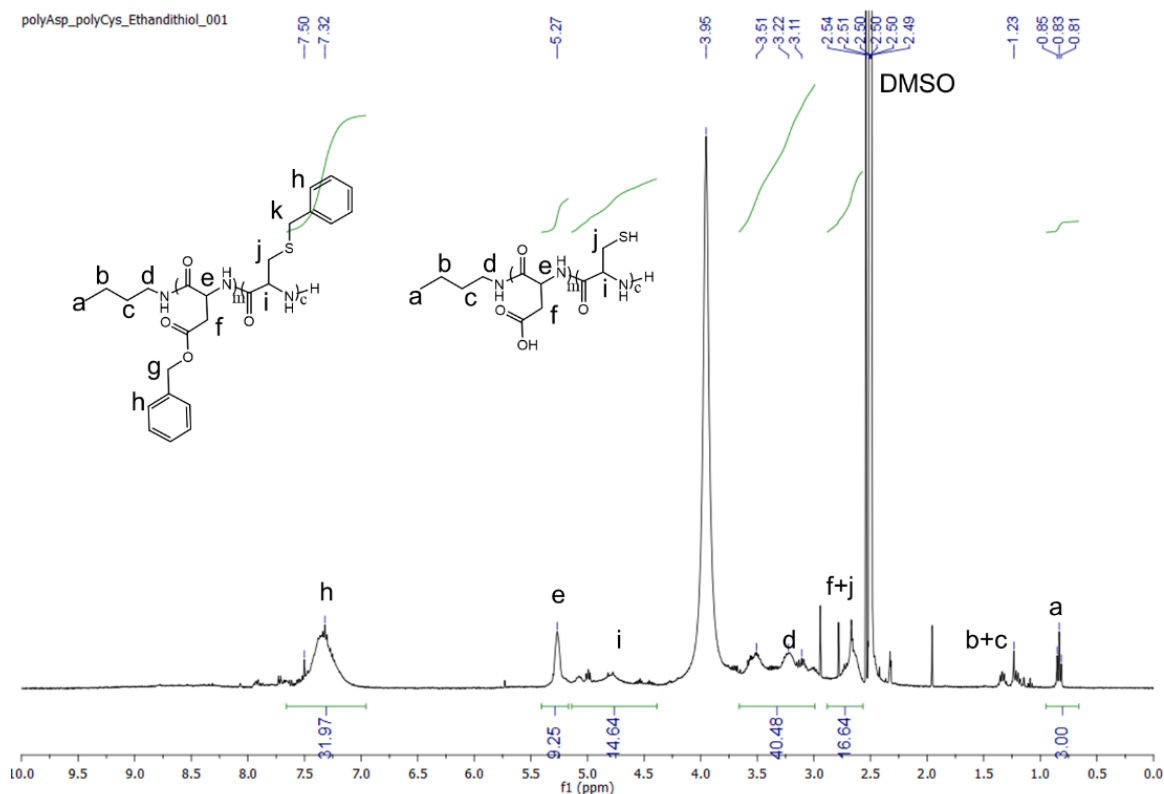


Figure 4.26  $^1\text{H}$  NMR spectrum of Bu-Asp<sub>11</sub>-Cys<sub>15</sub> (solvent: DMSO-*d*<sub>6</sub>) deprotected with 1,2-ethanedithiol as carbocation scavengers.

If only 1,2-ethanedithiol was used as carbocation scavenger for the deprotection of Bu-BnAsp<sub>11</sub>-CbzCys<sub>15</sub>, only around 6 Bn groups remain in each polymer chain according to the integrals of the signals a and h, which indicated that around 80% of Bn groups was removed (Figure 4.26). Around 39% of free thiol group can be detected in this case.

### 4.3 Investigation of PFD filled triblock polypeptide capsules

#### 4.3.1 Discussion of triblock polypeptide syntheses

Various triblock polypeptides consisting of aspartate block, cysteine block and phenylalanine block were synthesized using differently protected monomers and initiators.

The synthetic route of the polypeptide using NNPCbzCys as monomer and *n*-butylamine as initiator is shown in Figure 4.27.

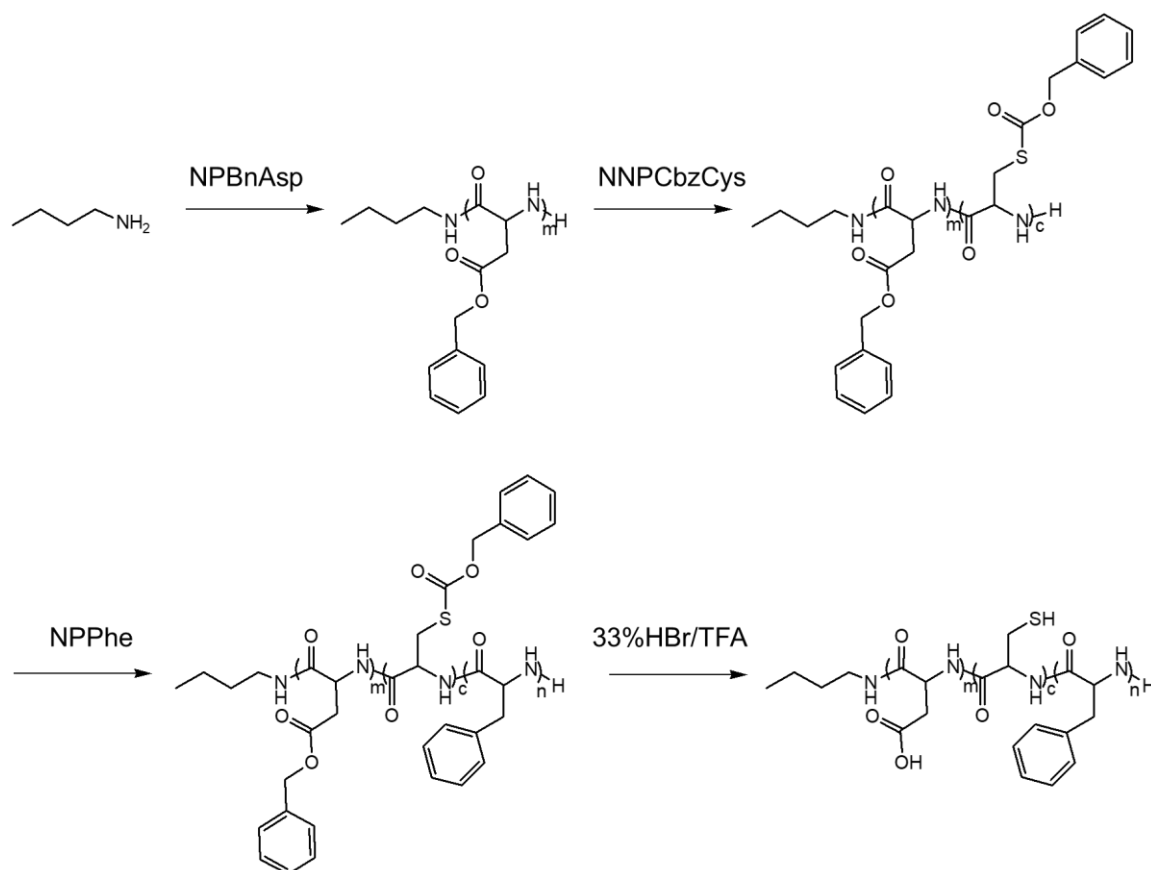


Figure 4.27 Synthetic route of triblock polypeptide using NNPCbzCys as monomer and *n*-butylamine as initiator.

Two triblock polypeptides were tried to be synthesized, including Bu-Asp<sub>31</sub>-Cys<sub>4</sub>-Phe<sub>3</sub> and Bu-Asp<sub>40</sub>-Cys<sub>5</sub>-Phe<sub>5</sub>. Their corresponding <sup>1</sup>H NMR spectra are shown in the appendices (Figure 7.13- Figure 7.21).

Polypeptides with longer cysteine block chain length are hardly obtained when NNPCbzCys was used as the monomer. The designed repeating units of CbzCys block are 30 for both triblock polypeptides. However, only 4 or 5 CbzCys were connected to Bu-BnAsp<sub>m</sub>. The efficiency of connecting Phe block to Bu-BnAsp<sub>m</sub>-CbzCys<sub>c</sub> is also low. These observations may be due to the possible intramolecular termination reaction of CbzCys block as mentioned in section 4.2. The integrals of <sup>1</sup>H NMR of CbzCys block in the polypeptides always decrease after polymerization of the third monomer NPPhe, which may be due to the loss of some self-polymerized oligocysteines during the precipitation process. When the polymerization is finished, the polypeptide DMAc solution will precipitate into diethyl ether to obtain the solid polypeptides. Some self-polymerized oligocysteines will dissolve into the diethyl ether, leading

to the decrease in the integrals of  $^1\text{H}$  NMR.

The synthetic route for the polypeptide using NPBnCys as monomer and n-butylamine as initiator is shown in Figure 4.28.

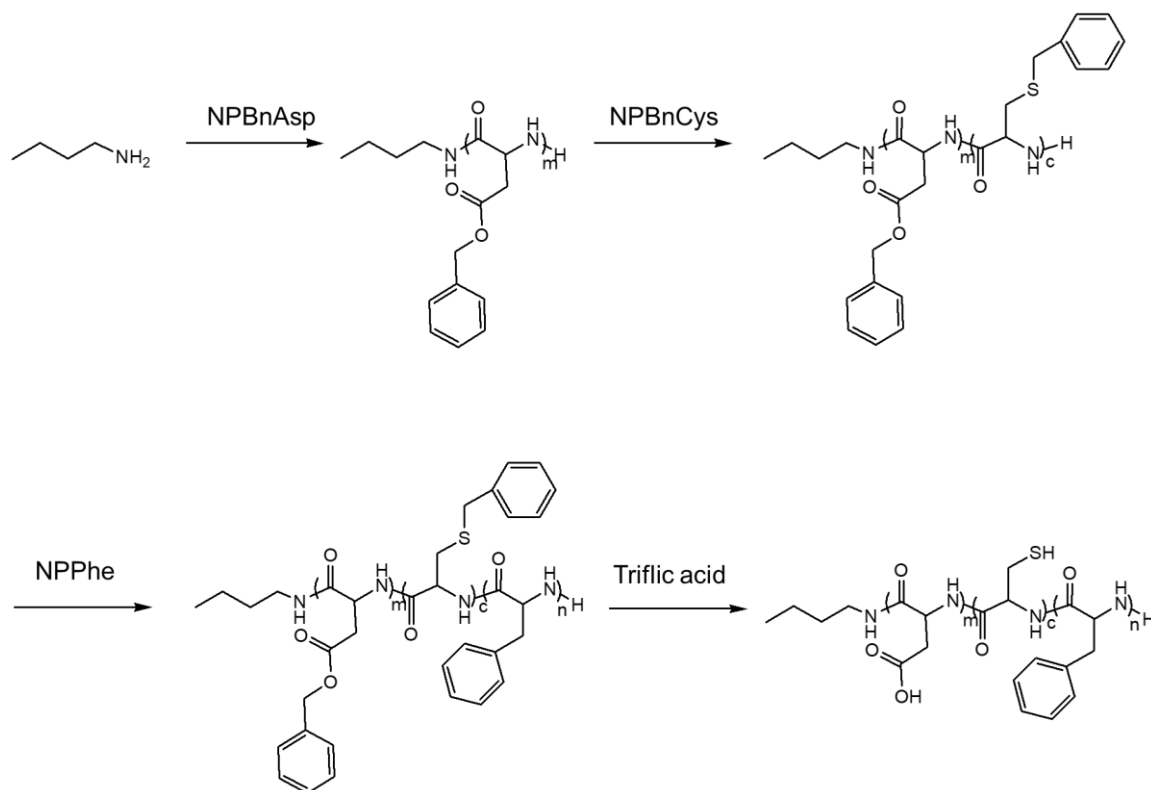


Figure 4.28 Synthetic route of triblock polypeptide using NPBnCys as monomer and n-butylamine as initiator.

Three triblock polypeptides from NPBnCys were successfully synthesized, including Bu-Asp<sub>6</sub>-Cys<sub>8</sub>-Phe<sub>8</sub>, Bu-Asp<sub>13</sub>-Cys<sub>6</sub>-Phe<sub>7</sub> and Bu-Asp<sub>7</sub>-Cys<sub>15</sub>-Phe<sub>2</sub>. Their corresponding  $^1\text{H}$  NMR spectra are shown in the appendices (Figure 7.22- Figure 7.34).

Triblock polypeptides can be efficiently synthesized if NPBnCys was used as monomers. All the polypeptides were synthesized with good yields. The efficiency of connecting the third block Phe is also high. These are because the polymerization of NPBnCys yield oligo- or poly-BnCys with free amine end and there is no self-polymerization happening for the monomer NPBnCys according to the MS result in Figure 4.15.

The synthetic route of the polypeptide using NPBnCys as monomer and 1,4-dibenzyl L-aspartate as initiator is shown in Figure 4.29.

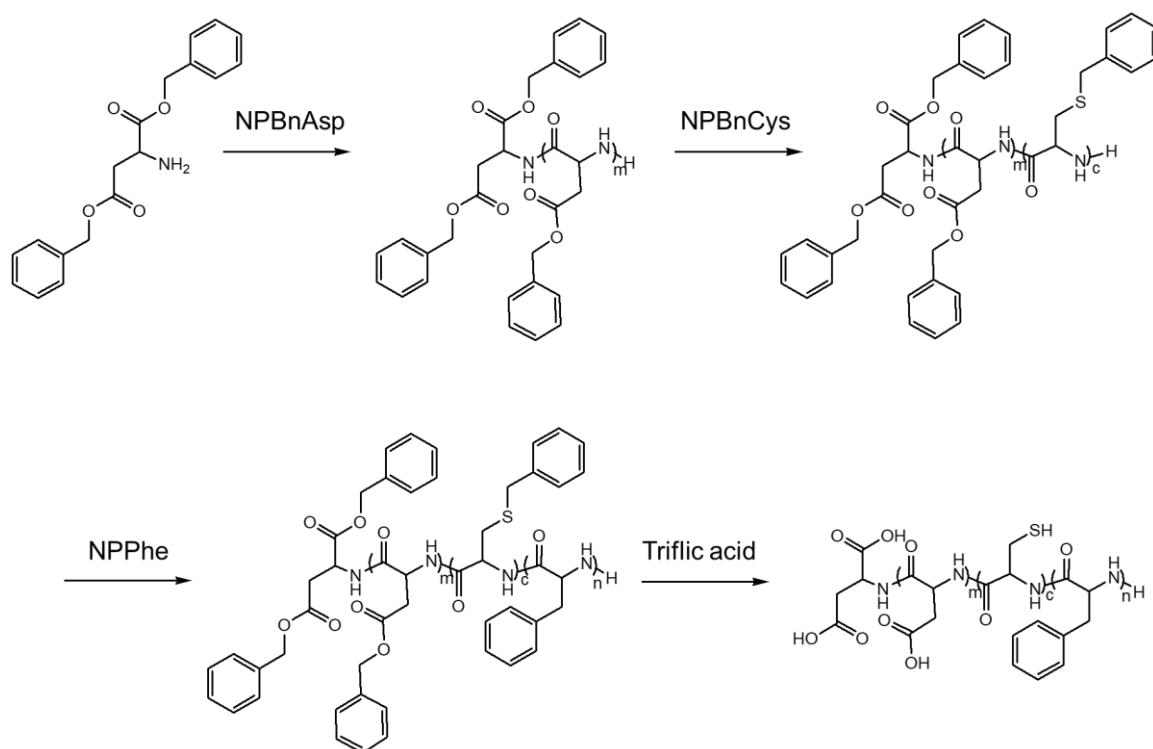


Figure 4.29 Synthetic route of triblock polypeptide using NPBnCys as monomer and 1,4-dibenzyl L-aspartate as initiator.

Triblock polypeptides Asp<sub>8</sub>-Cys<sub>4</sub>-Phe<sub>2</sub> were successfully synthesized. Triblock peptides can also be synthesized with 1,4-dibenzyl L-aspartate as initiator efficiently. Their corresponding <sup>1</sup>H NMR spectra are shown in the appendices (Figure 7.35- Figure 7.38).

#### 4.3.2 Discussion of PFD filled triblock polypeptide capsule

The appearance of a freshly prepared dispersion of PFD filled polypeptide capsules is shown in Figure 4.30. The capsules dispersion is well dispersed initially, but most capsules will settle down during 1 day. However, the capsule dispersion can be re-dispersed easily by shaking and remain well dispersed for several hours, which make it suitable for an application for blood replacement.



Figure 4.30 Photo of PFD filled polypeptide capsule dispersion.

We then analyzed the morphology of dried capsules by AFM. Figure 4.31 shows an AFM image of dried PFD filled Bu-Asp<sub>40</sub>-Cys<sub>5</sub>-Phe<sub>5</sub> capsules. A lot of regular round hollow structures were observed, which should be the collapsed capsules due to the leakage of PFD. The capsules have a diameter that ranges from 300 nm to 1150 nm. The capsule walls exhibited a certain mechanical strength as they can remain their round shape even though the PFD was evaporated. However, the vapor pressure of the PFD is high enough to destroy the capsule membranes.

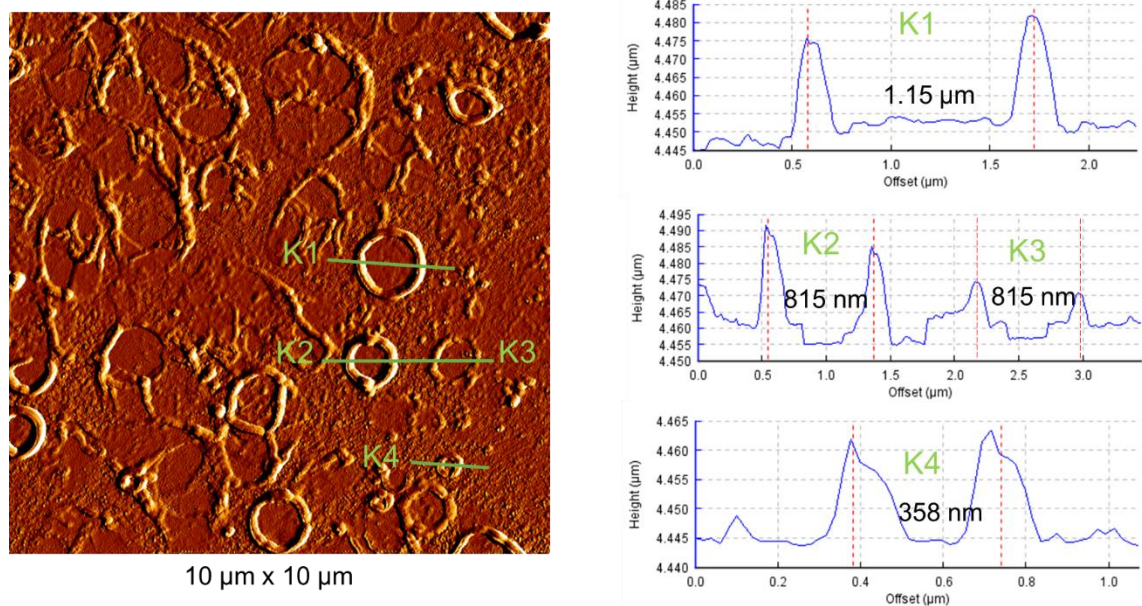


Figure 4.31 AFM image (left) and height profiles (right) of PFD filled Bu-Asp<sub>40</sub>-Cys<sub>5</sub>-Phe<sub>5</sub> capsules.

Most capsules are collapsed after drying possibly due to a relatively low content of cysteine residues. Therefore, the polypeptide Bu-Asp<sub>7</sub>-Cys<sub>15</sub>-Phe<sub>2</sub> with a longer cysteine chain length was synthesized and was used to encapsulate PFD to prepare capsules. Figure 4.32 shows the dried PFD filled Bu-Asp<sub>7</sub>-Cys<sub>15</sub>-Phe<sub>2</sub> capsules. Most of capsules exhibit a diameter that ranges from 300 nm to 1000 nm. Most capsules remain their spherical shape, which indicates their capsule walls exhibit enough mechanical strength to maintain their spherical structure even after drying.

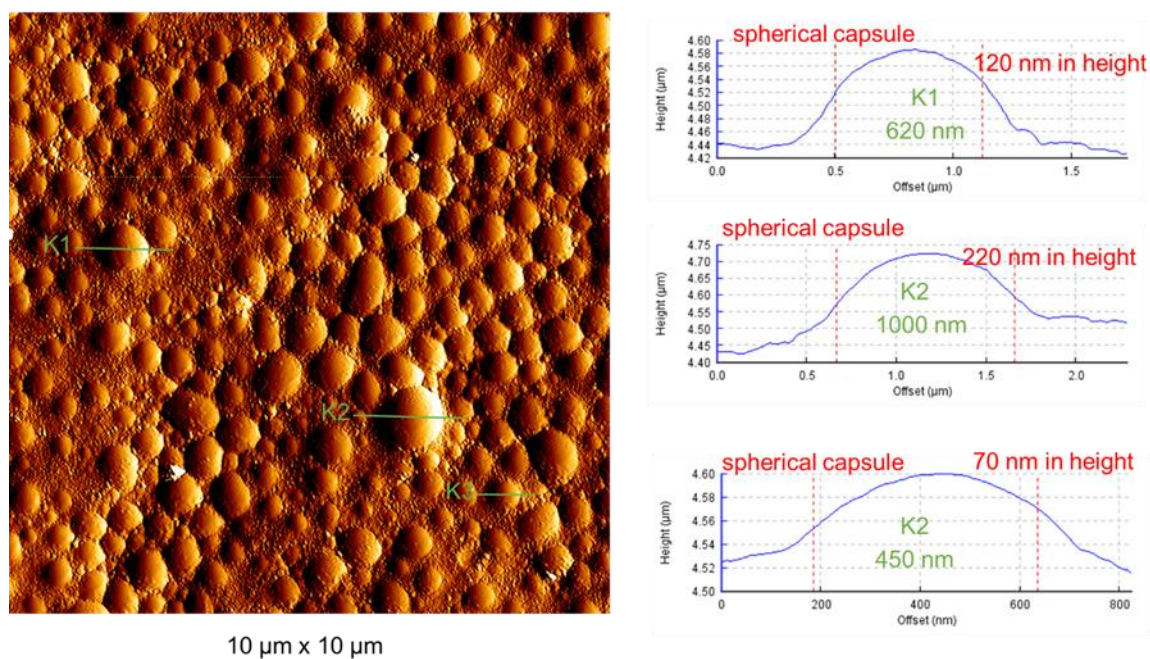


Figure 4.32 AFM image (left) and height profiles (right) of PFD filled Bu-Asp<sub>7</sub>-Cys<sub>15</sub>-Phe<sub>2</sub> capsules.

We also studied the influence of longer Phe chain length on the morphology of capsules. Figure 4.33 shows the AFM image of dried PFD filled Bu-Asp<sub>6</sub>-Cys<sub>8</sub>-Phe<sub>8</sub> capsules. Except for the spherical capsules and collapsed capsules, a large amount of very small nanoparticles with diameter of around 50 nm were observed as well, which should be self-assembled polypeptide micelles.

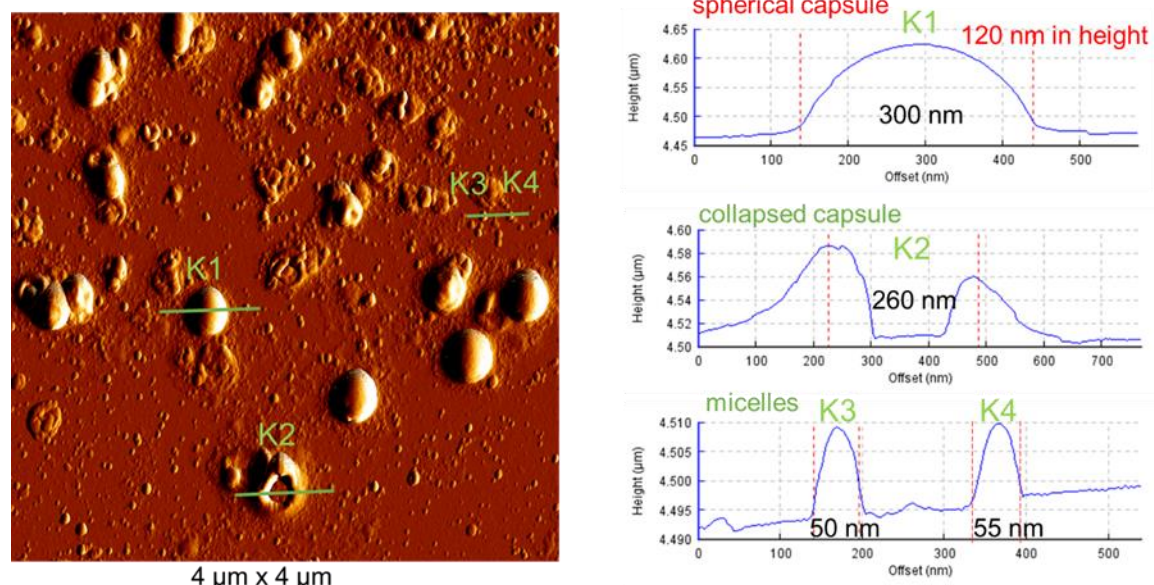


Figure 4.33 AFM image (left) and height profiles (right) of PFD-filled Bu-Asp<sub>6</sub>-Cys<sub>8</sub>-Phe<sub>8</sub> capsules

We also studied possibility of using di-block peptide Bu-Asp<sub>10</sub>-Cys<sub>15</sub> to encapsulate PFD to prepare capsules, as Bu-Asp<sub>10</sub>-Cys<sub>15</sub> is also amphiphilic with the ability to emulsify PFD. Figure 4.34 shows the AFM image of dried PFD filled Bu-Asp<sub>10</sub>-Cys<sub>15</sub> capsules. A lot of spherical capsules and collapsed capsules can be observed as well. This result indicates that Bu-Asp<sub>10</sub>-Cys<sub>15</sub> may be also suitable for encapsulating PFD to prepare capsules. The collapse of capsules may not really present a problem, as the planned use of the capsules for blood replacement would not include a drying step. It just means that the capsules should always be kept in a liquid environment for their medical application.

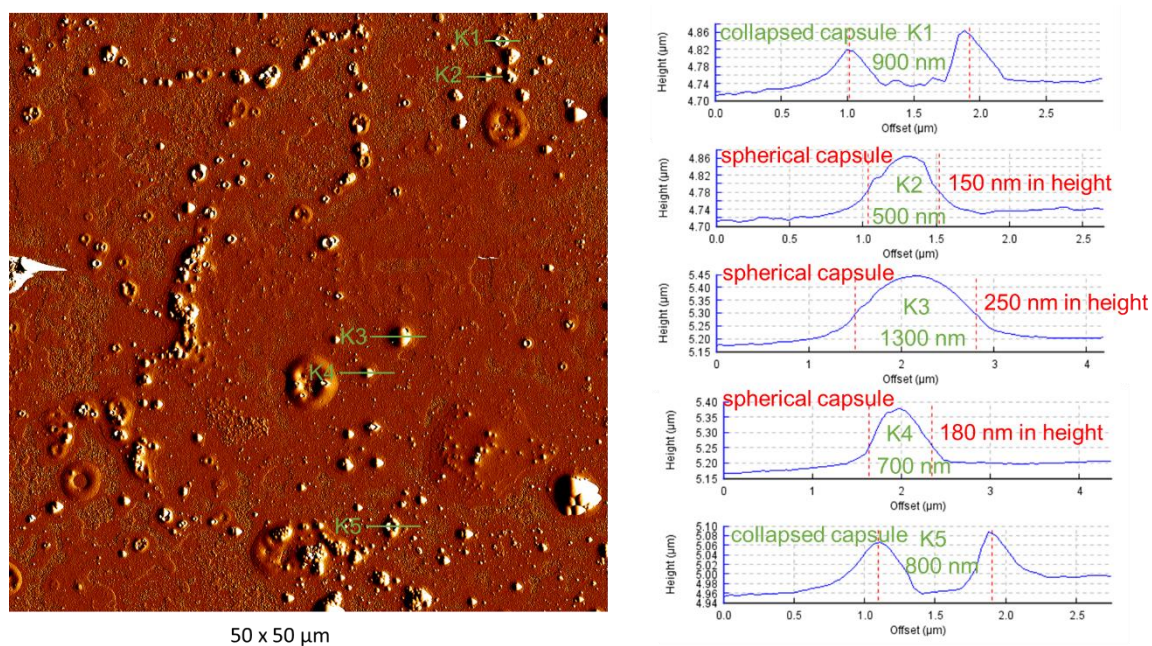


Figure 4.34 AFM image (left) and height profiles (right) of PFD-filled Bu-Asp<sub>10</sub>-Cys<sub>15</sub> capsules

Figure 4.35 shows the AFM image of collapsed dried PFD filled Bu-Asp<sub>10</sub>-Cys<sub>15</sub> capsules. Most collapsed capsules exhibit ring like structures, which may be formed by fold of peptide membrane after evaporation of PFD. The thickness of such ring like structures varies from 45 to 160 nm and depends strongly on the capsule diameter; smaller capsules are found to have thinner ring like structures.

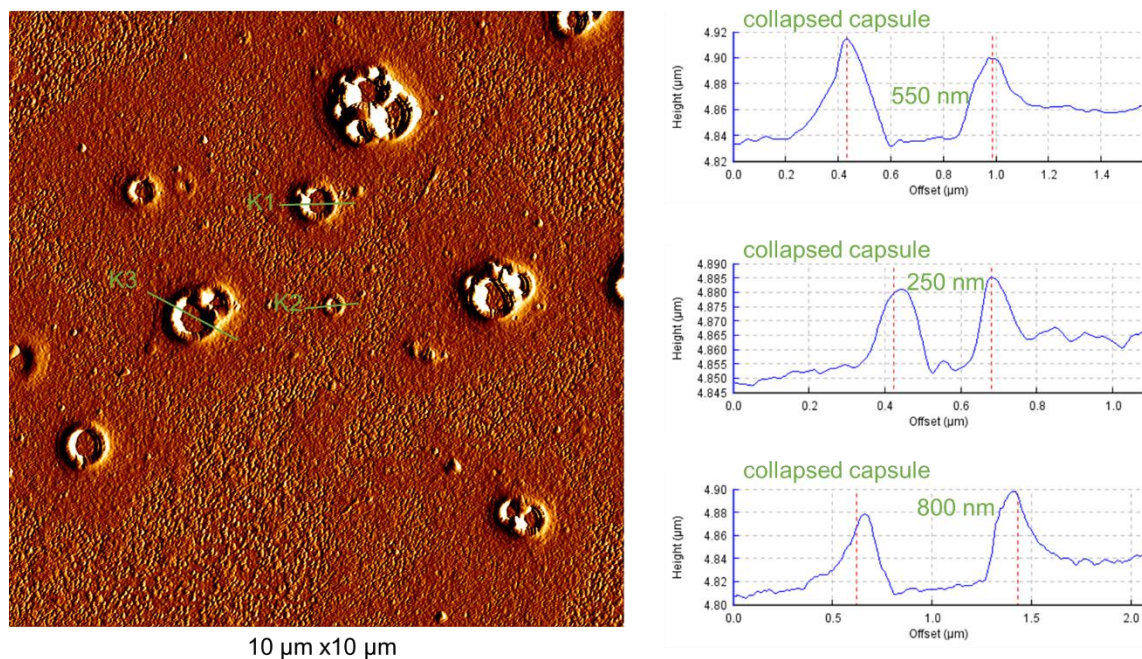
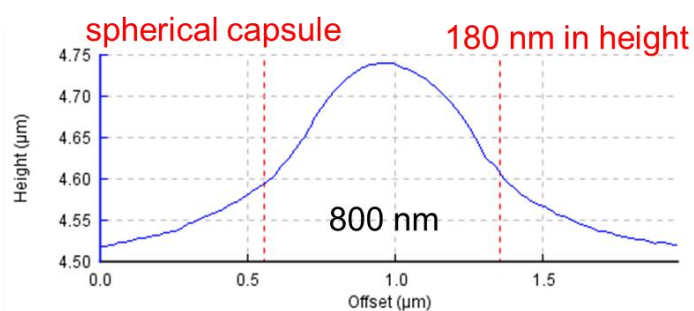
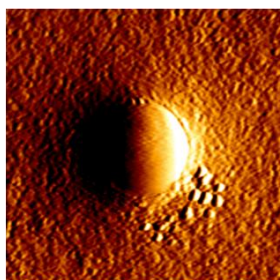


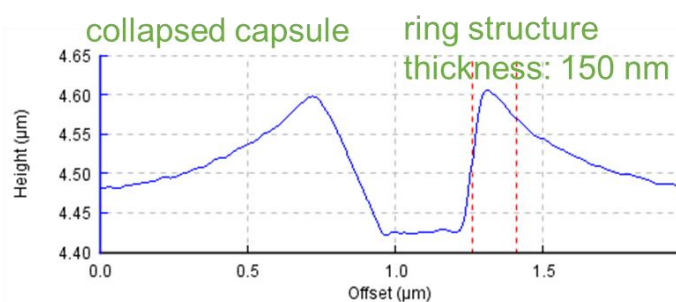
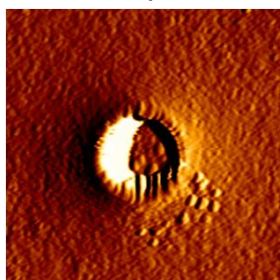
Figure 4.35 AFM image (left) and height profiles (right) of collapsed PFD-filled Bu-Asp<sub>10</sub>-Cys<sub>15</sub> capsules.

For study of mechanical performance of these capsules, we compressed some spherical capsules with an AFM tip. During the test, the cantilever holder was moved vertically towards the carrier surface by a distance of 1 μm in 0.5 sec. Some capsules remain intact after being compressed by the AFM tip, which indicates the good elasticity of these capsule walls. Some capsules were completely collapsed after compression tests as shown in Figure 4.36a. Some capsules show a characteristic folding after compression tests as shown in Figure 4.36b. The characteristic folding indicates the presence of a thin flexible capsule membrane surrounding a liquid core [2]. These results indicate that our capsule exhibit enough mechanical strength for using as artificial oxygen carriers.

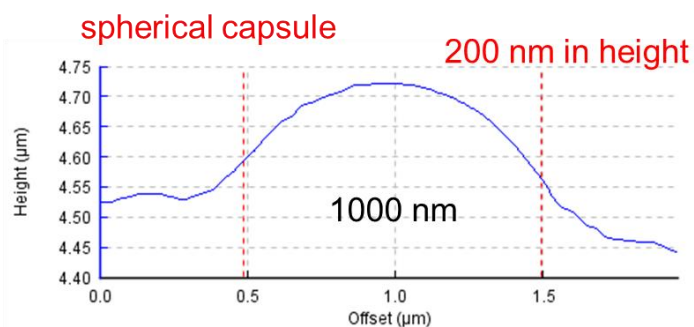
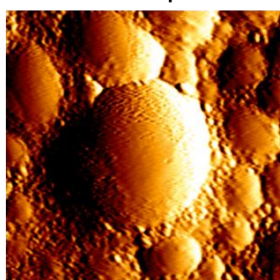
(a) Before compression



After compression



(b) Before compression



After compression

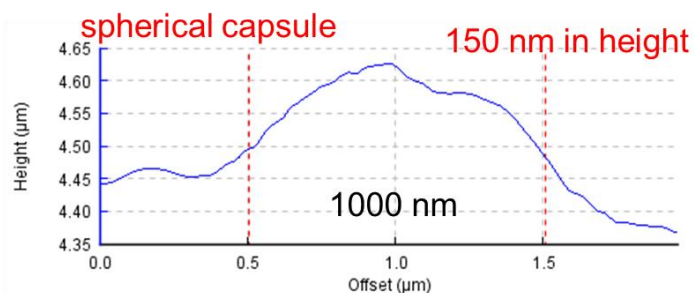
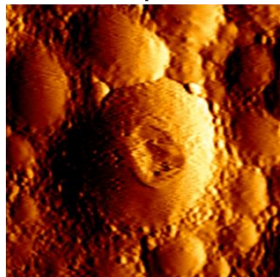


Figure 4.36 AFM images of some capsules before and after a single compression test. (a) a completely collapsed capsule after compression test. (b) a deformed capsule after compression test.

Mono-block peptide Bu-Cys<sub>20</sub> was also tried to be used to encapsulate PFD, because Bu-Cys<sub>20</sub> is also amphiphilic under neutral conditions. However, many white agglomerated precipitates appear in the capsule dispersion. These agglomerated precipitates couldn't be re-dispersed

by shaking the capsule dispersion. The remaining PFD capsules in the dispersions were observed by AFM. Figure 4.37 showed PFD filled Bu-Cys<sub>20</sub> capsules. Apart from that a large number of nanoparticles with a diameter of around 200 nm were observed, there are also many irregular hollow structures, which should be the collapsed capsules due to the leakage of PFD.

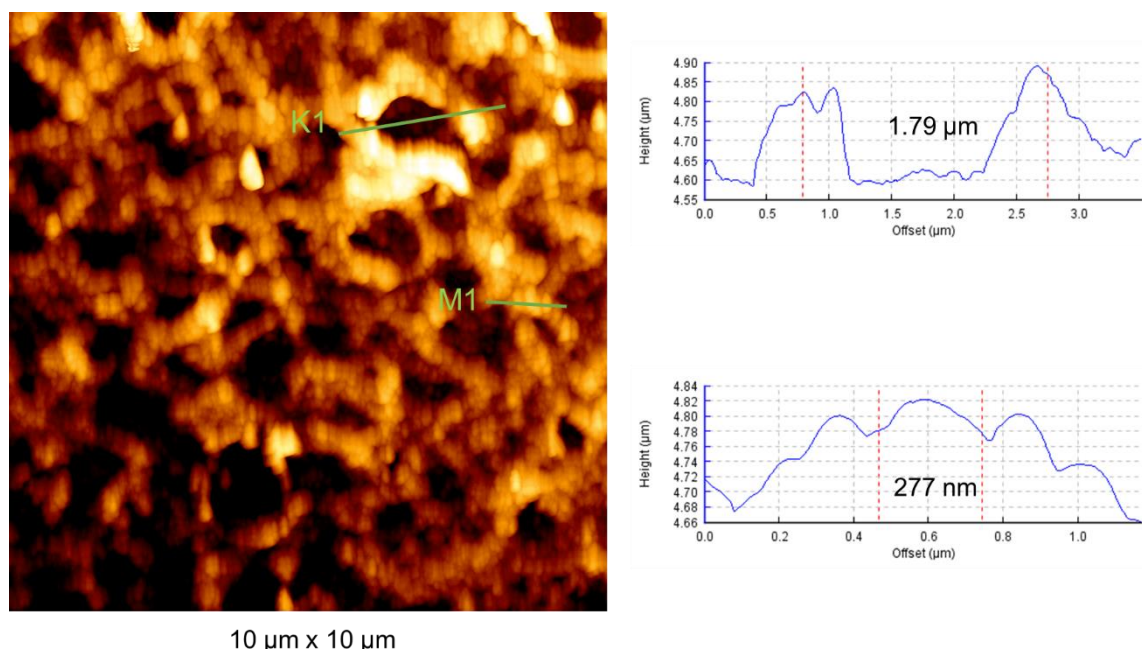


Figure 4.37 AFM image of PFD filled Bu-Cys<sub>20</sub> capsules.

Mono-block polycysteine is not suitable to encapsulate PFD to prepare stable capsule dispersions, as thiol groups on the surface of capsules may contact with another thiol groups on other capsules, leading to the formation of disulfide bridges among different capsules. The introduction of a hydrophilic aspartate block is essential, because most carboxylic groups in the side chains of polyaspartate will exist in  $\text{-COO}^-$  form at neutral conditions, which can provide both steric stabilization and electrostatic stabilization for PFD filled polypeptide capsules [50].

The oxygen absorption and release rates of PFD filled triblock polypeptide capsules were studied by  $^{19}\text{F}$  NMR, the result was shown in Figure 4.38. The chemical shift of the fluorine nuclei strongly depends on the oxygen concentration due to the paramagnetic influence of the oxygen. The time resolved plot obtained under periodic change of the purging gas between nitrogen and oxygen shows that it takes the PFD capsules less than 2 min to equilibrate to the new atmospheric conditions after switching from nitrogen to oxygen or vice versa. After 3 times of nitrogen and oxygen exchange, the capsule still maintains its original oxygen carrying

capacity. These results indicate that the capsules allow fast gas exchange and the gas exchange is completely reversible.

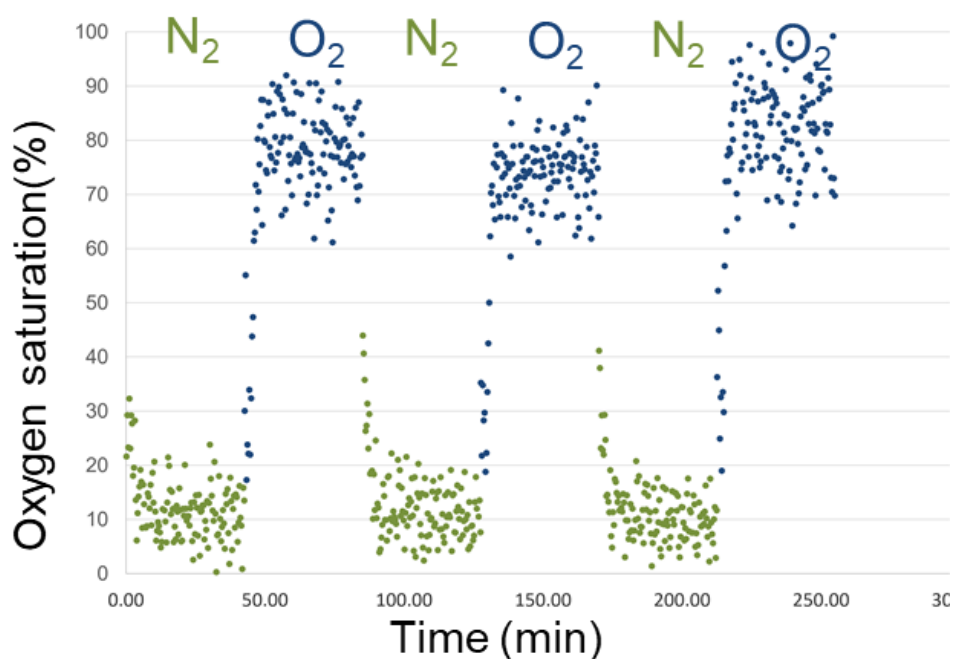


Figure 4.38 Gas exchange process in a dispersion of PFD-filled triblock-peptide Bu-Asp<sub>6</sub>-Cys<sub>8</sub>-Phe<sub>8</sub> capsules as determined by the chemical shift of the <sup>19</sup>F NMR signal.

The diffusion constant of PFD filled cysteine containing polypeptide capsules were studied by PFG NMR and the result was shown in Figure 4.39. Our results indicate that the capsules have a diffusion constant of  $2.05 \times 10^{-12} \text{ m}^2/\text{s}$ . This is about an order of magnitude larger than the self-diffusion constant of red blood cells, which means that our capsules can move faster in blood than red blood cells. Therefore, our capsules can deliver oxygen from lung tissues to the other tissues more quickly. In the meantime, perfluorodecalin inside the capsules also undergoes fast self-diffusion, which is good for the oxygen absorption and release. We can also determine that our capsules exhibit an average diameter of around 240 nm based on the diffusion constant of capsules according to Stocks-Einstein equation.

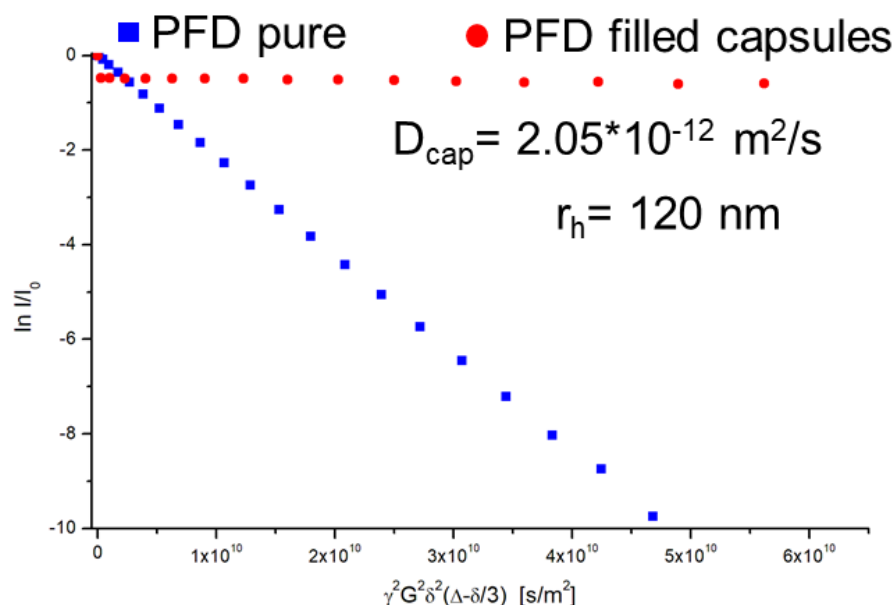


Figure 4.39 PFG-NMR echo decay plots for pure liquid PFD and the PFD in a dispersion of PFD-filled Bu-Asp<sub>7</sub>-Cys<sub>9</sub> capsules. The slopes of the decay corresponds to the self-diffusion constants of the observed nuclei.

The cytotoxicities of PFD filled polypeptide capsules were studied by use of the lactate dehydrogenase (LDH) Assay. The cell culture was conducted by Dr. Miriam Cantore.

LDH assay is a widely used method in cell toxicity research. LDH is an enzyme that is present in the cytoplasm of cells. When the cell membrane is damaged due to incubation with toxic chemicals or drugs, LDH is released from the cells, which can be detected to evaluate the damage rate of the cells. The cell damage rate is calculated according to the LDH released from cells after incubation with cell culture medium and the total LDH released from cells after incubation with Triton, a chemical to kill the cells. The LDH Assay result is shown in Figure 4.40. In the 4-h incubation test, the cells incubated with all capsules exhibited similar LDH values and kept a high cell viability comparable to control medium. For 24-h incubation test, the LDH values increase a little bit for every capsule treated group, but the cell viability is still very high. These results indicate that our capsules exhibit little cytotoxicity.

(a) Summary results: LDH release after 4 h (b) Summary results: LDH release after 24 h

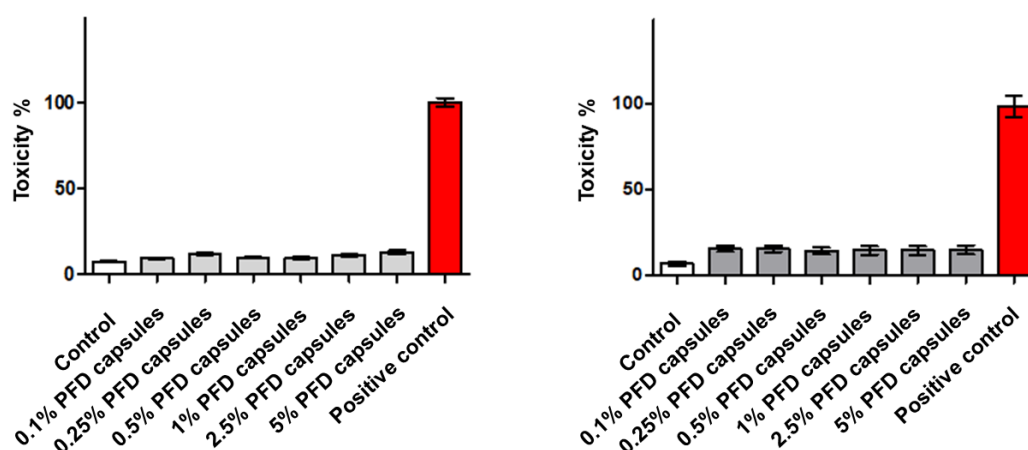


Figure 4.40 Cytotoxic effects of PFD-filled capsules on human HK-2 cells. To determine the disruption of cellular membrane integrity, LDH analyses was performed. Control cells were incubated for 4 h (A) or 24 h (B) with DMEM/F-12 with GlutaMAX (no supplements), whereas treatment groups were incubated for 4 h or 24 h with capsules at different concentrations (0.1 %, 0.25 %, 0.5 %, 1 %, 2.5 %, 5 %), respectively. The positive control group corresponded to Lysis Buffer treatment for 45 min. Values are expressed as means  $\pm$  SD ( $n = 12$ ) from 4 different experiments.

### 5 Summary and outlook

The goal of this Ph.D. thesis is to prepare perfluorodecalin (PFD) filled polypeptide capsules with both good mechanical and dispersion stability and good biocompatibility. To achieve this goal, a capsule membrane made from an artificial protein is to be prepared by cross-linking amphiphilic multiblock-peptides. The initial multiblock-peptide preferably consists of a hydrophobic section from Phe, a hydrophilic section from Asp, and a central section from Cys in order to allow for cross-linking via sulfur bridges.

Initial studies using the di-block polypeptides Asp<sub>40</sub>-Phe<sub>n</sub> with a variable number n reveal that the Phe section must remain short ( $n < 5$ ) in order to reach good stabilization for PFD droplets. Larger Phe sections with  $n > 5$  tend to form micelles and generally show excessive hydrophobicity. Cysteine, as an important moiety in the polypeptide structures, plays a vital role on the formation of solid capsule walls. Therefore, efforts were put on the synthesis and characterization of oligo- and poly-cysteine, which is particularly difficult as it requires selective activation and protection. Polymerization of NPBnCys gives PBnCys with good yields (around 80%) and narrow molecular weight distribution (PDI=1.2). The removal of benzyl group needs strongly acidic environments at higher temperature such as triflic acid at 40°C. Polymerization of NNPCbzCys gives PCbzCys with smaller yields (around 30%) and broad molecular weight distribution (PDI=1.8). The terminal structure is also unknown for PCbzCys, but the Cbz group can be easily removed using HBr at 25 °C. Free thiol group content of oligo- or poly-cysteine resulting from differently protected oligo- or poly-cysteine are for all types of protection and amount to 30%. Considering that triflic acid at 40 °C does not represent excessively harsh conditions, it is better to synthesize the triblock polypeptide based on the monomer NPBnCys.

All triblock oligo- or poly-peptides can stabilize PFD in water efficiently. The capsule dispersions can be easily redispersed by shaking even after 1 month. Most of the capsules exhibit a diameter that ranges from 100 nm to 1000 nm. The capsule wall exhibits sufficient mechanical strength for their use in dispersion and enough to maintain the intact spherical shape after drying process. The capsule wall allows for fast gas exchange and the gas exchange is completely reversible. The capsules also exhibit a large self-diffusion constant as around  $2.05 \times 10^{-12} \text{ m}^2/\text{s}$  in aqueous solution, which guarantees efficient oxygen delivery in the

environment of a blood vessel. The capsules also exhibit small cytotoxicity in a cell culture experiment.

In the future, more cell culture experiments and physiological testing on animals under laboratory conditions need to be conducted in order to check the capsules' biocompatibilities.

## 6 References

- [1] C.I. Castro, J.C. Briceno, Perfluorocarbon-based oxygen carriers: review of products and trials, *Artif Organs*, 34 (2010) 622-634.
- [2] J. Bauer, M. Zahres, A. Zellermann, M. Kirsch, F. Petrat, H. de Groot, C. Mayer, Perfluorocarbon-filled poly(lactide-co-glycolide) nano- and microcapsules as artificial oxygen carriers for blood substitutes: a physico-chemical assessment, *J Microencapsul*, 27 (2010) 122-132.
- [3] C. Stephan, C. Schlawne, S. Grass, I.N. Waack, K.B. Ferez, M. Bachmann, S. Barnert, R. Schubert, M. Bastmeyer, H. de Groot, C. Mayer, Artificial oxygen carriers based on perfluorodecalin-filled poly(n-butyl-cyanoacrylate) nanocapsules, *J Microencapsul*, 31 (2014) 284-292.
- [4] A. Wrobeln, J. Laudien, C. Gross-Heitfeld, J. Linders, C. Mayer, B. Wilde, T. Knoll, D. Naglav, M. Kirsch, K.B. Ferez, Albumin-derived perfluorocarbon-based artificial oxygen carriers: A physico-chemical characterization and first in vivo evaluation of biocompatibility, *Eur J Pharm Biopharm*, 115 (2017) 52-64.
- [5] K.B. Ferez, I.N. Waack, J. Laudien, C. Mayer, M. Broecker-Preuss, H. Groot, M. Kirsch, Safety of poly (ethylene glycol)-coated perfluorodecalin-filled poly (lactide-co-glycolide) microcapsules following intravenous administration of high amounts in rats, *Results Pharma Sci*, 4 (2014) 8-18.
- [6] J. Laudien, C. Gross-Heitfeld, C. Mayer, H. de Groot, M. Kirsch, K.B. Ferez, Perfluorodecalin-Filled Poly(n-butyl-cyanoacrylate) Nanocapsules as Potential Artificial Oxygen Carriers: Preclinical Safety and Biocompatibility, *J Nanosci Nanotechnol*, 15 (2015) 5637-5648.
- [7] K. Ferez, O. Karaman, S.B. Shah, Artificial red blood cells, *Nanotechnology for Hematology, Blood Transfusion, and Artificial Blood2022*, pp. 397-427.
- [8] K.B. Ferez, A.U. Steinbicker, Artificial Oxygen Carriers-Past, Present, and Future-a Review of the Most Innovative and Clinically Relevant Concepts, *J Pharmacol Exp Ther*, 369 (2019) 300-310.
- [9] J. Jagers, A. Wrobeln, K.B. Ferez, Perfluorocarbon-based oxygen carriers: from physics to physiology, *Pflugers Arch*, 473 (2021) 139-150.
- [10] K.B. Ferez, I.N. Waack, C. Mayer, H. de Groot, M. Kirsch, Long-circulating poly(ethylene glycol)-coated poly(lactid-co-glycolid) microcapsules as potential carriers for intravenously administered drugs, *J Microencapsul*, 30 (2013) 632-642.
- [11] A. Wrobeln, K.D. Schluter, J. Linders, M. Zahres, C. Mayer, M. Kirsch, K.B. Ferez, Functionality of albumin-derived perfluorocarbon-based artificial oxygen carriers in the Langendorff-heart (dagger), *Artif Cells Nanomed Biotechnol*, 45 (2017) 723-730.
- [12] M.M. Gromiha, *Protein Bioinformatics\_ From Sequence to Function*, Academic Press2010.
- [13] H.R. Kricheldorf, Polypeptides and 100 years of chemistry of alpha-amino acid N-carboxyanhydrides, *Angew Chem Int Ed Engl*, 45 (2006) 5752-5784.
- [14] H.A. Klok, *Protein-Inspired Materials: Synthetic Concepts and Potential Applications*, *Angewandte Chemie International Edition*, 41 (2002) 1509-1513.
- [15] H. Feng, J. Fabrizi, J. Li, C. Mayer, Syntheses of Polypeptides and Their Biomedical Application for Anti-Tumor Drug Delivery, *Int J Mol Sci*, 23 (2022).

- [16] David Van Vranken, G.A. Weiss, Introduction to Bioorganic Chemistry and Chemical Biology, Garland Science 2012.
- [17] B. Zheng, T. Bai, X. Tao, J. Ling, An Inspection into Multifarious Ways to Synthesize Poly(Amino Acid)s, *Macromol Rapid Commun*, 42 (2021) e2100453.
- [18] T.J. Deming, Living polymerization of  $\alpha$ -amino acid-N-carboxyanhydrides, *Journal of Polymer Science Part A: Polymer Chemistry*, 38 (2000) 3011-3018.
- [19] T. Endo, A. Sudo, Well-Defined Construction of Functional Macromolecular Architectures Based on Polymerization of Amino Acid Urethanes, *Biomedicines*, 8 (2020).
- [20] A.C. Farthing, R.J.W. Reynolds, Anhydro-N-carboxy-DL- $\beta$ -phenylalanine, *Nature*, 165 (1950) 647-647.
- [21] M. Szwarc, 'Living' polymers, *Nature*, 178 (1956) 1168-1169.
- [22] Y. Kamei, A. Nagai, A. Sudo, H. Nishida, K. Kikukawa, T. Endo, Convenient synthesis of poly( $\gamma$ -benzyl-L-glutamate) from activated urethane derivatives of  $\gamma$ -benzyl-L-glutamate, *Journal of Polymer Science Part A: Polymer Chemistry*, 46 (2008) 2649-2657.
- [23] Y. Kamei, A. Sudo, T. Endo, Synthesis of polypeptide having defined terminal structures through polymerization of activated urethane-derivative of  $\gamma$ -benzyl-L-glutamate, *Macromolecules*, 41 (2008) 7913-7919.
- [24] C. Mayer, Nanocapsules as drug delivery systems, *The International journal of artificial organs*, 28 (2005) 1163-1171.
- [25] H. Feng, Micro- and Nanocapsules Based on Artificial Peptides, *Molecules*, 27 (2022).
- [26] H. Jarrod Anders, Role of racemic hydrophobic segments in block copolypeptide assemblies, University of California, 2008.
- [27] J.A. Hanson, C.B. Chang, S.M. Graves, Z. Li, T.G. Mason, T.J. Deming, Nanoscale double emulsions stabilized by single-component block copolypeptides, *Nature*, 455 (2008) 85-88.
- [28] A. Berger, J. Noguchi, E. Katchalski, Poly-L-cysteine, *Journal of the American Chemical Society*, 78 (1956) 4483-4488.
- [29] C. Mayer, NMR Studies of Nanoparticles, 2005, pp. 205-258.
- [30] C. Mayer, Nuclear magnetic resonance on dispersed nanoparticles, *Progress in nuclear magnetic resonance spectroscopy*, 4 (2002) 307-366.
- [31] M.H. Levitt, Spin Dynamics Basics of Nuclear Magnetic Resonance (2nd edition) John Wiley & Sons 2013.
- [32] M.H. Levitt, Spin dynamics: basics of nuclear magnetic resonance, John Wiley & Sons 2013.
- [33] J. Keeler, Understanding NMR spectroscopy, Wiley 2005.
- [34] W. Gabuelse, molecular orientation and dynamics in poly(ethylene terephthalate) yarns: A Solid State NMR Study Shaker Publishing B.V. 1997.
- [35] J. Linders, Untersuchung nanoskaliger Systeme mit Feldgradienten NMR: Von Amphiphilen bis zur Nanokapsel., Universität Duisburg-Essen, 2014.
- [36] E.O. Stejskal, J.E. Tanner, Spin Diffusion Measurements: Spin Echoes in the Presence of a Time-Dependent Field Gradient, *Journal of Chemical Physics*, 42 (1965) 288-+.
- [37] C. Mayer, A. Bauer, Molecular exchange through capsule membranes observed by pulsed field gradient NMR, 2006.
- [38] A. Einstein, Investigations on the Theory of the Brownian Movement, Courier Corporation 1956.
- [39] S. Beuermann, Einbindung von Polyalkylcyanoacrylat-Nanokapseln in Metalloberflächen,

Universität Duisburg-Essen, 2015.

[40] C. Finder, M. Wohlgemuth, C. Mayer, Analysis of Particle Size Distribution by Particle Tracking, *Particle & Particle Systems Characterization*, 21 (2004) 372-378.

[41] P.J. de Pablo, Introduction to atomic force microscopy, *Methods Mol Biol*, 783 (2011) 197-212.

[42] NanoWizard AFM Handbook, JPK instruments AG2012.

[43] Y. Kamei, A. Sudo, H. Nishida, K. Kikukawa, T. Endo, Synthesis of polypeptides from activated urethane derivatives of  $\alpha$ -amino acids, *Journal of Polymer Science Part A: Polymer Chemistry*, 46 (2008) 2525-2535.

[44] S. Yamada, K. Koga, A. Sudo, M. Goto, T. Endo, Phosgene-free synthesis of polypeptides: Useful synthesis for hydrophobic polypeptides through polycondensation of activated urethane derivatives of  $\alpha$ -amino acids, *Journal of Polymer Science Part A: Polymer Chemistry*, 51 (2013) 3726-3731.

[45] S. Yamada, A. Sudo, M. Goto, T. Endo, Phosgene-free synthesis of polypeptides using activated urethane derivatives of  $\alpha$ -amino acids: an efficient synthetic approach to hydrophilic polypeptides, *RSC Adv.*, 4 (2014) 29890-29896.

[46] Y. Fujita, K. Koga, H.-K. Kim, X.-S. Wang, A. Sudo, H. Nishida, T. Endo, Phosgene-free synthesis of N-carboxyanhydrides of  $\alpha$ -amino acids based on bisarylcarbonates as starting compounds, *Journal of Polymer Science Part A: Polymer Chemistry*, 45 (2007) 5365-5370.

[47] Y. Yang, *Side Reactions in Peptide Synthesis*, Academic Press2015.

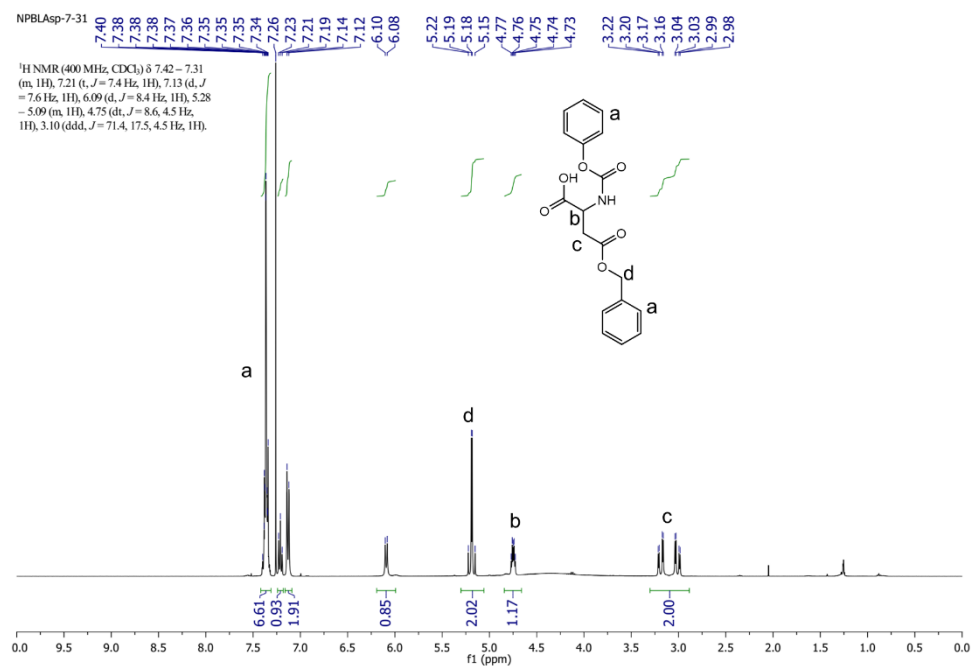
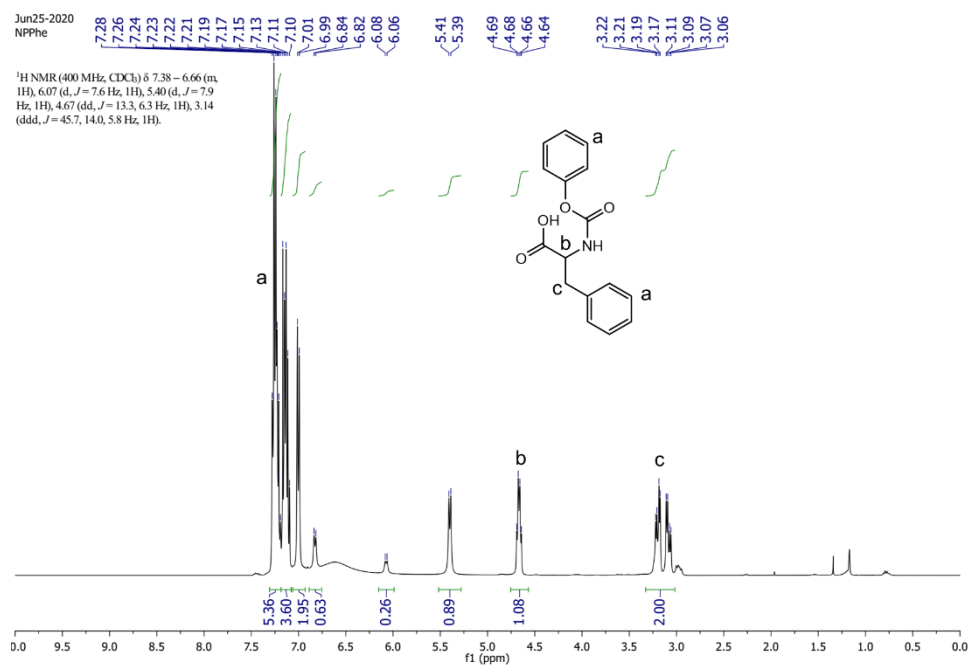
[48] H. Yajima, N. Fujii, H. Ogawa, H. Kawatani, Trifluoromethanesulphonic Acid, as a Deprotecting Reagent in Peptide Chemistry, *J Chem Soc Chem Comm*, (1974) 107-108.

[49] M. Bodanszky, *Principles of Peptide Synthesis*, Springer Science & Business Media2012.

[50] C. Mayer, Physical chemistry of dispersed nanostructures in blood, *Nanotechnology for Hematology, Blood Transfusion, and Artificial Blood.*, (2022).

## 7 Appendices

## 7.1 Supporting information

7.1.1 Measured  $^1\text{H}$  NMR spectraFigure 7.1  $^1\text{H}$  NMR spectrum of NPBLAsp (solvent:  $\text{CDCl}_3$ ).Figure 7.2  $^1\text{H}$  NMR spectrum of NPPhe (solvent:  $\text{CDCl}_3$ ).

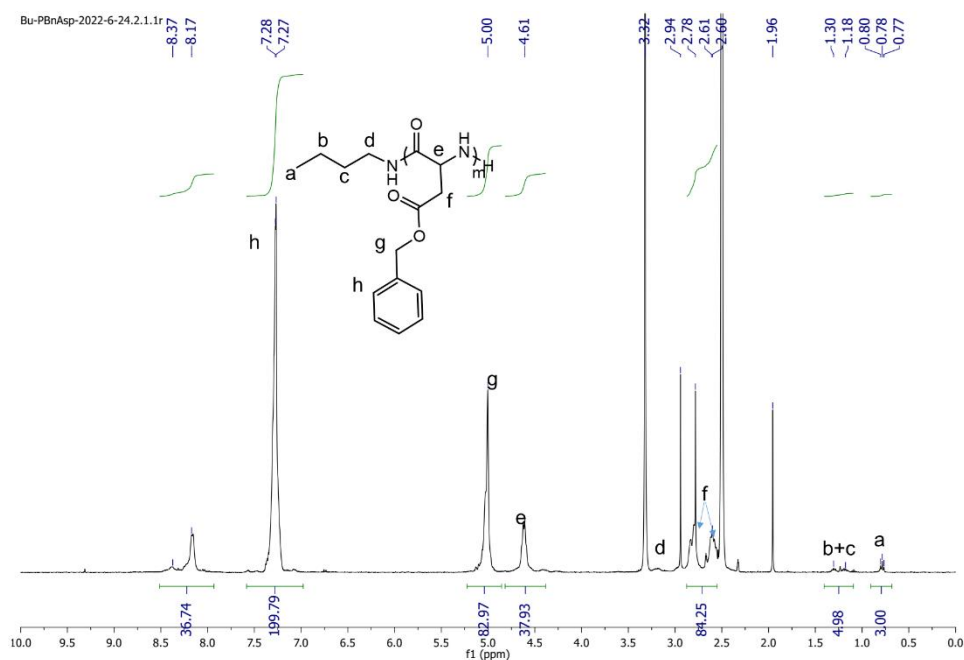


Figure 7.3  $^1\text{H}$  NMR spectrum of Bu-BnAsp<sub>40</sub> (solvent: DMSO- $d_6$ ).

According to the integrals of the signals a and h, the average number of Asp units is approximately 40.

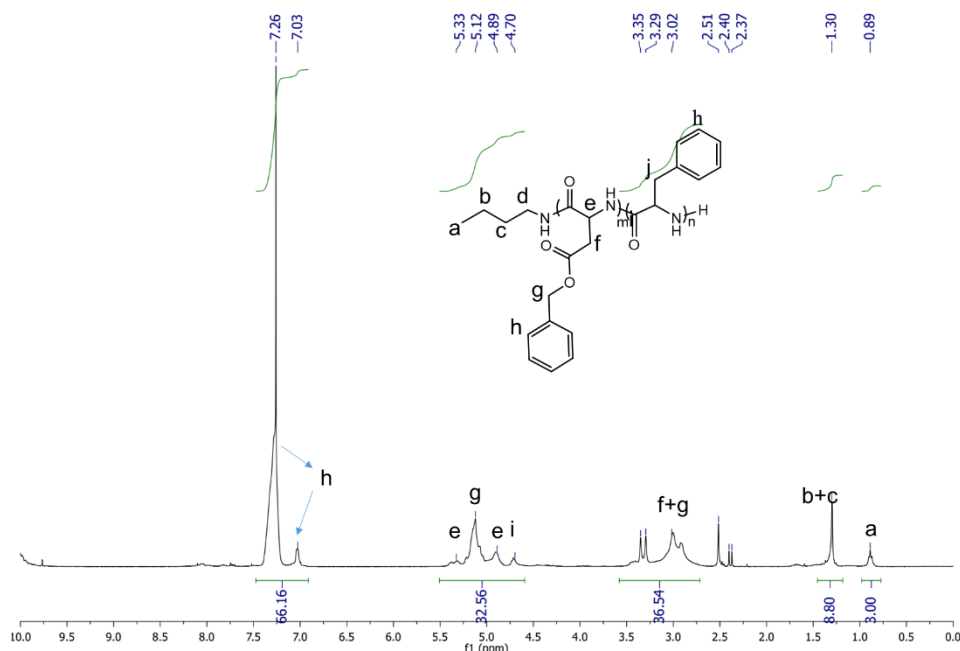


Figure 7.4  $^1\text{H}$  NMR spectrum of Bu-BnAsp<sub>40</sub>-Phe<sub>5</sub> (solvent: CDCl<sub>3</sub>/TFA- $d_1$ ).

Polypeptides with Phe block are not well dissolved into DMSO. Therefore, CDCl<sub>3</sub>/TFA- $d_1$  are used as the solvent. BnAsp block may react with TFA- $d_1$ , leading to the inaccuracy of the

integral. Therefore, the average number of Phe units was determined in the corresponding  $^1\text{H}$  NMR spectrum of the deprotected di-block peptide.

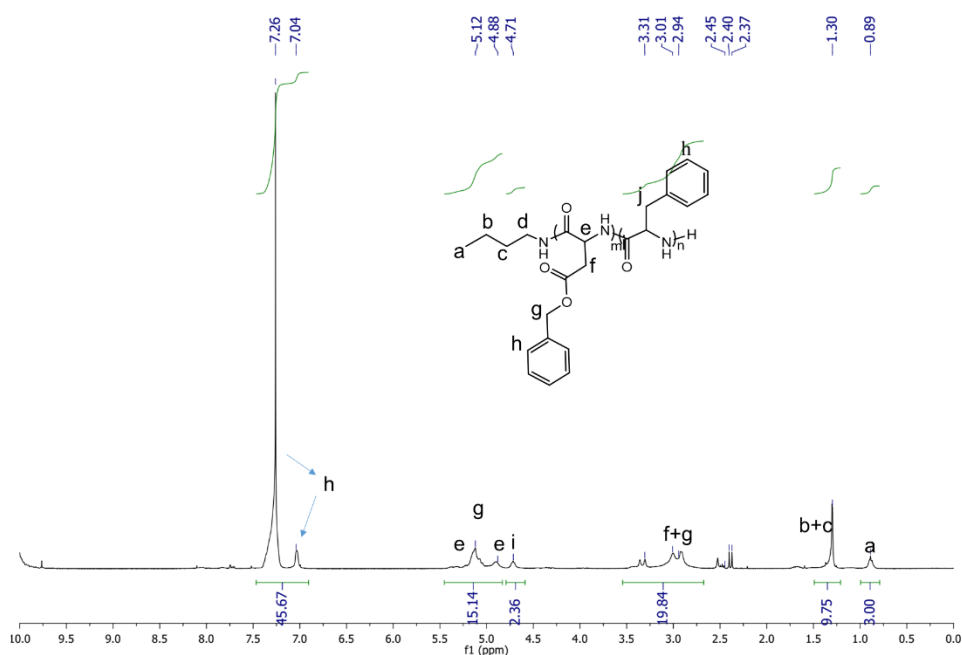


Figure 7.5  $^1\text{H}$  NMR spectrum of Bu-BnAsp<sub>40</sub>-Phe<sub>9</sub> (solvent: CDCl<sub>3</sub>/TFA-d<sub>1</sub>).

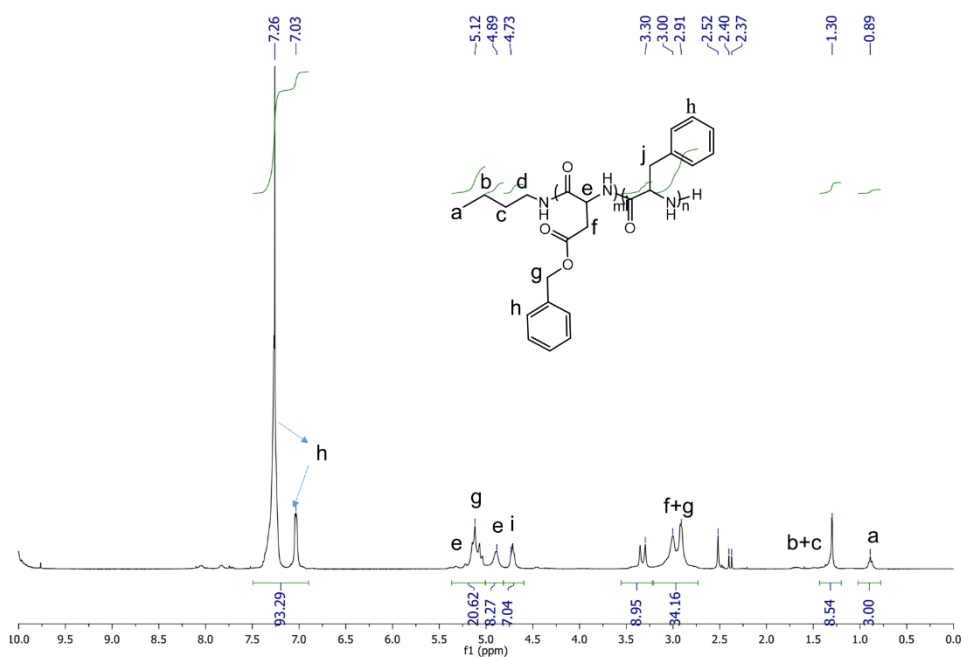


Figure 7.6  $^1\text{H}$  NMR spectrum of Bu-BnAsp<sub>40</sub>-Phe<sub>14</sub> (solvent: CDCl<sub>3</sub>/TFA-d<sub>1</sub>).

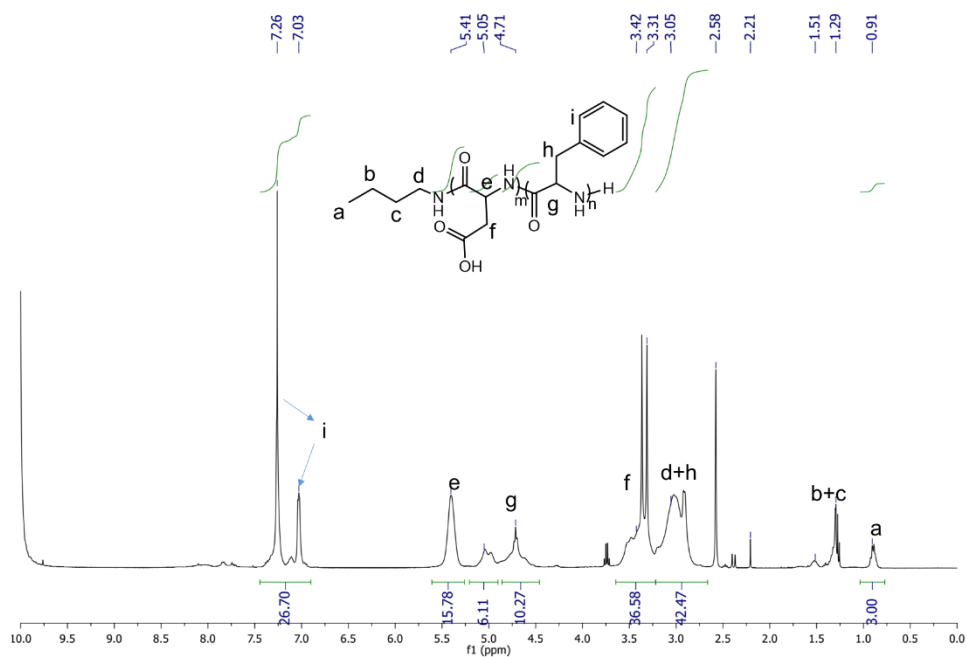


Figure 7.7 <sup>1</sup>H NMR spectrum of Bu-Asp<sub>40</sub>-Phe<sub>5</sub> (solvent: CDCl<sub>3</sub>/TFA-d<sub>1</sub>).

According to the integrals of the signals a and i, the average number of Phe units is approximately 5.

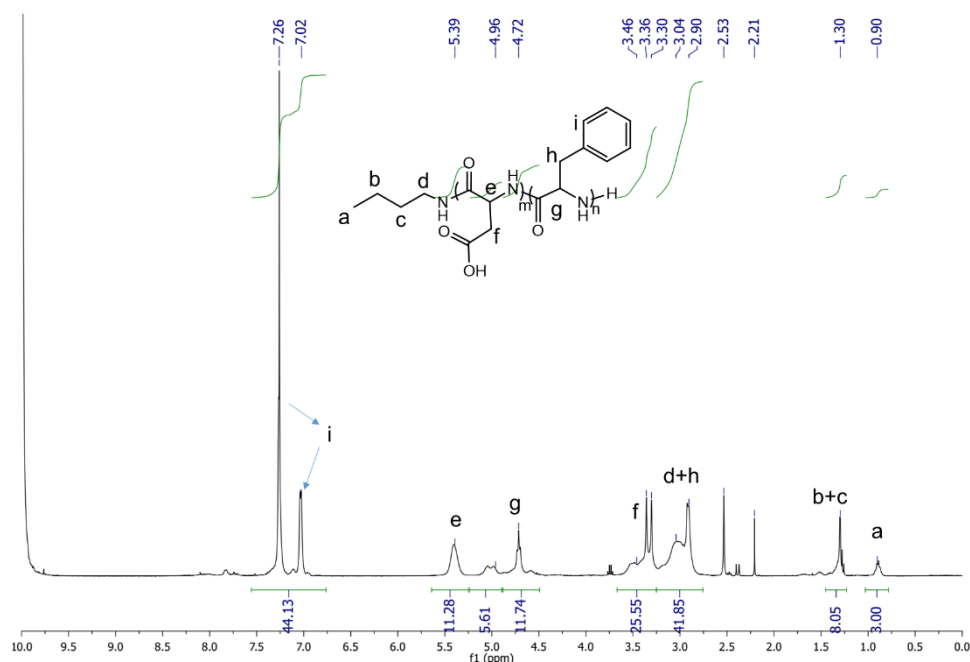


Figure 7.8 <sup>1</sup>H NMR spectrum of Bu-Asp<sub>40</sub>-Phe<sub>9</sub> (solvent: CDCl<sub>3</sub>/TFA-d<sub>1</sub>).

According to the integrals of the signals a and i, the average number of Phe units is approximately 9.

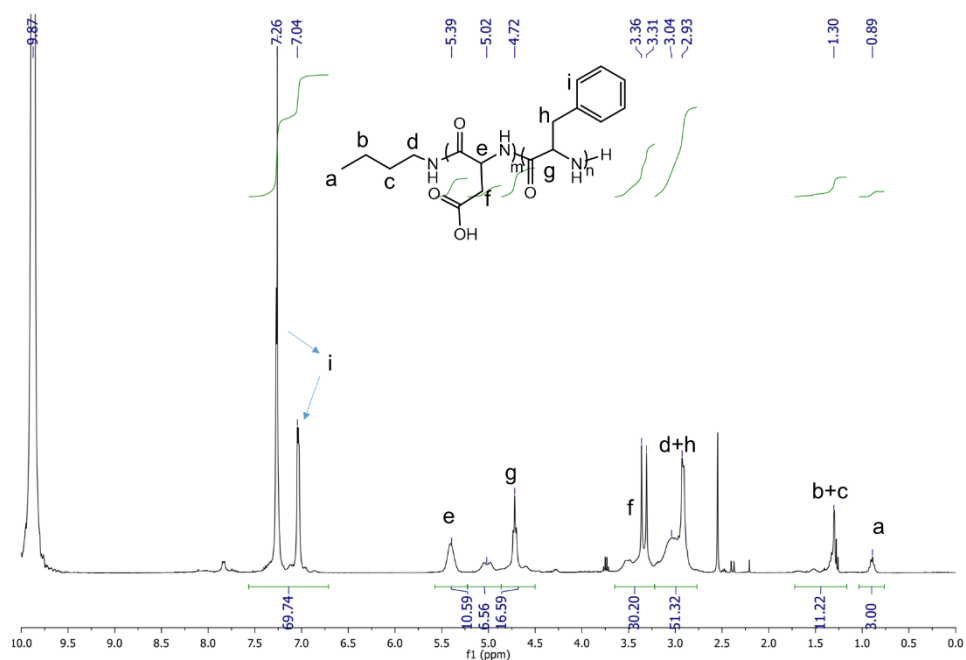


Figure 7.9 <sup>1</sup>H NMR spectrum of Bu-Asp<sub>40</sub>-Phe<sub>14</sub> (solvent: CDCl<sub>3</sub>/TFA-d<sub>1</sub>).

According to the integrals of the signals a and i, the average number of Phe units is approximately 14.

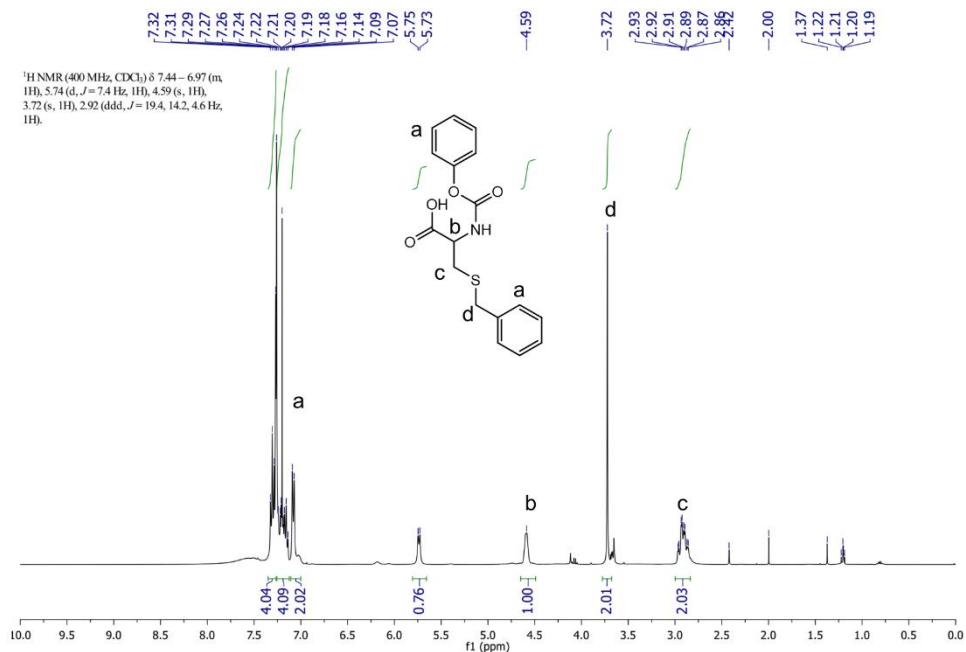
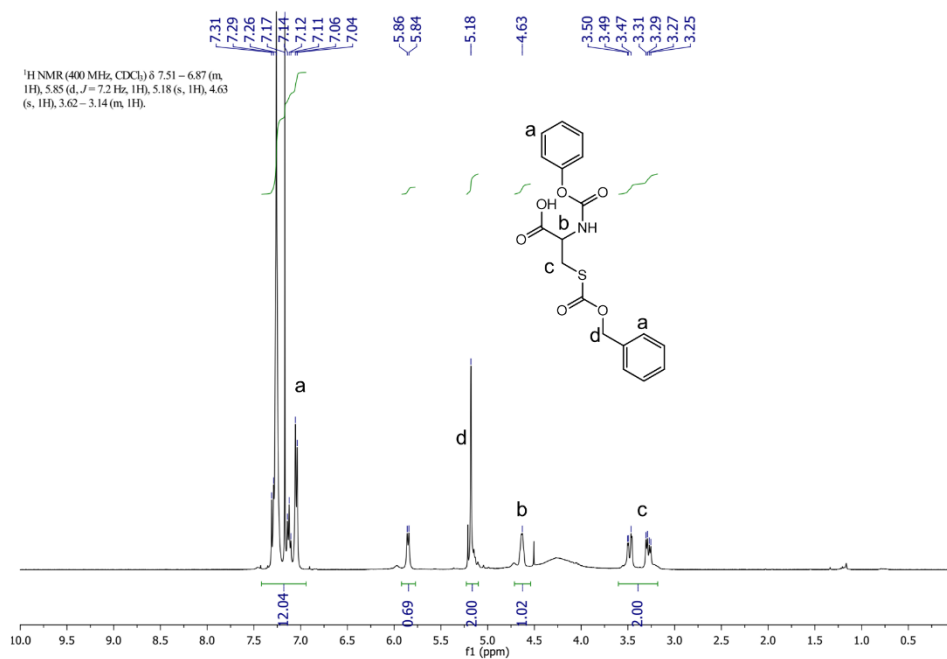
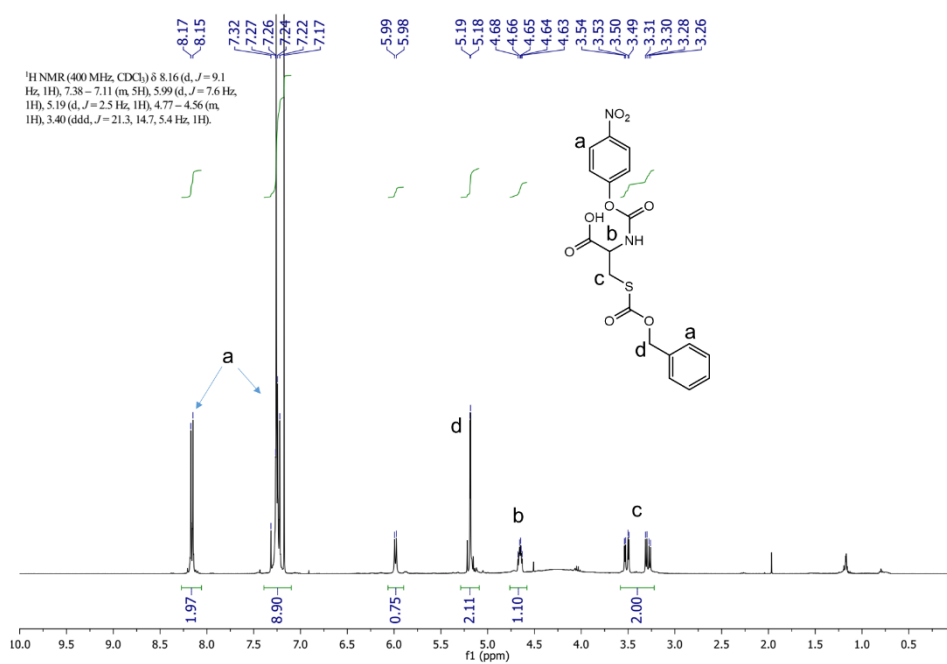


Figure 7.10 <sup>1</sup>H-NMR spectrum of NPBnCys (solvent: CDCl<sub>3</sub>).

Figure 7.11 <sup>1</sup>H-NMR spectrum of NPCbzCys (solvent: CDCl<sub>3</sub>).Figure 7.12 <sup>1</sup>H-NMR spectrum of NNPCbzCys (solvent: CDCl<sub>3</sub>).

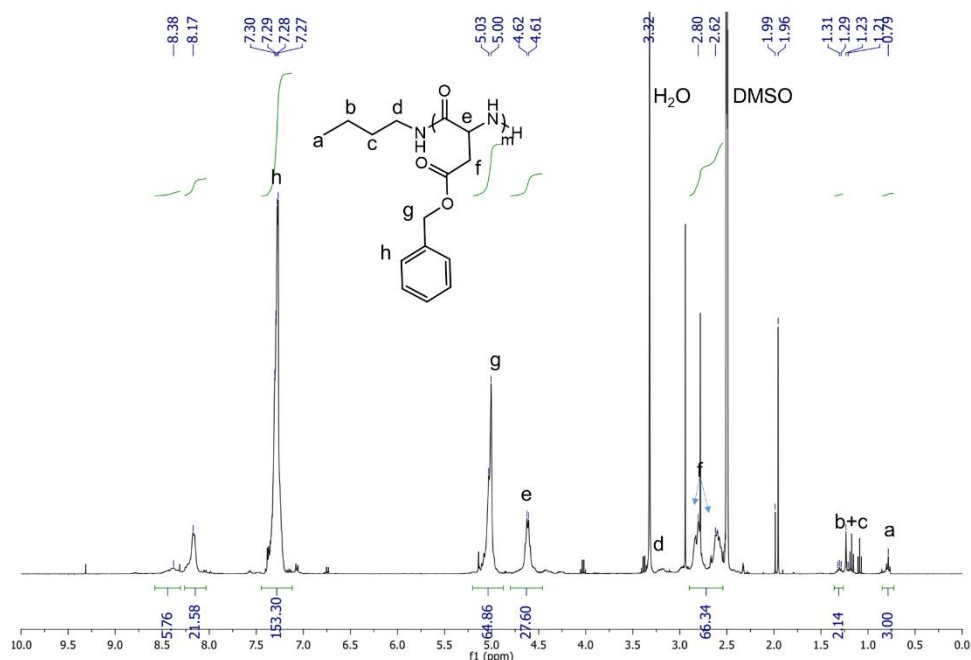


Figure 7.13 <sup>1</sup>H NMR spectrum of Bu-BnAsp<sub>31</sub> (solvent: DMSO-d<sub>6</sub>).

According to the integrals of the signals a and h, the average number of Asp units is approximately 31.

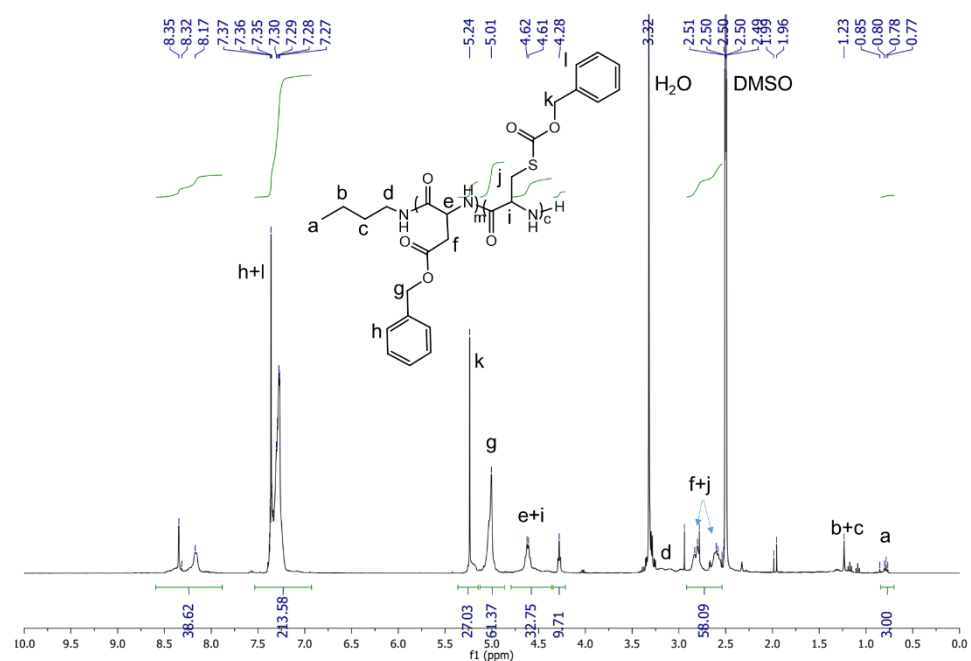


Figure 7.14 <sup>1</sup>H NMR spectrum of Bu-BnAsp<sub>31</sub>-CbzCys<sub>14</sub> (solvent: DMSO-d<sub>6</sub>).

According to the integrals of the signals a and k, the average number of Cys units is approximately 14.

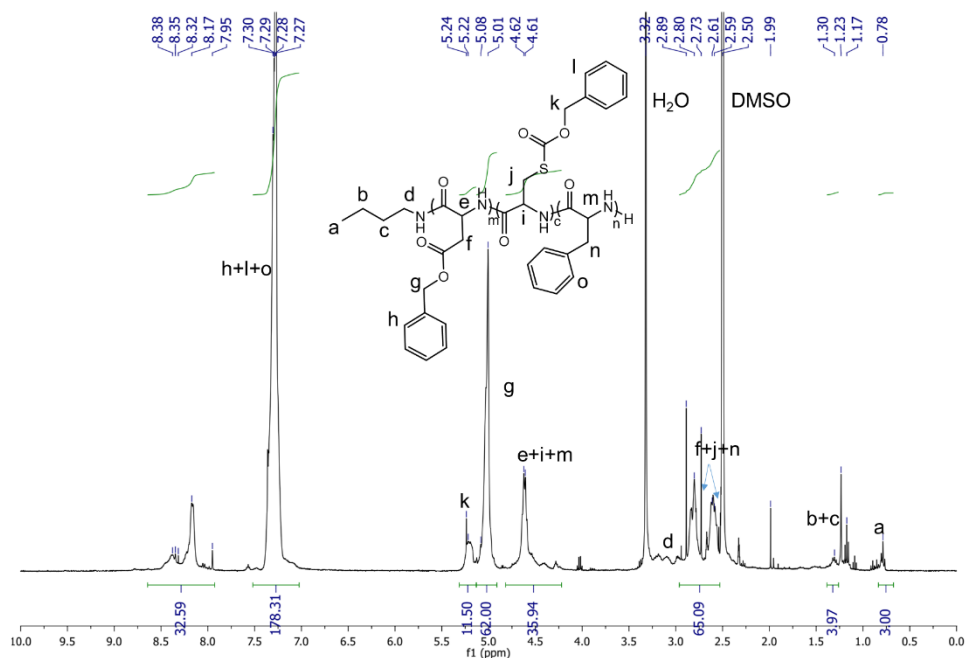


Figure 7.15  $^1\text{H}$  NMR spectrum of Bu-BnAsp<sub>31</sub>-CbzCys<sub>6</sub>-Phe<sub>n</sub> (solvent: DMSO-*d*<sub>6</sub>)

The integral for k decreased from 27 to 11.5, possibly due to the loss of self-polymerized oligo-CbzCys during the precipitation process.

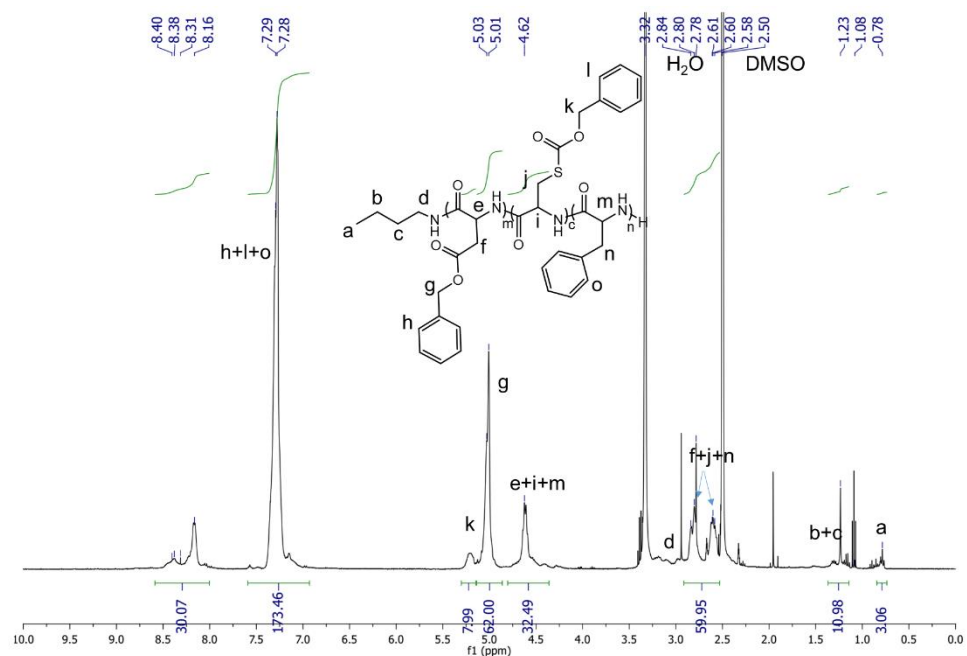


Figure 7.16  $^1\text{H}$  NMR spectrum of Bu-BnAsp<sub>31</sub>-CbzCys<sub>4</sub>-Phe<sub>n</sub> (solvent: DMSO-*d*<sub>6</sub>)

Again, the integral for k decreased from 11.5 to 7.99. Therefore, the average number for CbzCys in the polypeptides should be around 4. The average number of Phe units was

determined in the deprotected tri-block peptide.

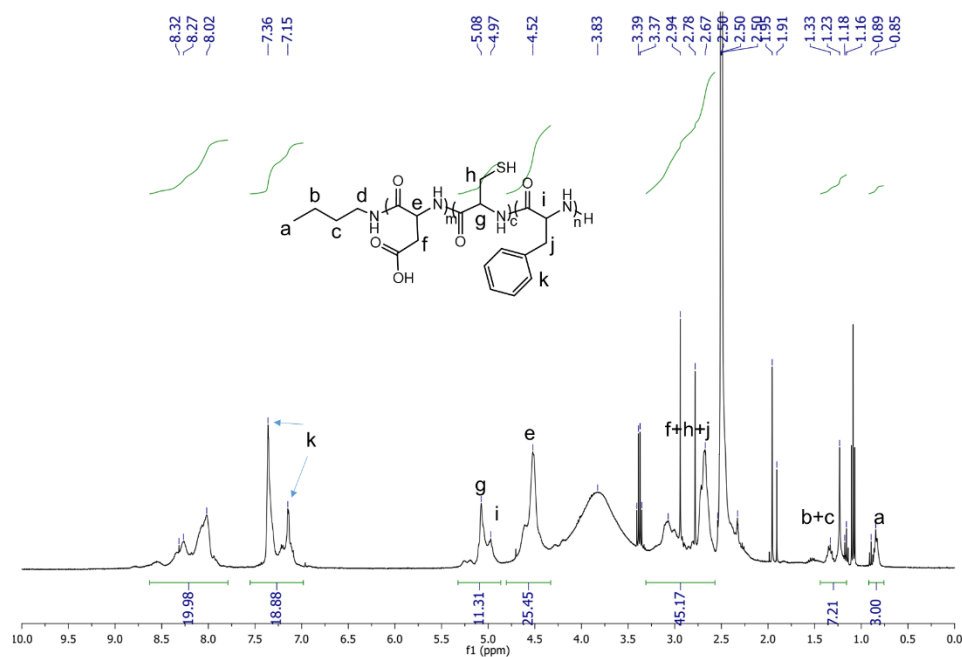


Figure 7.17 <sup>1</sup>H NMR spectrum of Bu-Asp<sub>31</sub>-Cys<sub>4</sub>-Phe<sub>3</sub> (solvent: DMSO-d<sub>6</sub>).

According to the integrals of the signals a and k, the average number of Phe units is approximately 3.

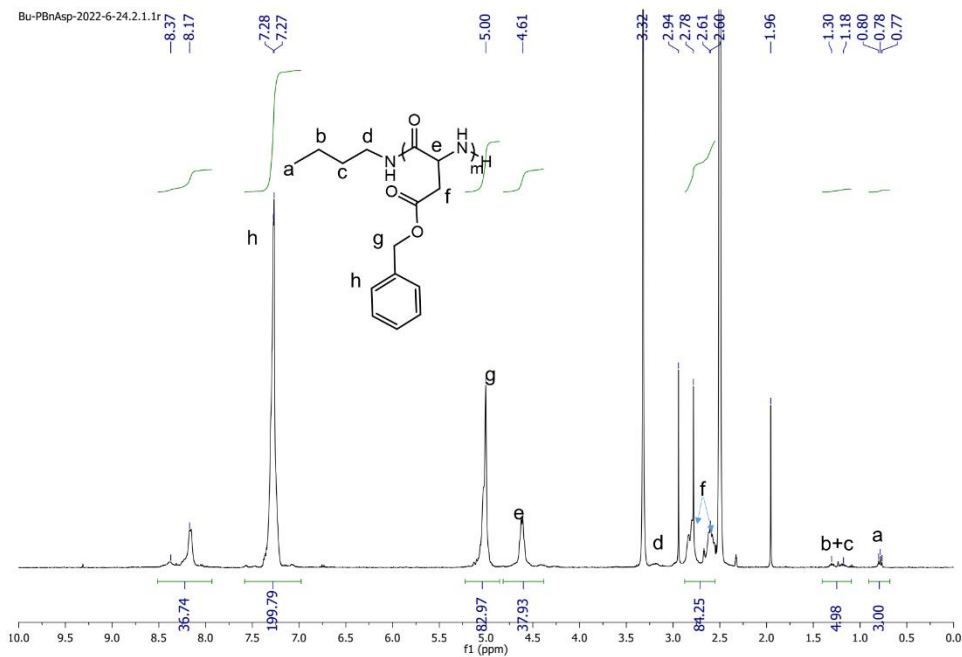


Figure 7.18 <sup>1</sup>H NMR spectrum of Bu-BnAsp<sub>40</sub> (solvent: DMSO-d<sub>6</sub>).

According to the integrals of the signals a and g, the average number of Asp units is approximately 40. (This figure is the same one as Figure 7.3. It is presented here again for a convenient comparison with the following figures)

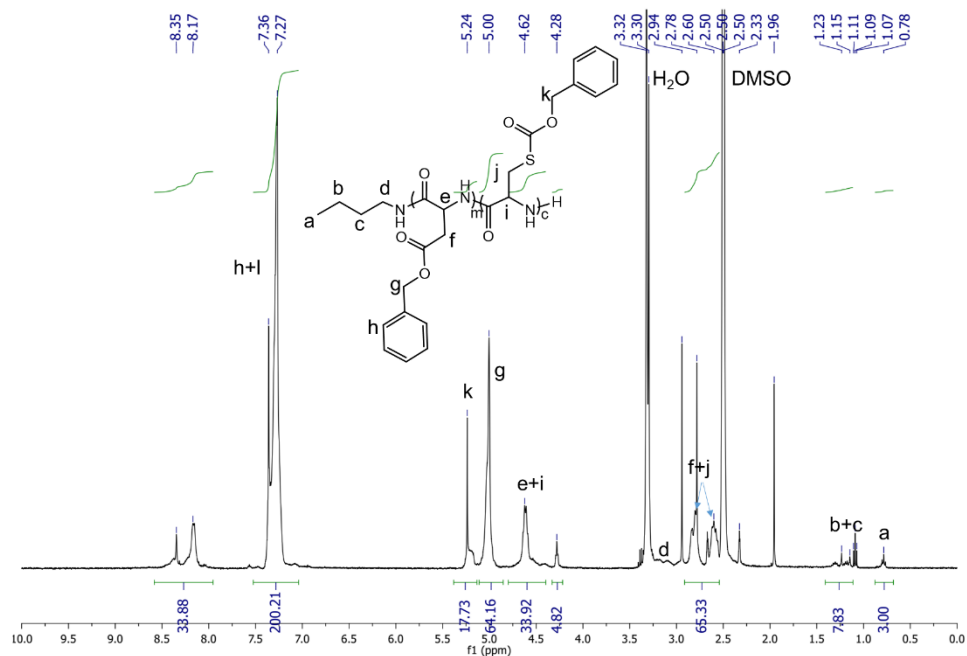


Figure 7.19  $^1\text{H}$  NMR spectrum of  $\text{Bu-BnAsp}_{40}\text{-CbzCys}_9$  (solvent:  $\text{DMSO-d}_6$ ).

According to the integrals of the signals a and k, the average number of Cys units is approximately 9.

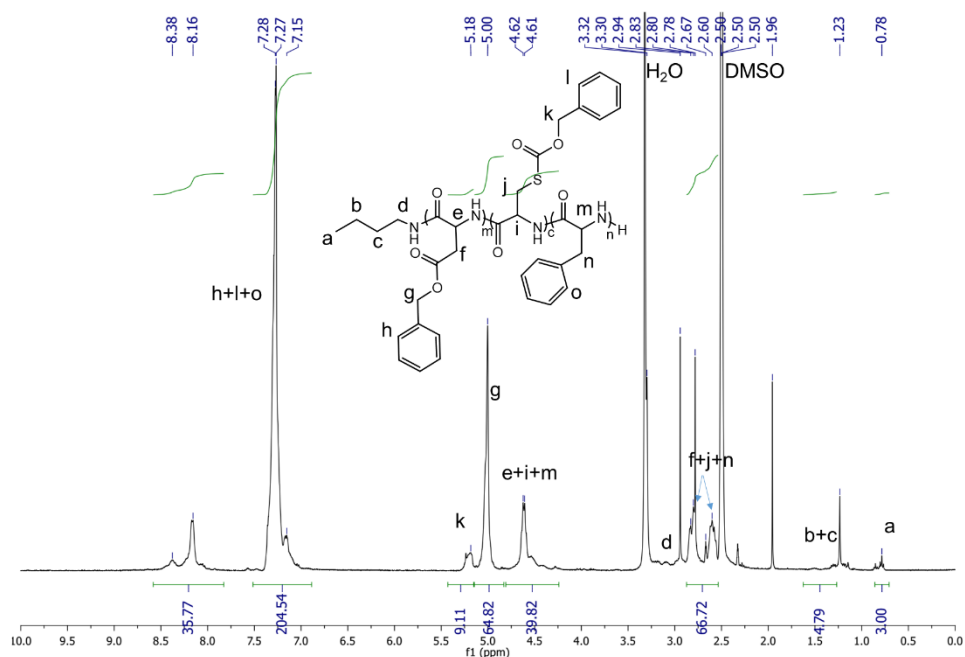


Figure 7.20  $^1\text{H}$  NMR spectrum of Bu-BnAsp<sub>40</sub>-CbzCys<sub>5</sub>-Phe<sub>n</sub> (solvent: DMSO- $d_6$ ).

Again, the integrals for CbzCys block decreases from 17.73 to 9.11, possibly due to the loss of self-polymerized oligo-CbzCys during the precipitation process. Therefore, the average number for CbzCys in the polypeptides should be around 5.

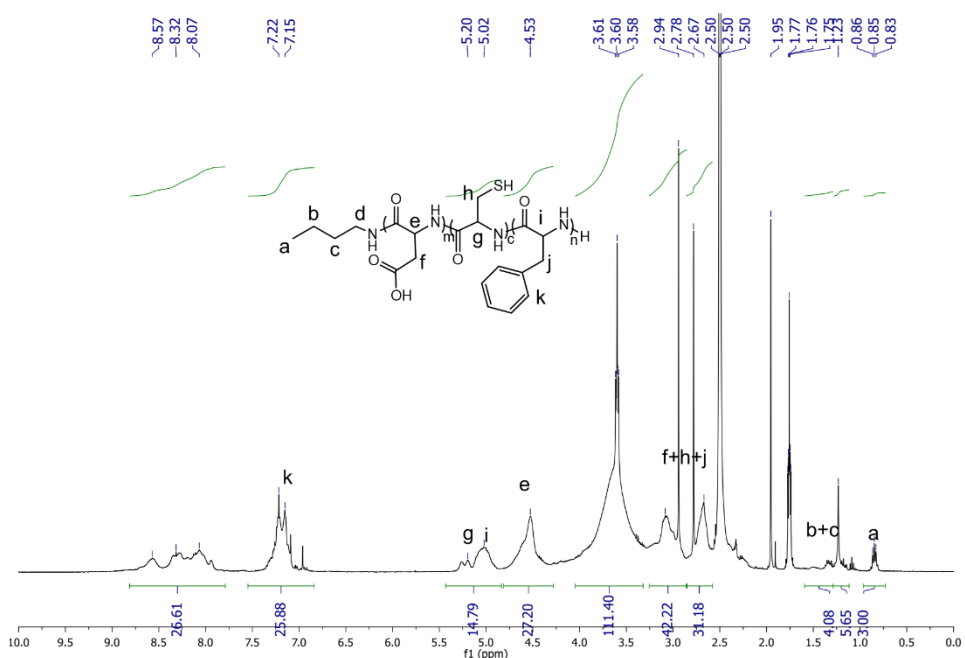


Figure 7.21  $^1\text{H}$  NMR spectrum of Bu-Asp<sub>40</sub>-Cys<sub>5</sub>-Phe<sub>5</sub> (solvent: DMSO- $d_6$ ).

According to the integrals of the signals a and k, the average number of Phe units is

approximately 5.

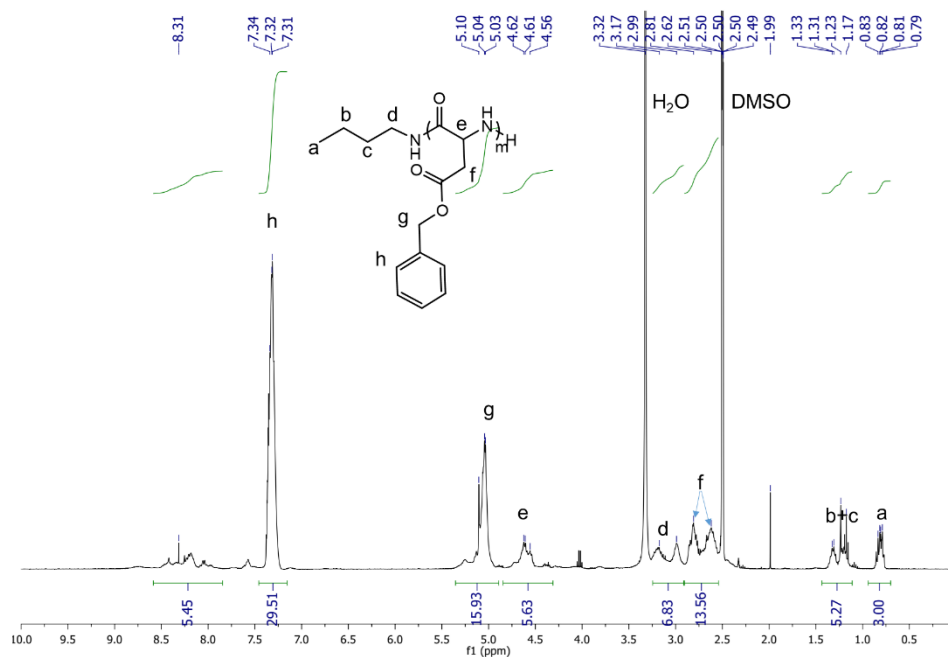


Figure 7.22  $^1\text{H}$  NMR spectrum of Bu-BnAsp<sub>6</sub> (solvent: DMSO-*d*<sub>6</sub>).

According to the integrals of the signals a and h, the average number of BnAsp units is approximately 6.

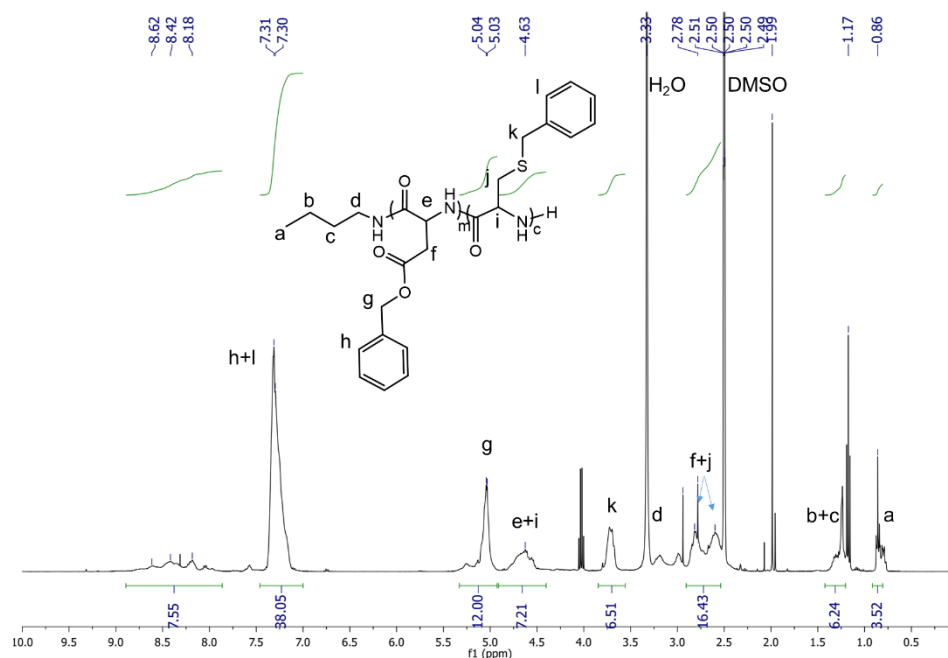


Figure 7.23  $^1\text{H}$  NMR spectrum of Bu-BnAsp<sub>6</sub>-BnCys<sub>3</sub> (solvent: DMSO-*d*<sub>6</sub>).

According to the integrals of the signals g and j, the average number of BnCys units is

approximately 3.

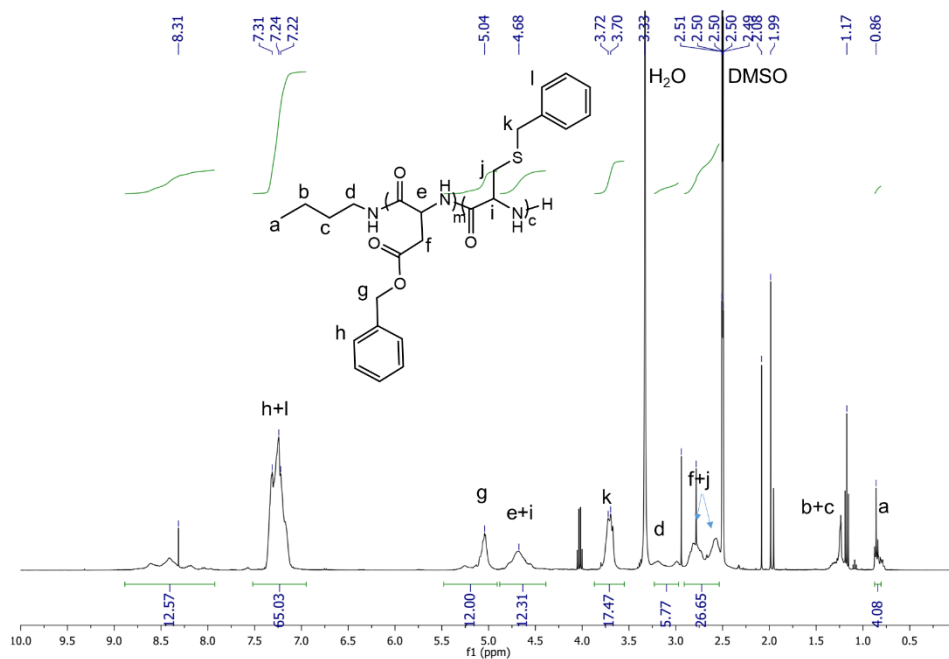


Figure 7.24  $^1\text{H}$  NMR spectrum of Bu-BnAsp<sub>6</sub>-BnCys<sub>8</sub> (solvent: DMSO-d<sub>6</sub>).

According to the integrals of the signals g and j, the average number of BnCys units is approximately 8. The polymerization of NPBnCys was repeated another time due to the low DP of first polymerization.

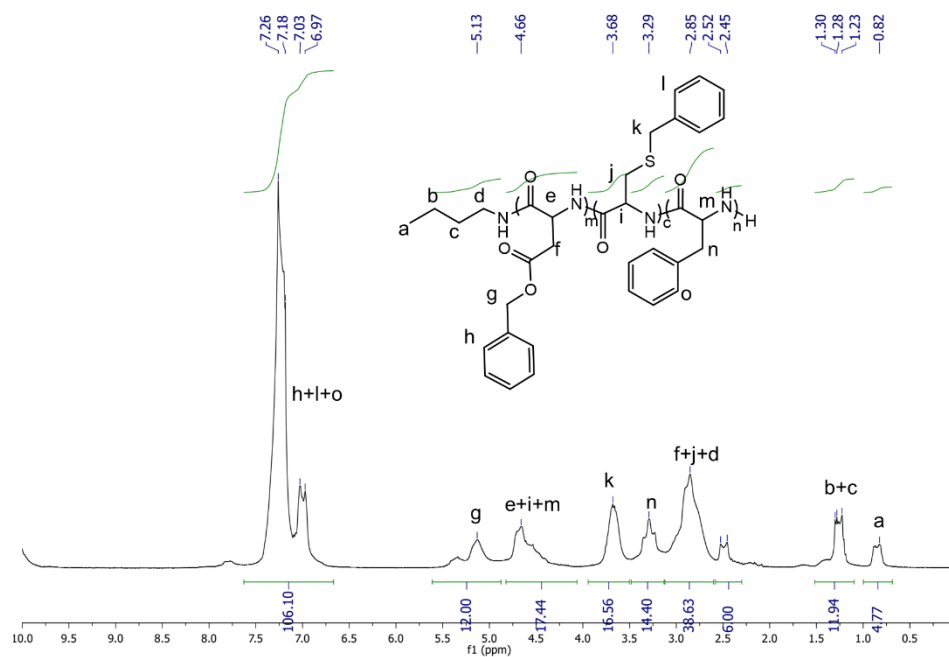


Figure 7.25  $^1\text{H}$  NMR spectrum of Bu-BnAsp<sub>6</sub>-BnCys<sub>8</sub>-Phe<sub>8</sub> (solvent: TFA-d<sub>1</sub>:CDCl<sub>3</sub>= 1:1).

According to the integrals of the signals g and k, the average number of Phe units is approximately 8.

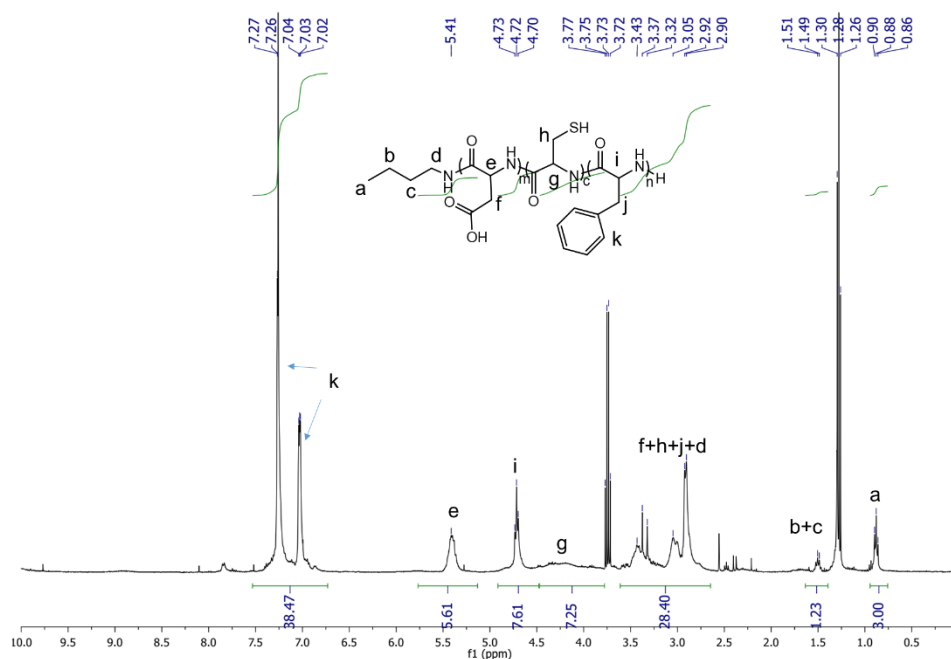


Figure 7.26 <sup>1</sup>H NMR spectrum of Bu-Asp<sub>6</sub>-Cys<sub>8</sub>-Phe<sub>8</sub> (solvent: TFA-d<sub>1</sub>: CDCl<sub>3</sub>= 1:1).

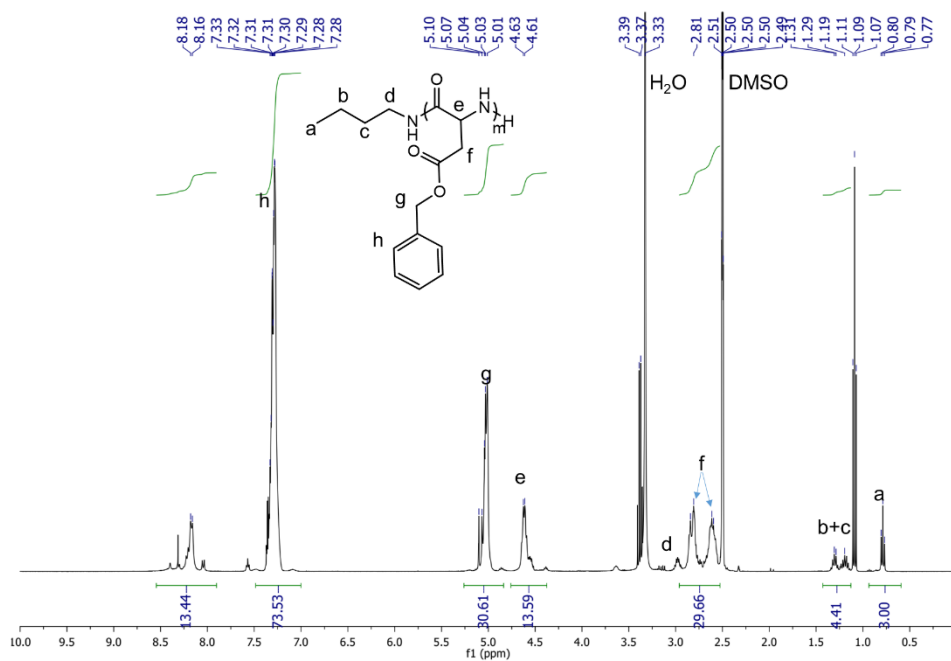


Figure 7.27 <sup>1</sup>H NMR spectrum of Bu-BnAsp<sub>13</sub> (solvent: DMSO-d<sub>6</sub>).

According to the integrals of the signals a and h, the average number of BnAsp units is approximately 13.

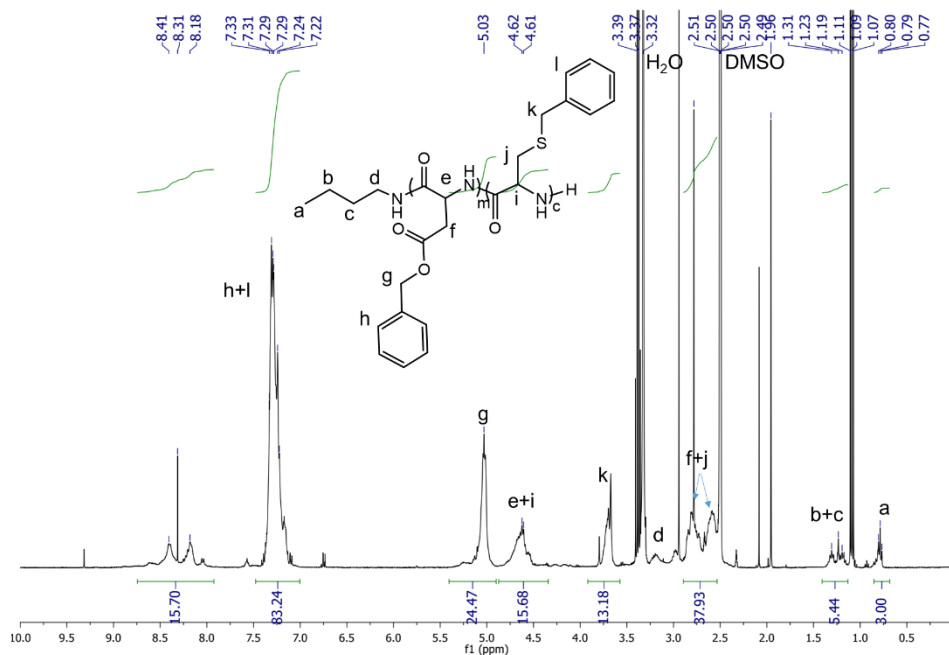


Figure 7.28  $^1\text{H}$  NMR spectrum of Bu-BnAsp<sub>13</sub>-BnCys<sub>6</sub> (solvent: DMSO-*d*<sub>6</sub>).

According to the integrals of the signals a and k, the average number of BnCys units is approximately 6.

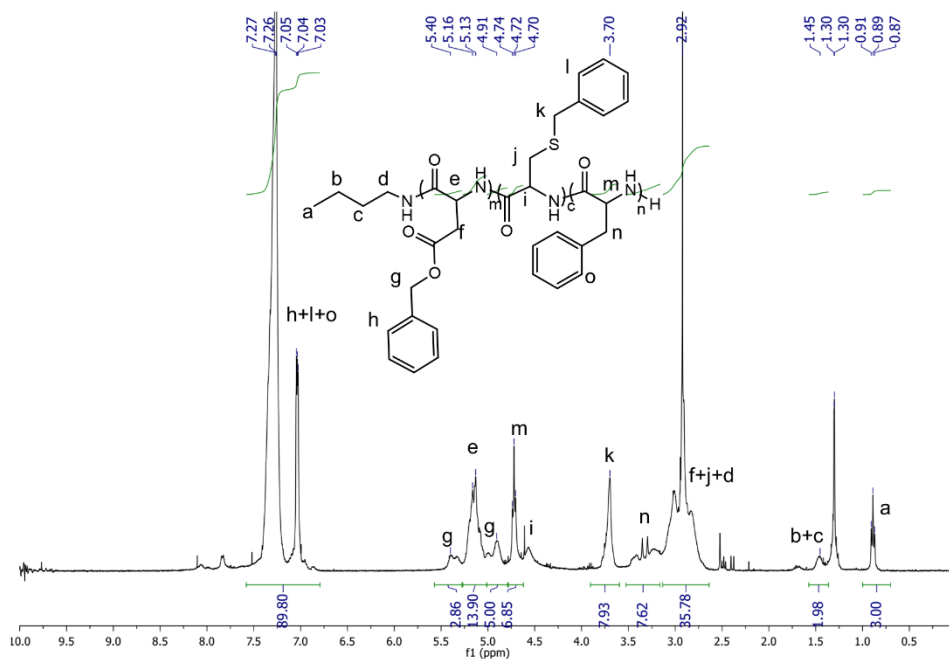


Figure 7.29  $^1\text{H}$  NMR spectrum of Bu-BnAsp<sub>13</sub>-BnCys<sub>6</sub>-Phe<sub>7</sub> (solvent: TFD-*d*<sub>1</sub> and CDCl<sub>3</sub>).

According to the integrals of the signals a and m, the average number of Phe units is approximately 7.

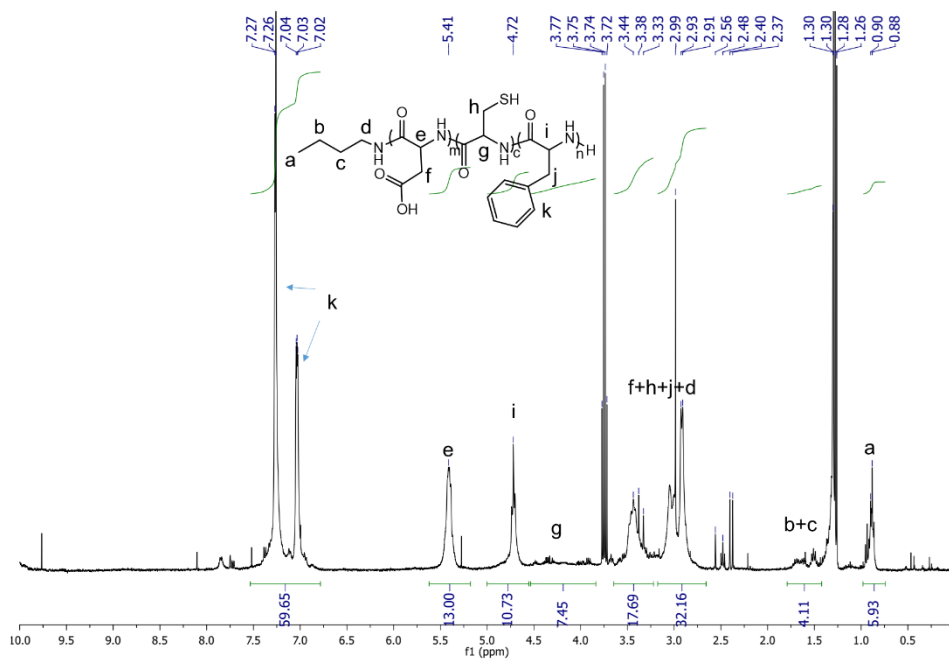


Figure 7.30 <sup>1</sup>H NMR spectrum of Bu-Asp<sub>13</sub>-Cys<sub>6</sub>-Phe<sub>7</sub> (solvent: TFA-d<sub>1</sub>: CDCl<sub>3</sub>= 1:1).

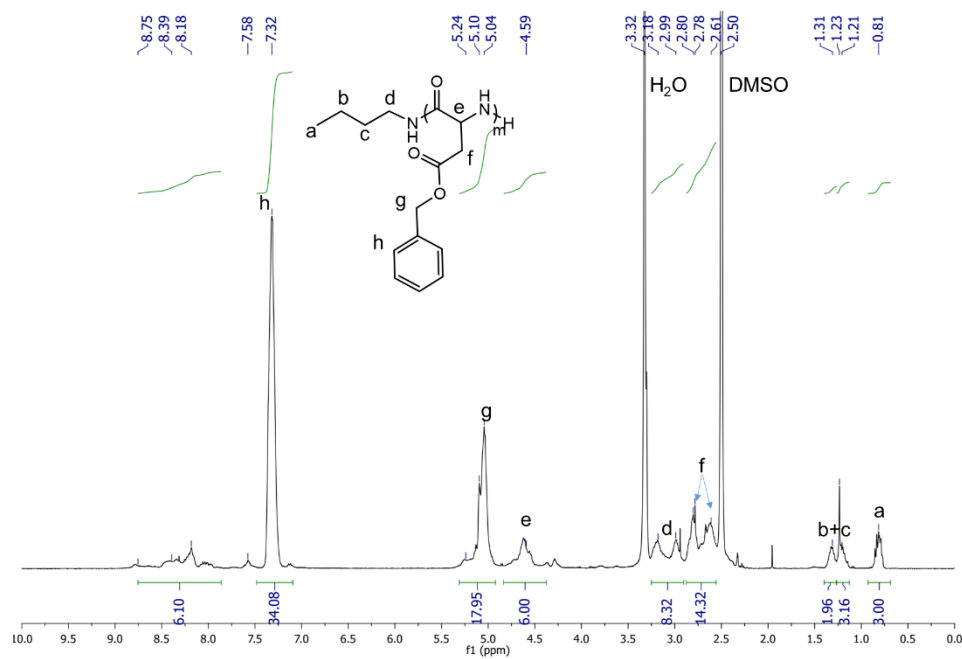


Figure 7.31 <sup>1</sup>H NMR spectrum of Bu-BnAsp<sub>7</sub> (solvent: DMSO-d<sub>6</sub>).

According to the integrals of the signals a and h, the average number of BnAsp units is approximately 7.

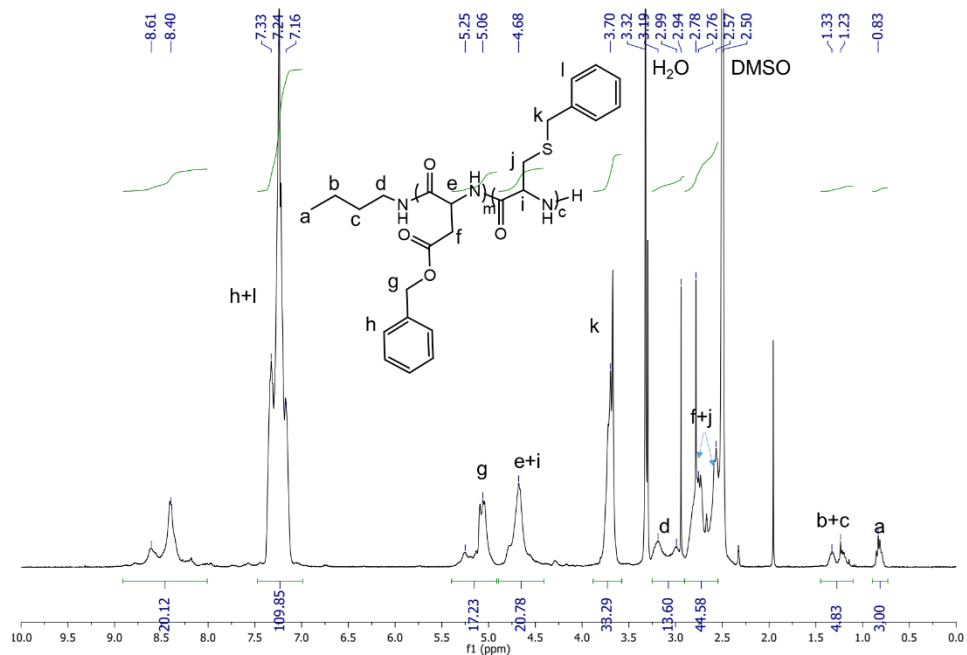


Figure 7.32 <sup>1</sup>H NMR spectrum of Bu-BnAsp<sub>7</sub>-BnCys<sub>15</sub> (solvent: DMSO-d<sub>6</sub>).

According to the integrals of the signals a and h+l, the average number of BnCys units is approximately 15.

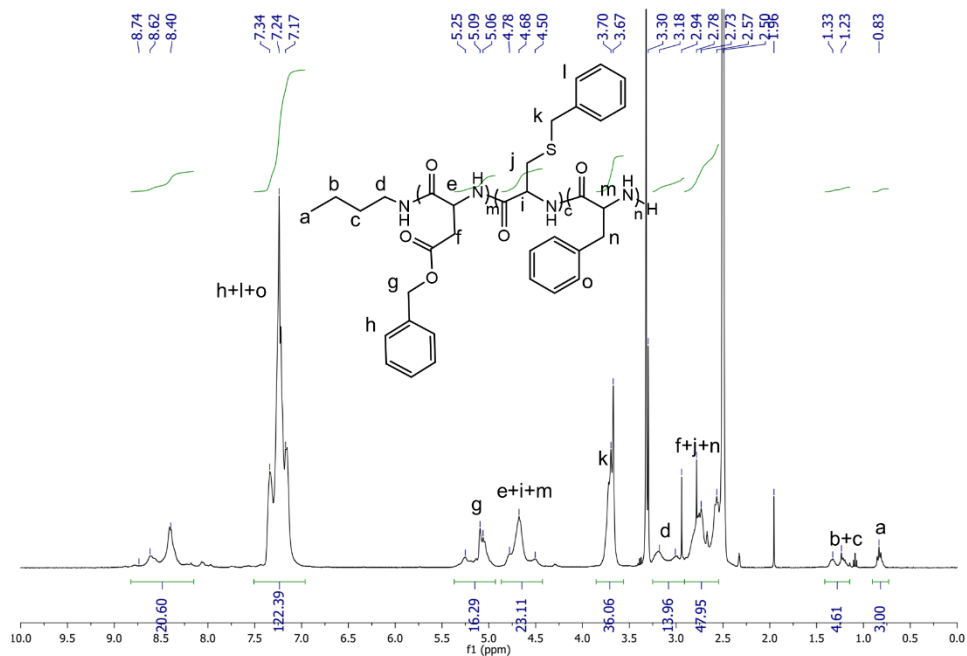


Figure 7.33 <sup>1</sup>H NMR spectrum of Bu-BnAsp<sub>7</sub>-BnCys<sub>15</sub>-Phe<sub>2</sub> (solvent: TFD-d<sub>1</sub> and CDCl<sub>3</sub>).

According to the integrals of the signals a and h+l+o, the average number of Phe units is approximately 2.

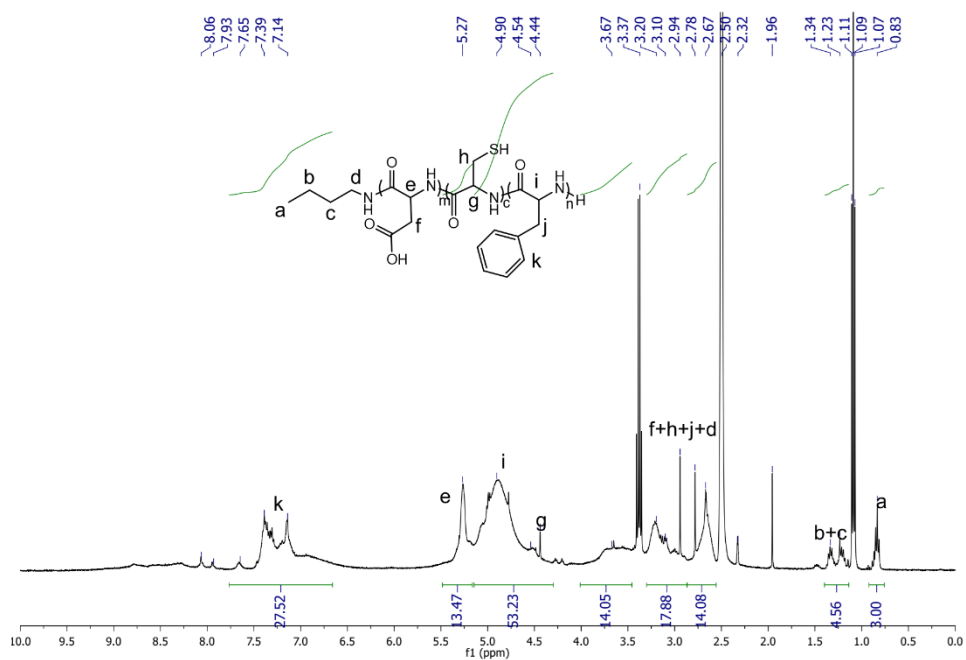


Figure 7.34 <sup>1</sup>H NMR spectrum of Bu-Asp<sub>7</sub>-Cys<sub>15</sub>-Phe<sub>2</sub> (solvent: DMSO-d<sub>6</sub>).

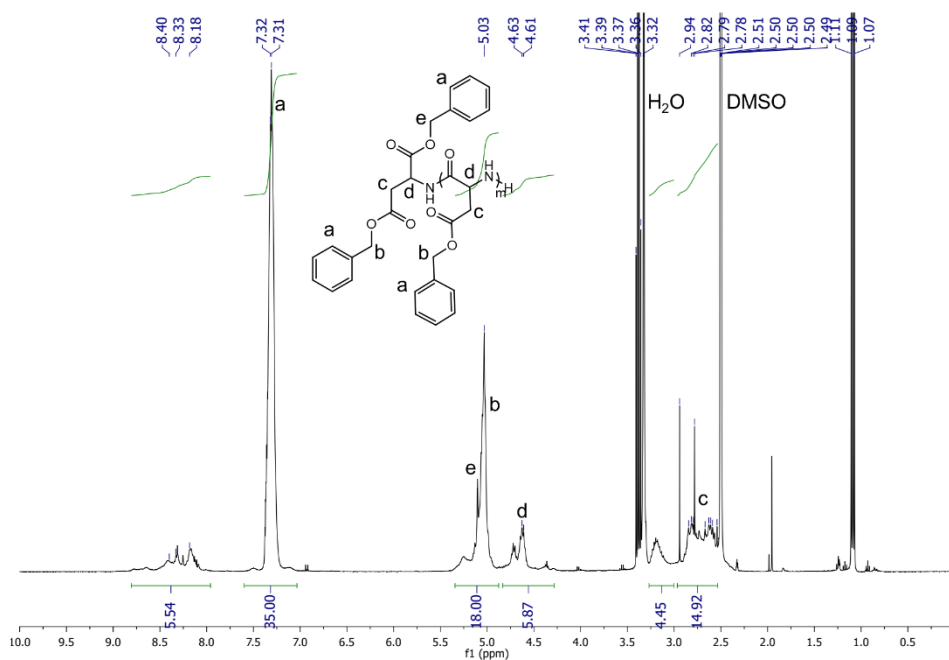


Figure 7.35 <sup>1</sup>H NMR spectrum of DBnAsp-BnAsp<sub>7</sub> (solvent: DMSO-d<sub>6</sub>).

According to the integrals of the signals b and e, the average number of BnAsp units is approximately 7.

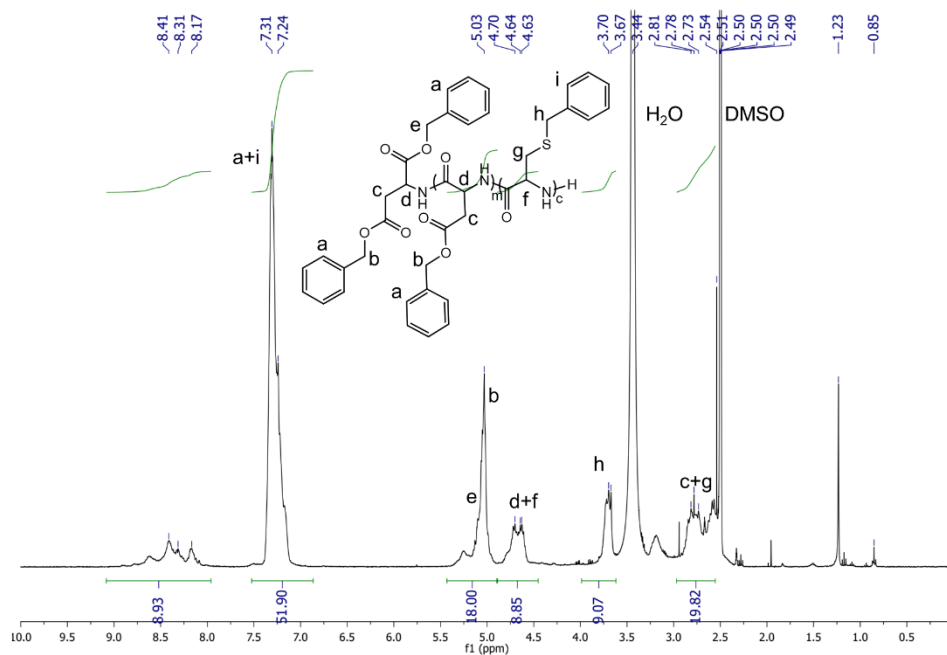


Figure 7.36  $^1\text{H}$  NMR spectrum of DBnAsp-BnAsp<sub>7</sub>-BnCys<sub>5</sub> (solvent: DMSO- $d_6$ ).

According to the integrals of the signals b and f, the average number of BnCys units is approximately 5 assuming that the average number of Asp in one chain is 8.

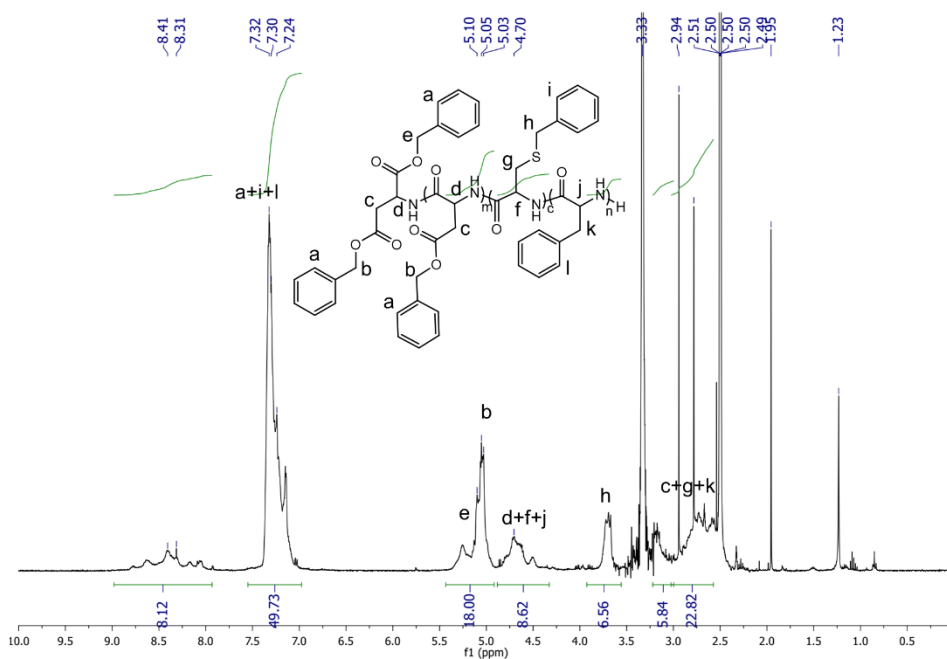


Figure 7.37  $^1\text{H}$  NMR spectrum of DBnAsp-BnAsp<sub>7</sub>-BnCys<sub>5</sub>-Phe<sub>n</sub> (solvent: DMSO- $d_6$ ).

The average number of Phe units is determined with the  $^1\text{H}$  NMR spectrum of deprotected product.

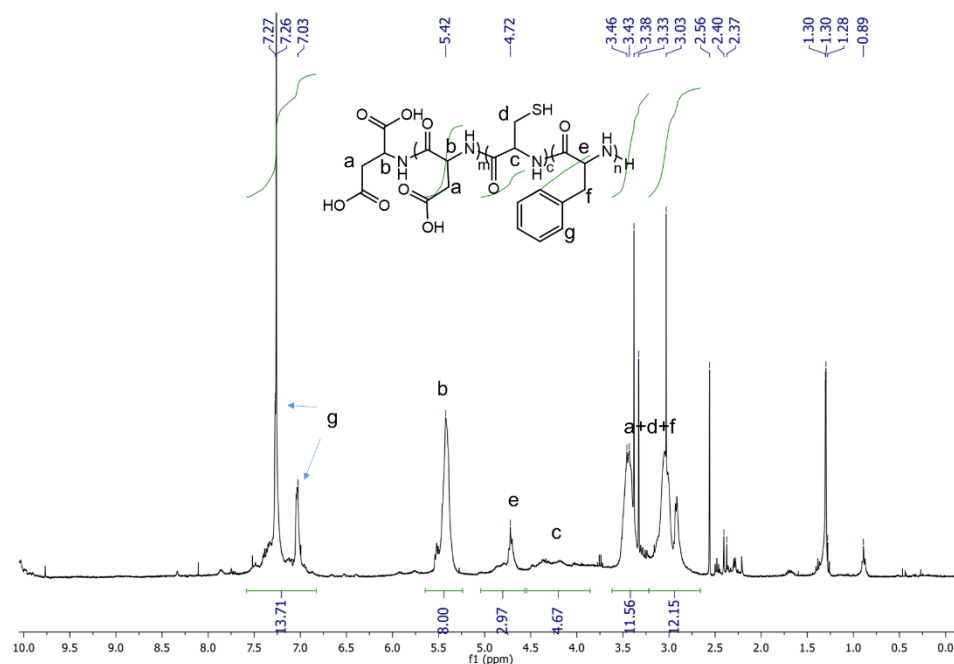


Figure 7.38 <sup>1</sup>H NMR spectrum of Asp<sub>8</sub>-Cys<sub>5</sub>-Phe<sub>3</sub> (solvent: TFA-d<sub>1</sub>: CDCl<sub>3</sub>= 1:1).

Assuming there are 8 aspartates in one chain, the average number of Phe unit is calculated as 3 according to the integral of signal b and e.

## 7.2 List of publications

1. Feng, H.<sup>1</sup>, Linders, J.<sup>1</sup>, Myszkowska, S., & Mayer, C. (2021). Capsules from synthetic diblock-peptides as potential artificial oxygen carriers. *Journal of Microencapsulation*, 38(5), 276-284.
2. Feng, H. (2022). Micro-and Nanocapsules Based on Artificial Peptides. *Molecules*, 27(4), 1373.
3. Feng, H., Fabrizi, J., Li, J., & Mayer, C. (2022). Syntheses of Polypeptides and Their Biomedical Application for Anti-Tumor Drug Delivery. *International Journal of Molecular Sciences*, 23(9), 5042.

## 7.3 Conference participation

2019 CENIDE-Jahresfeier, November 12<sup>th</sup>, 2019, Duisburg, German. Poster presentation, 'Nanocapsules from artificial peptides as oxygen carrier for blood substitutes'.

2022 ESB conference, 32<sup>nd</sup> Annual conference of the European society for biomaterials, September 4<sup>th</sup>-8<sup>th</sup>, 2022, Bordeaux, France.

2023 Uni Duisburg-Essen Neujahrskolloquium, January 18<sup>th</sup>, 2023, Essen, German. Oral presentation, 'Perfluorodecalin filled polypeptide capsules as artificial oxygen carriers'.

2023 3<sup>rd</sup> CENIDE Conference, May 2<sup>nd</sup>-4<sup>th</sup>, 2023, Bergisch Gladbach, German. Poster presentation, 'Cross-linked polypeptide capsules as potential oxygen carriers for artificial blood replacement'.

2023 35<sup>th</sup> CGCA Annual Conference, June 22<sup>nd</sup> -24<sup>th</sup>, 2023, Mainz, German. Oral presentation, 'Perfluorodecalin filled polypeptide capsules as artificial oxygen carriers'.

### 7.4 Students co-supervision

Jonas Fabrizi, Master's thesis, October 2021- September 2022, 'Synthesis and study of PFD-filled diblock polypeptide nanocapsules for medical purposes'.

Annika Kirsten, Practical course, January 2023- March 2023, 'PFD-filled polypeptide capsules as artificial oxygen carriers'.

Sascha Myszkowska, Practical course, March 2023- May 2023, 'PFD-filled polypeptide capsules as artificial oxygen carriers'.